DETERMINATION AND STATISTICAL EVALUATION OF THE EFFECT OF MINERALS AND MINERAL ASSOCIATIONS IN SPECIFIC DENSE MEDIUM FRACTIONS ON ASH FUSION TEMPERATURE

ASHRITI GOVENDER

Hons. B.Sc. (Chemistry) (University of Natal)

B.Sc. (Chemistry and Applied Chemistry) (University of Natal)

Thesis submitted for the degree Master of Science (Engineering Science) at the North-West University

Supervisor: **Prof. F.B. Waanders**

Co-supervisor: **Mr. J.C. van Dyk**

2005

Potchefstroom Campus

ACKNOWLEDGEMENTS

I would like to thank the following people and organisations for their help and support throughout this study:

Mr. JC van Dyk for his input as line manager.

Prof. FB Waanders for his assistance and guidance as supervisor.

Sasol Technology, Research and Development Division for funding this research project

My husband and family for all their encouragement, interest and support.

SOLEMN DECLARATION

I declare herewith that the thesis entitled:

DETERMINATION AND STATISTICAL EVALUATION OF THE EFFECT OF MINERALS AND MINERAL ASSOCIATIONS IN SPECIFIC DENSE MEDIUM FRACTIONS ON ASH FUSION TEMPERATURE

which I herewith submit to the North-West University in completion of the requirements set for the degree Master of Science (Engineering Science) is my own work and has not already been submitted to any other university.

SYNOPSIS

During Sasol-Lurgi Fixed Bed Dry Bottom coal gasification, the mineral matter in coal undergoes various transformations. Heat induced transformation due to low ash fusion temperatures leads to agglomeration of the ash particles to sizes varying from tiny particles to lumps larger than 100mm. Channel burning and instability in the ash bed can occur as a result. It is therefore important to understand and anticipate the reactions of the mineral matter prior to feeding the coal into a gasifier.

The principal aims of this thesis were to investigate the effect of minerals and mineral associations on the ash fusion temperature of coal. Ash fusion temperature was used as a measure of the expected behaviour of the ash bed during gasification.

Representative samples of run-of-mine coal from three sources were density separated and then comprehensively characterised. The predominant basic oxides present were identified to be Ca, Mg and Fe due to the presence of calcite, dolomite and pyrite. The results showed highest linear correlations with SiO_2 and CaO and confirmed literature that low ash fusion temperatures may be attributed to increased basic oxide levels and low SiO_2/Al_2O_3 ratios.

The combined removal of Ca, Mg and Fe by chemical fractionation resulted in an increase in ash fusion temperature. Different combinations of minerals were removed by different leaching agents. Chemical fractionation selectively altered the mineral content of coal which in turn provided valuable information on mineral interactions. This was clearly illustrated in the models developed for the calculation of ash fusion temperature.

OPSOMMING

Gedurende die Sasol-Lurgi Vastebed-droëvoer steenkoolvergassing ondergaan die minerale in die steenkool verskeie transformasies. Hitte-geïnduseerde transformasies as gevolg van lae as-smeltpunte lei tot agglomerasie van die aspartikels, die groottes waarvan varieer vanaf klein partikels tot klonte groter as 100mm. Kanaalverbranding en onstabiliteit in die asbed kan as gevolg hiervan voorkom. Dit is daarom belangrik om die mineraalreaksies te verstaan en te voorsien voordat die steenkool in 'n vergasser ingevoer word.

Die hoofdoelwitte van hierdie verhandeling is om die invloed van minerale en mineraalassosiasies op die smelttemperatuur van steenkoolas na te gaan. Die as-smelttemperatuur is gebruik as 'n maatstaf vir die verwagte gedrag van die asbed gedurende vergassing.

Verteenwoordigende monsters van onveredelde steenkool uit drie bronne is op grond van digtheid geskei en uitvoerig gekarakteriseer. Die mees prominente basiese oksiedes teenwoordig is geïdentifiseer as dié van Ca, Mg en Fe as gevolg van die teenwoordigheid van kalsiet, dolomiet and piriet. Die resultate toon die hoogste lineêre korrelasies met SiO_2 en CaO en bevestig literatuurgegewens wat daarop dui dat lae as-smelttemperature toegeskryf kan word aan hoë vlakke van basiese oksiedes en lae SiO_2/Al_2O_3 -verhoudings.

Die gesamentlike verwydering van Ca, Mg en Fe deur chemiese fraksionering het gelei tot 'n toename in die smelttemperatuur. Verskillende kombinasies van minerale is verwyder met verskillende loogmiddels. Chemiese fraksionering het die mineraalinhoud van die steenkool selektief verander en ook waardevolle inligting gelewer oor mineraalinteraksies. Dit is geïllustreer deur die modelle wat ontwikkel is vir die berekening van die smelttemperatuur.

TABLE OF CONTENTS

LIST OF TABLES

LIST OF FIGURES

CHAPTER 1

INTRODUCTION

1.1 BACKGROUND

Coal is fundamentally composed of the fossilised remains of plant debris which have undergone progressive physical and chemical alteration through geological time (Falcon and Snyman, 1986). Coal is not a homogeneous material as it is composed of a number of microscopic organic and inorganic constituents, which occur together in various proportions or associations (Falcon and Falcon, 1987). The term "mineral matter" usually applies to all the inorganic non-coal material occurring in coal and includes those inorganic elements which may occur in organic combination (Bryers *et al.*, 1976). The most abundant mineral groups found in South African coals are clays, carbonates, sulphides and quartz (Falcon and Snyman, 1986). The behaviour of these minerals during gasification is of interest to the operation of the gasifier, the selection of coals and the utilisation of the gasification ash.

During Sasol-Lurgi Fixed Bed Dry Bottom coal gasification, the mineral matter in coal undergoes various transformations. Heat induced transformation due to low ash fusion temperatures leads to agglomeration of the ash particles (slagging or fouling) to sizes varying from tiny particles to lumps larger than 100mm. Channel burning and instability in the ash bed can occur as a result. It is therefore important to understand and anticipate the reactions of the mineral matter prior to feeding the coal into a gasifier in order to have a prediction of what can happen during gasification. Research on ash fusion properties of mineral matter needed to be done in order to have a better fundamental understanding.

1.2 THESIS AIMS AND SCOPE

The principal aims of this thesis are to investigate the effect of minerals and mineral associations on the ash fusion temperature of coal. Ash fusion temperature is used, amongst others, in this study as a measure of the expected behaviour of the ash bed during gasification. Chemical fractionation

tests will also be conducted in order to provide further information on the significance and interaction of mineral elements with respect to the thermal properties of coal. The correlations between mineral elements and ash fusion temperatures will then be examined. Finally, empirical equations to calculate the ash fusion temperatures from the chemical compositions of coal will be determined. This will not simply develop equations for calculating ash fusion temperatures, but also highlight which variables in mineral composition affect ash properties.

1.3 STRUCTURE OF THESIS

The thesis begins with a comprehensive review of the literature pertaining to the project in Chapter 2. Experimental methods and procedures used are outlined in Chapter 3.

The results and general discussion on the coals characterisation results are discussed in Chapter 4. The findings from the chemical fractionation tests are presented in Chapter 5. Chapter 6 formulates the statistical correlation between coal analysis and ash fusion temperatures as well as the empirical equations to calculate ash fusion temperature.

Finally, the major findings of the research are summarised in Chapter 7.

CHAPTER 2

LITERATURE REVIEW

In this chapter an overview is given of the available literature and begins by broadly describing the origin, composition and characteristics of coal and more specifically, the minerals present in coal. This is followed by an introduction to coal gasification. Then, to complete the picture, a discussion on coal mineralogy and its relationship to coal ash chemistry, melting and slagging properties and specifically ash fusion temperature.

2.1 INTRODUCTION TO COAL

This section provides a broad description on the origin and constituents of coal.

2.1.1 DEFINITION OF COAL

Coal is fundamentally composed of the fossilised remains of plant debris which have undergone progressive physical and chemical alteration through geological time (Falcon and Snyman, 1986). Sanders (1996) proposed that "coal is a compact stratified mass of metamorphosed plants which have, in part, suffered arrested decay to varying degrees of completeness".

Coal is an organic sedimentary rock, formed by the action of temperature and pressure on plant debris. Coal is a complex mixture of organic matter containing carbon, hydrogen and oxygen, together with smaller amounts of nitrogen, sulphur and trace elements (Grainger *et al.*, 1981).

Coal is a generic term referring to a family of solid fossil fuels with a wide range of physical and chemical compositions. Coal is actually a heterogeneous rock composed of different kinds of organic matter which vary in their proportions in different coals, and no two coals are absolutely identical in nature, composition or origin (Sanders, 1996).

2.1.2 COAL FORMATION

Coalification is the process of metamorphism which takes place over time, and under conditions of higher temperature and pressure, and results in the transformation of the original peat swamp through the progressive stages of lignite, sub-bituminous, bituminous coals, anthracite and graphite (Falcon and Snyman, 1986). This process may be distinguished into a *biochemical stage*, which includes the whole of the peat-forming process, and a *geochemical stage*, during which metamorphosis takes place.

(i) Biochemical Stage

The principal initiating requirements for coal formation are a swampy or marshy environment, climatic conditions favourable for rapid plant growth, with enough depth of water to restrict oxygen supply during the breakdown of the original plant material when it dies and falls into the water (Grainger *et al.*, 1981). During this stage the grade of the coal is determined and is dependant on the amount of inorganic mineral material washed into the system. Grade refers to the mineral matter composition (Falcon and Snyman, 1986).

Micro-organisms in the presence of water induce a chemical change in the plant material resulting in the formation of peat. Continued subsidence of the swamp allows further growth and accumulation of plant material (Grainger *et al.*, 1981).

The proportions and chemical composition of the organic constituents formed during the peatification stage are the precursors of the macerals which impart to the fossilised plant material its characteristic organic composition (type) (Falcon and Snyman, 1986).

(ii) Geochemical Stage

The differing degrees of pressure and heat over different periods of time in the geochemical stage, which act on the peat-like deposits, were responsible for the difference in coalification, referred to as the rank of the coal (Grainger *et al.*, 1981). Rank refers to the degree of maturity or metamorphosis undergone by a coal seam, usually in response to time, temperature or pressure. The

most reliable parameter used in South Africa to define rank is the reflectance of vitrinite, which is measured petrographically under oil immersion (Falcon and Falcon, 1987).

The proportions of organic constituents (type) and the process of maturation (rank) are independent of one another (**Figure 2.1**) (Falcon and Snyman, 1986).

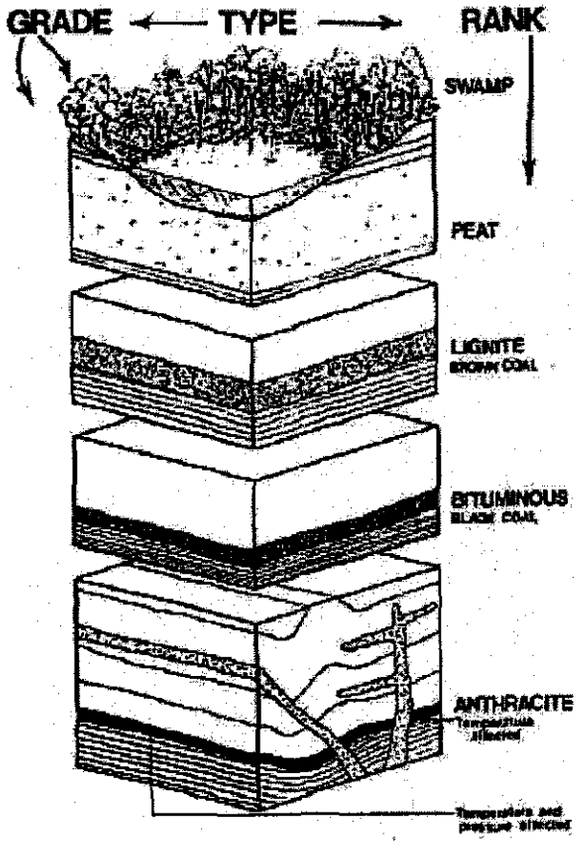

Figure 2.1 Formation of coal in terms of rank, type and grade
(Falcon and Snyman, 1986)

2.1.3 Coal Composition

Coal is not a homogeneous material as it is composed of a number of microscopic organic and inorganic constituents, which occur together in various proportions or associations (Falcon and Falcon, 1987).

The term "maceral" is used to represent the different organic plant tissue from which the coal was originally formed. Vitrinite, liptinite and inertinite are the

main maceral categories. Vitrinite is relatively oxygen-rich and is derived from cell walls and cell contents of precipitated gels preserved under water. Liptinite is the hydrogen-rich maceral type formed from algae, spores and waxy leaves. Inertinite originated from plant tissue that had oxidised, altered, degraded or burnt in the peat stage of coal formation, and is carbon-rich (Falcon and Falcon, 1987).

The term "mineral matter" usually applies to all the inorganic non-coal material occurring in coal and includes those inorganic elements which may occur in organic combination (Bryers *et al.*, 1976). According to Ward (2002), the term mineral matter in coal encompasses dissolved salts in the pore water, inorganic elements associated with the organic compounds, as well as discrete crystalline and non-crystalline mineral particles. The dissolved salts and inorganic elements are usually prominent in the mineral matter of lower-rank coals, such as brown coals and lignites. However, these are removed by expulsion of moisture and changes in the chemical structure of the organic matter with rank advance. Discrete crystalline and non-crystalline minerals may occur in both low-rank and higher-rank coals (Ward, 2002).

The organic and inorganic constituents of coal combine in various associations to form microscopic layers termed microlithotypes which, by definition, are greater than 50 μm in width. They may be composed of pure macerals or varying proportions of different macerals.

A succession of microlithotypes forms macroscopically identifiable layers of 5mm or more, called lithotypes. There are four main classifications of lithotypes (Falcon and Falcon, 1987):

(i) Vitrain (bright coal) which forms the vitreous and brittle bands in bituminous coal.

(ii) Clarain (bright-banded intermediate coal) occurs in laminated bands. It is commonly associated with vitrain.

(iii) Durain (dull coal) represents agglomerations of oxidised and carbonised plant remains.

(iv) Fusain (soft and friable) represents remnants of dried, oxidised wood.

2.1.4 Origin of minerals in coal seams

Minerals occur in sedimentary rocks, such as siltstones, shale, and sandstones, interbedded between coal bands or seams, and as mineral grains within the organic matrix of a seam (Falcon and Falcon, 1987).

The minerals in coal (**Figure 2.2**) can be classified into two major categories, namely intrinsic and extrinsic mineral matter, depending on its origin (Falcon and Snyman, 1986):

(i) Intrinsic (included) inorganic matter was present in the original living plant tissue. These are trapped in coal in the form of sub-microscopic mineral grains and as organo-metallic complexes.

(ii) Extrinsic (excluded) mineral matter was introduced from external sources and can be further subdivided into two classes:

(a) Syngenetic minerals that arise from the accumulation of the minerals at the time of peat accumulation by means of wind and water or precipitation *in situ*.

(b) Epigenetic minerals that were deposited by percolating waters into fissures and cracks long after the initial peat had accumulated.

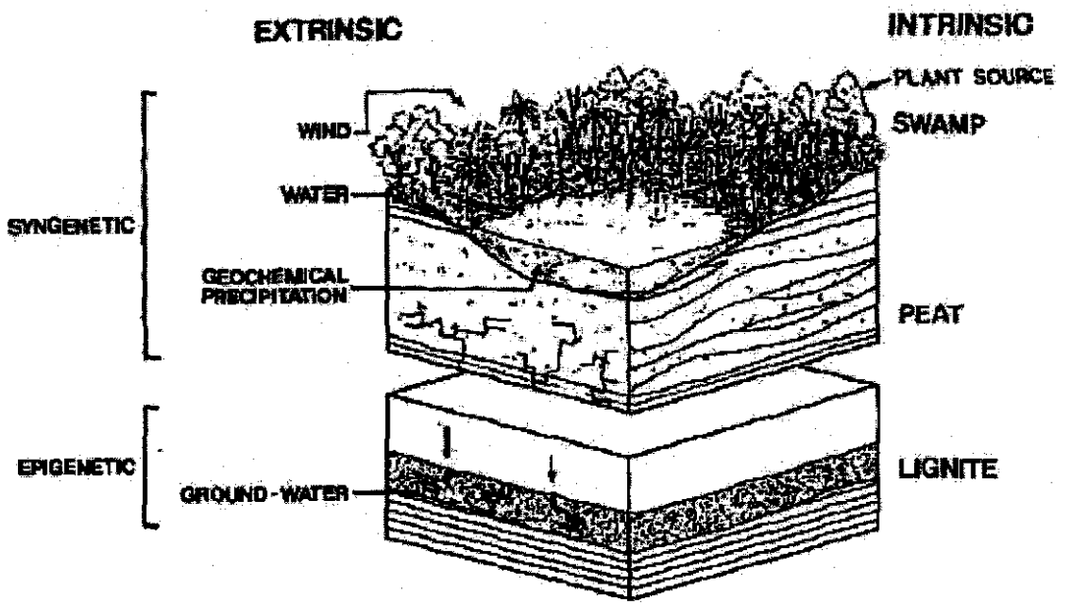

Figure 2.2 The origin and types of mineral matter in coal
(Falcon and Snyman, 1986)

According to Creelman *et al.* (2000), minerals in coal occur as:

(i) Excluded inorganic matter completely liberated from the coal which will oxidise, melt, may form voids, but has no opportunity to combine with other minerals prior to deposition.

(ii) Inherent species organically attached to the coal structure which originated from living plant tissues or were ion exchanged with the coal structure during coalification.

(iii) Included mineral dispersions bound to the coal will oxidise, melt, form voids, adhere to the char surface, possibly agglomerate, and be released from the coal.

2.1.5 Abundant mineral groups in South African coals

The most abundant mineral groups found in South African coals are clays, carbonates, sulphides, quartz and glauconite (Falcon and Snyman, 1986). **Table 2.1** lists the common minerals in South African coals.

Table 2.1 Distribution of the common minerals in South African coals (Falcon and Snyman, 1986)

Mineral group	**Mineral name**	**Chemical formula**
Clays	Kaolinite	$Al_2Si_2O_5(OH)_4$
	Illite/Muscovite	$(K,H)Al_2(Si,Al)_4O_{10}(OH)_2$
	Montmorillonite	$(½\ Ca,Na)_{0-7}(Al,Mg,Fe)_4(Si,Al)_8O_{20}(OH)_4.nH_2O$
Carbonates	Calcite	$CaCO_3$
	Dolomite	$(Ca,Mg)(CO_3)_2$
	Aragonite	$CaCO_3$ (orthorhombic)
	Siderite	$FeCO_3$
Sulphides	Pyrite	FeS_2
	Marcasite	FeS_2
Oxides	Haematite	Fe_2O_3
Silicates	Quartz	SiO_2

An important point to note is that coal does not contain ash, it contains minerals. Mineral matter in coal transform on heating to form ash. Molten ash will readily coalesce to form a large molten mass or cause the agglomeration of ash particles (Slaghuis, 1993). In order to understand the negative effect of that, the basics of the Sasol-Lurgi fixed bed dry bottom gasification operation need to be known.

2.2 INTRODUCTION TO COAL GASIFICATION

Coal is used by Sasol as a feedstock to produce synthesis gas via the Sasol-Lurgi Fixed Bed Dry Bottom gasification process.

The Sasol-Lurgi Fixed Bed Dry Bottom gasifier operates on lump sized coal. Therefore, once the coal is mined, it is crushed down to less than 100mm and screened at a bottom size of 5 to 8 mm. The coal enters the top of the gasifier through a lock-hopper system while reactant gases (steam and oxygen) are introduced at the bottom of the gasifier. The reactant gases flow upwards through the spaces between the coal lumps. The counter-current operation results in a temperature drop in the reactor, with the result that five characteristic zones (**Figure 2.3**) can be identified in a fixed bed gasifier (Slaghuis, 1993).

As the coal descends it is first dried and devolatilised by the heat of the rising gas. The devolatilised coal, better known as char, then enters a gasification zone and residual char is finally burnt to ash. Ash is removed at the bottom of the gasifier by a rotating grate and lock hopper.

During high-temperature gasification, the mineral matter in coal undergoes various transformations. The final product of these transformations is ash or agglomerates of ash particles. The size of the ash particle agglomerates (which is called clinker) can vary from tiny particles to lumps larger than 100mm. Ash clinkering inside the gasifier can lead to channel burning, pressure drop problems and unstable gasifier operation.

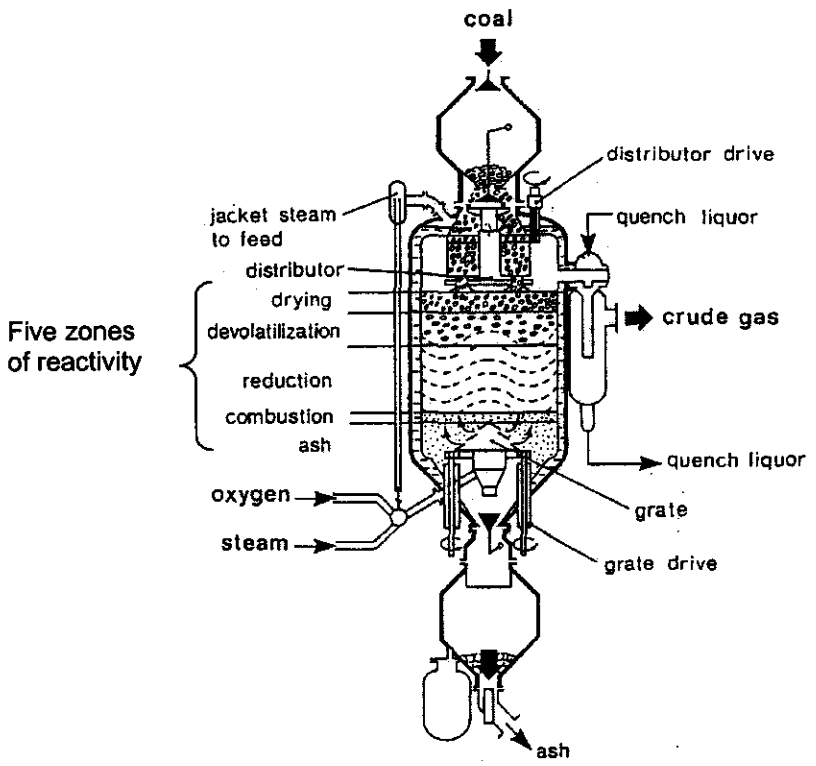

Figure 2.3 Representation of the gasifier showing the zones of reactivity (Slaghuis, 1993)

The Sasol-Lurgi Dry Bottom gasifier technology requires that the temperature of the ash must not exceed the ash fusion temperature (flow) in the above lying combustion zone. When the temperature in the combustion zone exceeds the melting point of the ash, the ash will melt/flow and agglomerate (Slaghuis, 1993).

It is, therefore, necessary to understand the effect and interaction of mineral matter during heating. This can only develop once the mineral matter present in the coal and its associations with each other and the macerals present has been identified and the coal is comprehensively characterised.

2.3 DEVELOPING AN UNDERSTANDING OF COAL

In order to build an understanding of how critical elements behave during gasification, what minerals are present in the coal and how such minerals interact during utilisation, one needs to obtain as complete a description of the coal as possible.

2.3.1 Coal characterisation

Coal characterisation techniques include proximate, ultimate and petrographic analyses as well as the determination of the mineralogy by x-ray powder diffractometry; chemical analysis and optical and scanning electron microscopy. The determination of the mineralogy of a coal provides valuable information about the inorganic matter in coal that cannot be obtained from chemical analysis alone (Huggins, 2002).

Methods to determine the mineral matter in coal should preferably be done without separation of the mineral matter from the coal so that association of minerals with macerals and of minerals with other minerals might also be determined (Huggins, 2002). It is, however, difficult to determine the separate effects of the different coal properties from the whole coal. One way to alleviate that problem is to density separate the coal.

Density separation reduces the great heterogeneity of the coal particles and allows the preparation of series of samples that cover the full range of mineral contents in raw coal particles. The study of the density separated samples allows the gathering of information on mineral distribution in the coal particles and its degree of association with the organic components, as well as to understand the influence of mineral matter composition and distribution within the particles on the behaviour of the whole coal. The segregation of both macerals and minerals and the variable degree of association of macerals and organic/inorganic matter are known to occur during the preparation of density fractions (Mendez *et al.*, 2003).

2.3.1.1 Ash fusion temperature (AFT)

The ash fusion temperature provides an indication as to the extent of ash agglomeration and clinkering likely to occur within the gasifier. Ash clinkering inside the gasifier can cause channel burning, pressure drop problems and unstable gasifier operation. More information on AFT is provided in **Section 2.4.2.1**.

2.3.1.2 **Proximate analysis** (Govender, 2004)

The proximate analysis of a coal describes its composition in terms of the relative amounts of moisture, volatile matter, and ash content. The fixed carbon in the coal is calculated by difference. The volatile matter provides an indication of the reactivity of a coal, as well as the amount of tar and oils that might be produced during gasification. Although this is not a direct method for tar and oil determination, it is in good correlation with the tar determination via the Fischer Assay analysis. The ash content gives an indication of the amount of inorganic material in the coal and includes mineral matter inherent in the coal structure, as well as out-of-seam inorganic contamination.

The proximate analysis parameters are usually determined on an air-dried sample, where the coal sample is spread out and allowed to come into equilibrium with the laboratory atmosphere. Since coal is hydroscopic, its moisture content will vary with changes in the humidity. Thus it can be noted from the outset that the same coal could have different moisture values assigned by different laboratories.

2.3.1.3 **Ultimate analysis** (Govender, 2004)

An ultimate analysis determines the total amounts of each of the principal chemical elements present in coal, namely carbon, hydrogen, sulphur, nitrogen and oxygen by difference. Carbon and hydrogen determinations are used in material balance calculations on coal conversion calculations. Nitrogen data can be used to evaluate the potential formation of nitrogen oxides as a source of atmospheric pollution. Results of the sulphur analysis may be used to evaluate coal preparation, evaluate potential sulphur emissions from coal conversion processes, and evaluation of the coal quality in relation to specifications.

2.3.1.4 **Ash composition** (Govender, 2004)

A compositional analysis of the ash in coal is often useful in the total description of the quality of the coal. Ash is composed of complex oxides and the ash analysis expresses this composition in terms of its oxides of Si, Al, Fe,

Ti, P, Ca, Mg, Na, K, and S. Further information on ash oxides is provided in **Section 2.4.2.2.**

2.3.1.5 **X-ray diffraction (XRD)** (Govender, 2004)

X-ray powder diffraction (XRD) is an instrumental technique that uses the principles of Bragg's Law to determine the type and relative amount of crystalline substances in a bulk sample. It is based on the unique characteristic diffraction of X-rays from the crystal structure of each mineral. This method is however, at best, semi-quantitative due to variations in the mineral crystallinity, preferred orientation in the sample mount, and differential absorption of X-rays by the minerals in the mixture.

2.3.1.6 **Fischer assay** (Govender, 2004)

The yield of tar, water, gas and char for a given coal is measured using the Fischer assay.

2.3.1.7 **Petrographic Analyses** (Govender, 2004)

Petrographic analyses of coal provide information about the rank, the maceral and microlithotype compositions and the distribution of mineral matter in the coal.

2.3.1.7.1 **Maceral analysis** (Govender, 2004)

Macerals represent the primary microscopic organic building blocks of coal. There are three major groups, namely vitrinite, liptinite and inertinite; each group is divided into sub-categories. For South African coals only the inertinite group is sub-divided and determined; reactive and inert semifusinite, reactive and inert inertodetrinite and micrinite. Each of the three major groups possesses significantly different chemical, physical and performance characteristics which impart to that coal its inherent technological behaviour. Comparatively, vitrinite is considered to be oxygen-rich, liptinite hydrogen-rich and inertinite carbon-rich. The rank of the coal (degree of maturity) will affect these proportions.

Of the three groups, vitrinite is the most brittle, is highly reactive in combustion environments (although liptinite is more reactive), devolatilises easily, can swell and will become porous on heating. Inertinite requires far more oxygen to ignite, does not swell and is harder to crush. Typically the results are reported to include total reactive macerals (vitrinite + liptinite + reactive semi-fusinite and reactive inertodetrinite) indicating the proportion of particles expected to devolatilise and become porous and swell to varying degrees on heating. Total inertinite (inert semi-fusinite + fusinite / sclerotinite + micrinite + inert inertodetrinite) indicates the proportion of less reactive particles; fusinites particularly may pass through a heating process unaltered, and hence not contributing to the process. The influence of pressure is likely to increase the reactivity of the inert particles. The role of the different macerals during utilization is dependant on particle size, oxidizing/reducing environments, time in system, as well as the organic and inorganic interactions between and within the particles.

2.3.1.7.2 **Microlithotype analysis** (Govender, 2004)

Microlithotypes represent the natural associations of macerals to each other and inorganic matter. Macerals may occur as mono-macerals, or mixed in varying degrees of complexity. The degree of banding or mixing and mineral intergrowths between the macerals further influences the technological and mechanical properties of the coal. Rank will affect these properties.

The results of the maceral group analysis can be interpreted more meaningfully from knowledge of the microlithotype composition, assisting in the consideration of the behaviour of coal during utilisation. Information on microlithotypes can assist with seam correlations and coal genesis investigations, hardness and bulk densities.

2.3.1.7.3 **Mineral group analysis** (Govender, 2004)

This analysis is based on the visible representation of the various broad mineral groups, namely clays & quartz, carbonate group minerals, and pyrite group minerals. By this means it is possible to establish trends regarding the form, size and nature of distribution of the major mineral groups. These

factors can influence mineral liberation in coal, beneficiation, abrasion, spontaneous combustion and so on.

The proportions and distribution (including size distribution and distribution within the organic matter) of minerals can influence performance behaviour, ash formation and clinkering. High proportions of sulphide minerals will increase SOx and H_2S production. High proportions of carbonates can influence the clinkering and slagging behaviour of the coal. High proportions of quartz will render the coal more abrasive and could increase the titanium content. These results should be used in conjunction with XRD and CCSEM data; petrography provides a broader picture at a fraction of the price of CCSEM analysis.

2.3.1.7.4 **Rank** (Govender, 2004)

Rank is an indication of the degree of maturity of coal and may be determined very accurately by the reflectance of light emanating from the polished surface of vitrinite. Rank can also be inferred from the volatile matter and carbon content of a coal, but this method is not very accurate. The distribution of reflectance readings and standard deviation number can indicate the "purity of rank" (i.e. whether the sample is from a single seam, or a blend of seams/coals, or heat affected). If a coal sample is a blend of different ranks, or includes heat affected material, predicted utilization characteristics based on average chemical composition may be inaccurate. Coals of a lower rank have a higher volatile matter and lower carbon contents, and thus react differently to higher rank coals, where the volatile content is lower and the carbon content higher.

2.3.1.7.5 **Weathering** (Govender, 2004)

The analysis can provide useful information regarding the general condition of the coal; that is the degree of weathering, oxidation, or other anomalies such as heat affect, pseudovitrinite, inherent fissures and cracks.

2.3.1.8 CCSEM analysis

The Computer Controlled Scanning Electron Microscope (CCSEM) is a scanning electron microscope, which has being configured to quantify and qualify the minerals in coal, ash and clinkers, according to elemental proportions.

The principal component of a CCSEM is a scanning electron microscope (SEM), which is automatically controlled by microanalysis system (Oxford ISIS system). The ISIS microanalysis system controls stage movements, image acquisition, positioning of the electron beam, acquisition and interpretation of energy dispersive (EDS) X-rays obtained and image processing routines (Van Alphen, 2003).

The CCSEM procedure used to analyse the samples in this study is as follows (Van Alphen, 2003):

1) Prepared polished sections are placed in a sample holder.
2) The automated stage positions the sample holder at the first field of view. A backscattered electron (BSE) image is acquired. A low atomic weight phase such as the carbonaceous material (coal) is dark whereas a high atomic weight phase such as pyrite (FeS_2) is white (**Figure 2.4**).
3) An automated image analysis routine processes the BSE image and produces a binary image of the particles in the field of view. A binary grid of regularly spaced points is superimposed over the particle binary image. Analytical points are defined as the intersection between the processed image and a superimposed binary grid (**Figure 2.4**).
4) The electron beam is positioned at each analytical point in the field of view. At each point a 100 msec X-ray spectrum is obtained. From the X-ray spectrum, X-ray counts for predefined elements are computed and recorded.
5) The stage positions the next field of view and the process is repeated until all the field of views have been analysed.

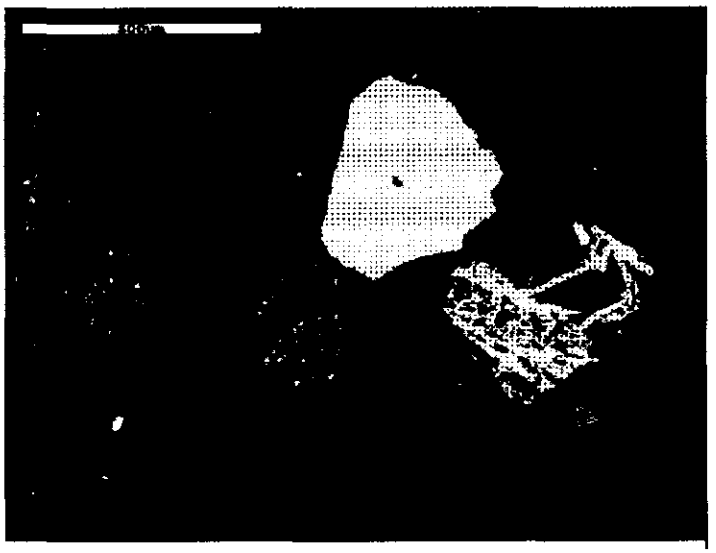

Figure 2.4 Processed BSE image illustrating the position of the analytical points. Coal is black, epoxy resin is grey and mineral matter white. Point spacing is 11.21 µm. (scale bar represents 500 µm)

Mineral identification is based on the elemental counts derived for each analytical point and by applying unique mineral identification rules based on the principals of fuzzy logic. In context of this investigation, coal is considered as a "mineral" defined by its high carbon content (**Figure 2.5**).

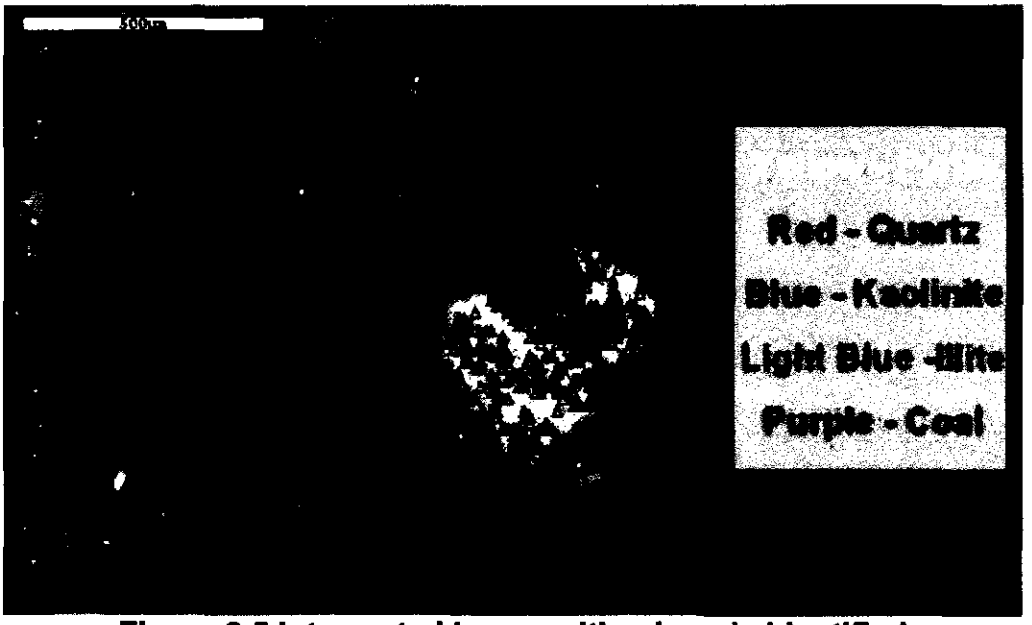

Figure 2.5 Interpreted image with minerals identified

The development of mineral identification rules based on the principals of fuzzy logic is crucial for CCSEM analysis. The rules are developed by

examining the polished section and identifying the minerals present prior to undertaking an automated CCSEM analysis.

The principal requirement of this investigation is to establish the association characteristics of mineral matter with coal. Since the X- and Y-coordinates of each analytical point are recorded it is possible to reconstruct the particles analysed and to determine the minerals present for each particle identified. With this data, the particle size, included mineral and coal grain sizes and mineral matter to coal associations can be determined (**Figure 2.4** and **Figure 2.5**).

2.3.1.9 Mössbauer spectroscopy

Mössbauer spectroscopy plays an important role to study minerals containing iron, as well as to identify different iron transformations. According to Cohen (1976), the Mössbauer effect is the recoilless emission by radioactive nuclei and resonant re-absorption of γ-rays, which arises from the nuclear excited states. These γ-rays are electromagnetic radiation and have no electrical charge and are absorbed or scattered by energetic collisions when passing through matter. The very small energy changes can be measured by the Mössbauer effect to give information about the surroundings of the nucleus. In **Figure 2.6**, a schematic representation of the nuclear decay and excitation process is given.

In **Figure 2.6** the horizontal lines represent nuclear energy levels of the source and absorber. The source nucleus decays from the excited state to the ground state, emitting a γ-ray. The γ-ray is subsequently absorbed in the absorber, thus raising the absorber nucleus to its excited state. Since every isotope has absorption energy in a different energy region, γ-rays of each nucleus (e.g. ^{57}Fe) can only be reabsorbed by nuclei of the same type (Cohen, 1976).

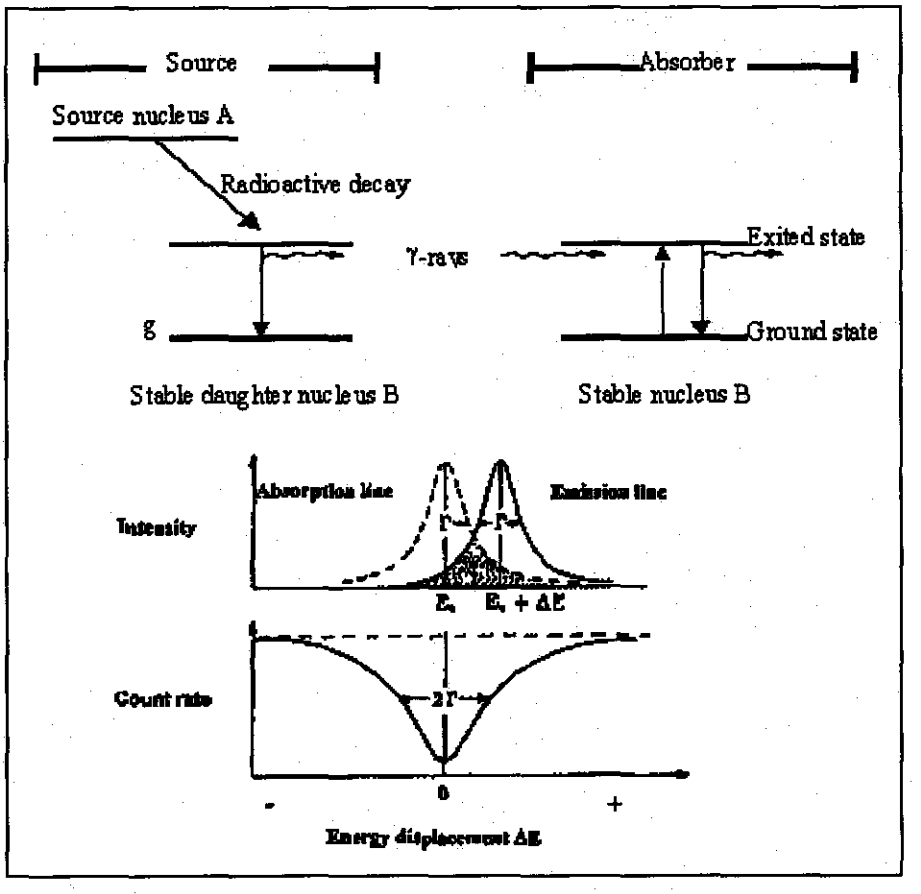

Figure 2.6 Schematic representation of the events occurring in MS
(Cohen, 1976)

Small perturbations in the energy of nuclear levels in the absorber can be measured by observing the change in γ-ray energy required for the γ-ray to be resonantly absorbed. These measurements are usually performed by scanning the gamma-ray energy, using the Doppler shift, produced by moving the source with known velocities (Cohen, 1976).

The resultant spectrum is normally displayed as a spectrum of count rate versus γ-ray energy shift (see **Figure 2.6**). The nuclear resonance will cause an increased absorption at γ-ray energies, matching the possible excitation energies in nuclei in the absorber and will result in an absorption line. This dip (or series of dips) is known as a Mössbauer spectrum. The energy shifts, at which resonant absorption occurs, as well as the relative line intensities, are the principal measured parameters in most Mössbauer spectroscopy

experiments and are determined by electronic effects on the nuclear energy levels.

The energy shift arises from the interactions of electrons with the nuclei, and these measurements allow various conclusions to be drawn about the electronic structure of the material being studied. These effects, called "hyperfine parameters", are the isomer (chemical) shift,δ, (electric) quadrupole splitting,Δ, and the magnetic hyperfine Zeeman splitting. The isomer shift and quadrupole splitting are expressed as a value with units of $mm.s^{-1}$ and the magnetic hyperfine Zeeman splitting in terms of the magnetic field strength measured in Tesla (Cohen, 1976).

In the present investigation, use was made of a ^{57}Co-source emitting λ-rays of 14.4 keV energy, decaying to ^{57}Fe, of which the energy level diagram is shown in **Figure 2.7.**

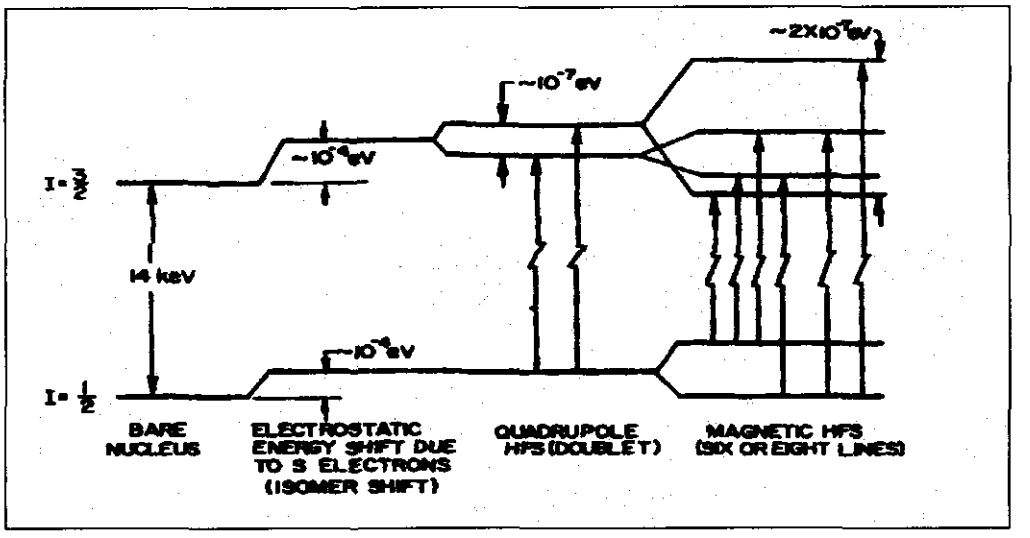

Figure 2.7 Energy level diagram for ^{57}Fe
(Cohen, 1976)

(i) Isomer shift (δ)

The total electron density on the Mössbauer atom is measured by the isomer shift (see **Figure 2.8**). Strictly, it is the electron density at the nucleus that is important and it is measured relative to that in a standard material. The nucleus interacts with the electrons in a manner, which raises the energy

levels by an amount that is proportional, both to the size of the nucleus and to the magnitude of the electron density (Cohen, 1976).

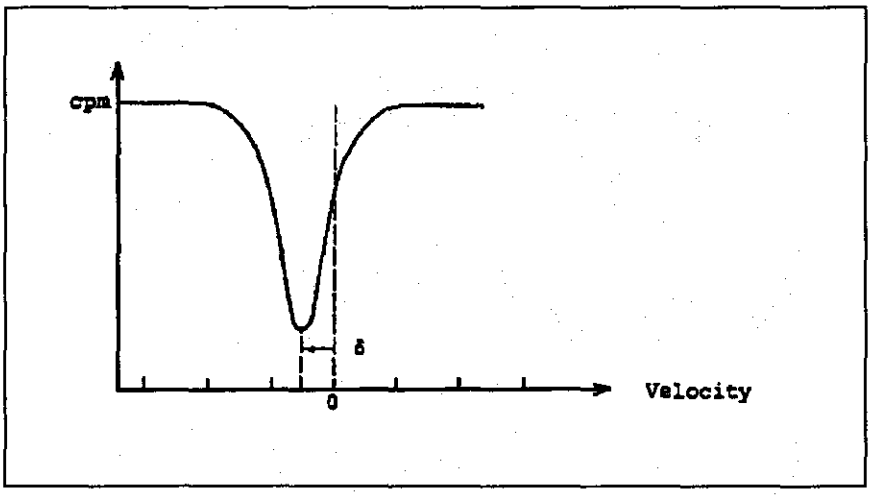

Figure 2.8 Characteristic parameter of a Mössbauer spectra: isomer shift (singlet)

The isomer shift is determined by the interaction between the nucleus and the charge distribution of electrons in the region of the nucleus. The isomer shift depends on the fact that the spacing of the nuclear energy levels depend on the chemical environment of the nucleus.

(ii) Quadrupole interactions (Δ)

Cohen (1976) stated that a Mössbauer nucleus can be used as an 'observer' or probe to get information about site symmetries and field gradients within a crystal and to give details of imbalance of *p* and *d* electrons. The nuclear energy levels, represented by the electric quadrupole and magnetic dipole hyperfine interactions, may be split, in addition to energy level changes, produced by the isomer shift. This splitting leads to a number of possible absorption energies, resulting in a number of absorption lines. A split between the nuclear excited state (I=3/2) and ground state (I=1/2) of ^{57}Fe-nucleas results in the formation of two absorption lines, namely a doublet. This type of interaction is illustrated in **Figure 2.9**.

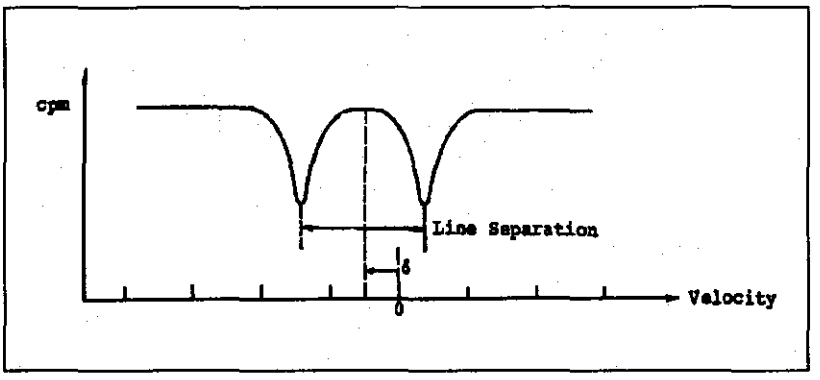

Figure 2.9 Characteristic parameter of Mössbauer spectra: electric quadrupole splitting (doublet)

(iii) Hyperfine magnetic interactions (Zeeman splitting)

The third of the major types of interaction that can be investigated by Mössbauer spectroscopy is the hyperfine magnetic interactions (Zeeman splitting) of the nuclear energy levels in a magnetic field, resulting in a sextet (six lines) as illustrated in **Figure 2.10**. Cohen (1976) stated that the magnetic hyperfine interaction arises from the coupling of the nuclear magnetic moment with effective magnetic fields at the nucleus and results in splitting of the nuclear ground and excited states if they have a nuclear spin larger than zero.

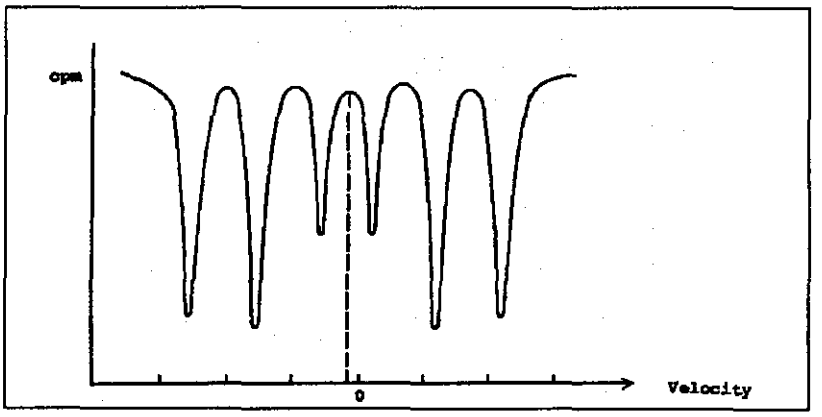

Figure 2.10 Characteristic parameter of Mössbauer spectra: nuclear Zeeman splitting (sextet)

The data obtained from the Mössbauer spectra are then interpreted by referring to the Minerals Data Handbook (Stevens *et al.*, 1998).

2.3.2 CHEMICAL FRACTIONATION TESTS

Chemical fractionation tests result in coal with different mineral properties which can be used to explain the effect of specific minerals on ash fusion temperature. The experimental procedure, obtained from Baxter (2002), uses selective extraction of elements, based on solubility, which reflects their association in the coal. The tests provide further information on the significance and interaction of mineral elements with respect to the thermal properties of coal.

The leaching agents used were water, ammonium acetate (NH_4OAc), hydrochloric acid (HCl) and nitric acid (HNO_3). The first extraction is by water only and is intended to remove water-soluble elements such as sodium. The second extraction uses ammonium acetate to remove elements such as sodium, calcium and magnesium that are ion exchangeable. The third and fourth extractions use acid (HCl and HNO_3) to remove acid soluble species such as alkaline earth sulphates, carbonates, etc. The residual material typically consists of silicates, oxides and sulphides.

2.3.3 STATISTICAL EVALUATION

Two statistical software packages were employed to analyse the analytical data obtained.

2.3.3.1 Calculation of correlation coefficients

The correlation coefficients between two data sets (ash elements and ash fusion temperatures) were calculated using the Data Analysis Tool Pack in Microsoft Excel. Correlation coefficients determine whether two ranges of data move together. **Equation 1** is used in order to determine the correlation coefficient, *r* (Mack, 1975).

$$r = \sum_{i=1}^{N}(x_1-\bar{x})(y_1-\bar{y}) \Big/ \left[\sum_{i=1}^{N}(x_i-\bar{x})^2 \sum_{i=1}^{N}(y_i-\bar{y})^2\right]^{1/2} \quad (1)$$

The correlation coefficient, r, can be proven mathematically to never be greater than +1 nor less than -1 whatever the x and y-values. It is a measure of the linear association between the random variables, x and y.

If r has a value between +0.8 and +1, it indicates that there is a strong positive correlation while r values between -0.8 and -1 indicate a strong negative correlation (Mack, 1975).

2.3.3.2 Development of a model to predict ash fusion temperature

The Design Expert (version 6) package was utilised to derive empirical equations to calculate the ash fusion temperatures from the chemical compositions of coal.

$$y = constant + b_1x_1 + b_2x_2 + \ldots + b_n x_n \quad (2)$$

The equation is developed in the form shown in **Equation 2**, where the response y is one of the four ash fusion temperatures. The b_i $(i = 1,2,\ldots,n)$ are the respective regression coefficients and the x_i $(i = 1,2,\ldots,n)$ refers to the chemical properties such as ash oxide percents or ash oxide indices.

The objective of this exercise was not simply to develop equations for calculating ash fusion temperatures, but rather to determine which variables in ash composition affect ash properties.

2.4 EFFECT OF COAL MINERALOGY ON COAL PROPERTIES

An extended knowledge of the inorganic matter and its behaviour during heating can be of great importance in understanding the fusion characteristics of coal ash, as well as the reactions taking place during coal use.

2.4.1 THERMAL BEHAVIOUR OF MINERALS

It is reasonable to expect that the known thermal behaviour of some of the individual minerals would provide information which is consistent with the interactions of the various minerals in ash.

- Kaolinite: The decomposition starts at 550-600°C due to the release of water leading to the formation of meta-kaolinite. Meta-kaolinite remains unaltered up to a temperature of 950-1000°C, at which it decomposes to mullite. Presence of iron accelerates the formation of mullite from kaolinite, whilst potassium retards the formation (Gupta *et al.*, 1998).

- Illite: At 350°C illite loses hygroscopic moisture resulting in a mass loss. The conversion of illite to semimetaillite occurs at about 550°C while the conversion of this semimetaillite to metaillite occurs at about 900°C (Tomeczek *et al.*, 2002). Potassium and iron oxides are key fluxing elements (Gupta *et al.*, 1998).

- Calcite: Decomposition starts at around 900°C. The decomposition of calcite is influenced by partial pressure of carbon dioxide in the environment (Tomeczek *et al.*, 2002).
- Pyrite: Decomposition starts at around 700°C and occurs in two steps. In the first step, $Fe_{1.25}S$ is produced which decomposes later into Fe and S_2 in the second step above 1000°C. In oxidising atmosphere, the pyrite combustion reaction starts at about 600°C (Tomeczek *et al.*, 2002).

- Quartz: Tridymite and cristobalite are two major phase inversions of quartz, which occur at 870 °C and 1470 °C, respectively. The presence of potassium, iron or calcium oxide can give rise to the formation of silicate glasses at much lower temperatures (<1300°C) (Gupta *et al.*, 1998).

The findings of Vassilev *et al.* (1995) on the effect of temperature on minerals, is summarised in **Table 2.2.**

Table 2.2 Effect of temperature on minerals

TEMPERATURE	EFFECT OBSERVED
55°C – 110°C	Loss of absorbed water.
130°C – 180°C	Dehydration of gypsum (endothermic).
200°C – 400°C	Dehydroxylation of Fe.
300°C – 600°C	Dehydroxylation of Al.
340°C – 530°C	Pyrite and siderite decomposition. Clay minerals dehydroxylation and destruction.
350°C – 620°C	Dehydroxylation of Ca-Mg.
470°C – 810°C	Decomposition of Fe sulphates.
570°C – 575°C	Quartz inversion (endothermic).
680°C – 915°C	Calcite and dolomite decomposition.
>800°C	Continuation of clay mineral destruction and carbonate decomposition.
850°C – 1000°C	Continuation of clay mineral destruction. Formation of spinel, mullite, corundum and amorphous phases.
965°C – 1000°C	Solid state reactions (mainly between CaO and silicates).
>1000°C	Crystallisation of amorphous silica to cristobalite. Formation of corundum, spinels, mullite, Ca silicates, pyroxenes and olivines. Anhydrite decomposition. Some reactions between phases. Melting or solutions of different phases.

2.4.2 EVALUATION OF CLINKERING AND SLAGGING POTENTIAL

Various analytical techniques are used to evaluate the potential of coals to clinker and slag. These include the ash fusion test, the analysis of ash (expressed as the elemental oxides), phase diagrams and the estimation of indices based on ratios of the elemental ash oxides (Huggins, 2002).

Different approaches can be used to predict the clinker/slagging propensity of a coal. The common approach is to measure ash fusion temperatures under

reducing and oxidising conditions or to use the numerous slagging indices which are available and are based on the acid to base composition of the ash.

2.4.2.1 Ash fusion temperature (AFT)

The ash fusion temperature of a coal source gives an indication to what extent ash agglomeration and ash clinkering is likely to occur within the gasifier.

The ASTM Fusion Temperature Test is a documented observation of the melting process occurring in coal ash shaped like a small cone, and placed in a furnace with increasing temperatures. As the ash heats, particles sinter and fuse and eventually form a liquid slag, these changes providing the basis for characterising the fusion processes (Huggins, 2002).

When coal ash melts it occurs on both a large scale and a microscopic scale. On the large or bulk scale the ash behaves like a glass. As the temperature of the material increases, its viscosity decreases. At temperatures less than 1000 °C, the ash may appear solid. On a microscopic scale several minerals may have all ready melted, but their concentrations are low when compared to other minerals with higher melting temperatures. As the temperature is increased the ash becomes less viscous or more liquid like. Many reactions are now occurring between the minerals as they melt and become more fluid. As the molten components mix they become more like molten glass. This molten material starts to dissolve the non molten materials like quartz and other minerals. In this way the melting temperature of minerals such as sandstones and shales are lowered by other minerals such as pyrite and limestone (Hatt, 2001).

The AFT operator observes changes in a standard ash cone as it is heated through a temperature range of 1000-1600°C (Wall *et al.*, 1999). The ash fusion temperatures recorded as the characteristic of various stages of ash melting are:

- The deformation temperature (DT) when ash just begins to flow (as shown by the first sign of deformation or rounding of the apex of the pyramid).

- The softening temperature (ST) which tends to correlate with the temperature of critical viscosity (when the height of the ash becomes equal to the width of the base).
- The hemispherical temperature (HT) which represents the temperature yielding a hemispherically shaped droplet (when the height of the fused ash becomes equal to half of its width).
- The flow temperature (FT) at which the ash is supposedly freely fluid (when the height becomes 1/16th of the width).

The atmosphere of the furnace is controlled to either an oxidizing (like air) or a reducing (CO present) condition. This is important due to the oxidation behavior of iron (Fe) atoms. Reduced iron lowers melting and fusion temperatures of ash much better than the oxidized form. In coals that have significant iron levels, the oxidation state of the iron is critical (Hatt, 2001).

Sasol coal sources have an initial deformation temperature greater than 1250°C and an ash melting temperature above 1300°C. Operating experience with the Sasol-Lurgi gasifiers has indicated that ideal gasifier operation is to operate at a temperature above the initial deformation temperature in order to obtain enough agglomeration to improve bed permeability, but also to operate below the ash melting temperature to prevent excessive clinkering (Van Dyk, 2001).

2.4.2.2 Ash composition

Ash is composed of complex oxides and the ash composition analysis expresses this composition in terms of the component oxides. The eight predominant oxides are classified as follows (Hatt, 2001):

(i) Acids or glass formers

- Silicon dioxide SiO_2
- Aluminum oxide Al_2O_3
- Titanium dioxide TiO_2

(ii) Bases or fluxing agents

- Iron oxide Fe_2O_3
- Calcium oxide CaO
- Magnesium oxide MgO
- Potassium oxide K_2O
- Sodium oxide Na_2O

Some studies indicated that the principal factors associated with coal ash melting and subsequent slag flow properties were the SiO_2/Al_2O_3 ratio and basic oxide levels (Bryant *et al.*, 2000).

Slag deposits may be enhanced in Fe and Ca compared to the coal ash, originally occurring as pyrite and calcite in the coal. The deposit may also be enhanced in Na, Mg, K, Ca and Fe which may have originally been organically bound in the coal (Kahraman *et al.*, 1999).

Patterson and Hurst (2000) stated that the relative amounts of the major minerals: quartz; clays; siderite and other carbonates, control ash and slag characteristics. These features result in relatively high silica contents, high SiO_2/Al_2O_3 ratios and low concentrations of basic oxides and account for the high ash fusion temperatures of Australian bituminous coal ashes.

2.4.2.3 Phase Diagrams

Phase diagrams are used to determine the effect of ash chemistry on the potential of a fuel to slag and form clinkers. In addition to predicting melting and clinker formation, phase diagrams can be used to predict the composition of the clinkers and possibly obtain an idea of the temperature history to which the clinker was exposed (Magasiner *et al.*, 2000).

The two critical temperatures derived from a phase diagram are the solidus and liquidus temperatures. During the heating of a solid, the solidus (Sh) is the temperature at which the solid will start melting and the liquidus (Lh) is the temperature at which melting is complete. During cooling, the liquidus (Lc) is the temperature at which the first phase will crystallise from the molten melt

and the solidus (Sc) is the temperature when crystallisation is complete (Magasiner *et al.*, 2000).

Thus, phase diagrams can be used to predict the temperature at which the phases will melt during heating (solidus Sh) or the temperature (liquidus Lc) at which phases will start crystallising from a molten mass during cooling. In terms of forming solid clinkers, the liquidus (Lc) temperature is an indication of when the crystals will start crystallising from the melt, initiating clinker formation (Magasiner *et al.*, 2000).

Depending on the number of elemental components, a binary, ternary or quarternary phase diagram is used. Based on the distribution of the components in the ash analysis, a phase diagram is selected and the ash elemental analysis is normalised and plotted. Phase diagram selection is dependant on the dominant elemental components of the ash. Ideally, the components should account for more than 90% of the total elemental composition (Magasiner *et al.*, 2000).

In a ternary phase diagram (**Figure 2.11**), each point of the triangle represents 100% of that component. The liquidus point can be easily defined by the composition of the three ash components selected. The solidus point depends on which of the many compounds present will melt first (Magasiner *et al.*, 2000).

Figure 2.11 shows that an ash with 45% SiO_2, 20% CaO and 35% Al_2O_3 (composition A) will start to melt at 1170 °C, whereas an ash with 45% SiO_2, 19% CaO and 36% Al_2O_3 (composition B) will start melting at 1345 °C. Thus a 1% difference in the Al_2O_3 and CaO content results in 175 °C variation in predicted melting points. Interpreting a complex phase diagram such as the SiO_2-Al_2O_3-CaO diagram requires a good understanding of the principles of phase diagrams and what they represent and hence how to move from composition A or B to the respective solidus temperatures (Magasiner *et al.*, 2000).

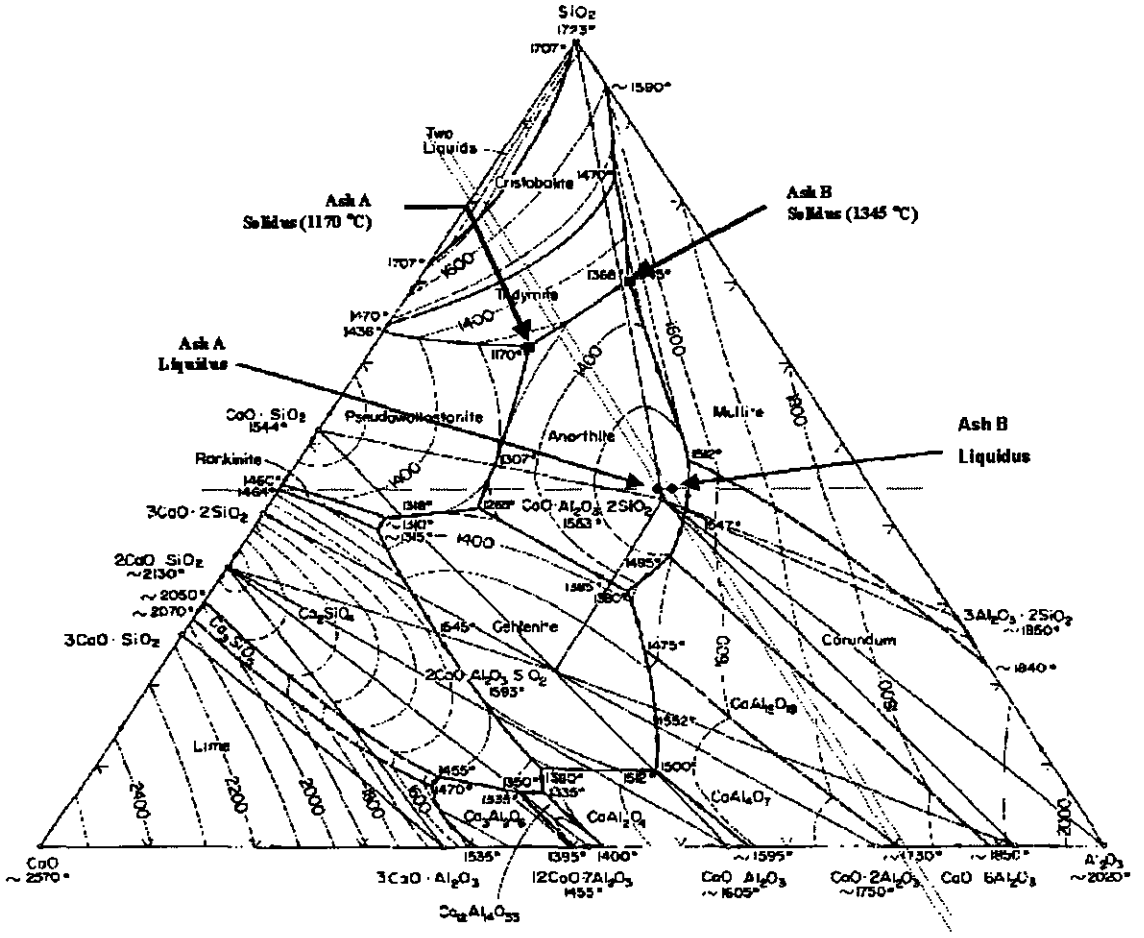

Figure 2.11 SiO_2-Al_2O_3-CaO phase diagram
Circle indicates liquidus temperature (Lh totally molten) and square indicates solidus temperature (Sh start melting) for idealised compositions A and B
(Magasiner *et al.*, 2000)

Creelman *et al.* (2000) concluded that mixed particles of FeO-Al_2O_3-SiO_2, Na_2O-Al_2O_3-SiO_2, and CaO-Al_2O_3-SiO_2 melt at temperatures below the deposit surface temperatures of 1200 to 1350°C and are therefore responsible for slagging in combustion. Most nearly pure minerals will not cause slagging.

2.4.2.4 Mineral ratios (Coal ash indices)

Coal ash based ratios are used to predict the ash deposition and fusion characteristics of coals. There are a number of coal ash indices that have been reported in literature by various authors (DeMaris *et al.*, 1988; Gray, 1987; Winegartner and Rhodes, 1975 and Lolja *et al.*, 2002), expressing the fusibility of the ash as a function of the content of the eight principal oxides frequently found in coal ash.

% Base = $Fe_2O_3 + CaO + MgO + K_2O + Na_2O$

The base oxides are also known as the fluxing agents.

% Acid = $Al_2O_3 + SiO_2 + TiO_2$

The base to acid ratio (B/A) of a coal provides a rough indication of slagging potential because it reflects a potential for ash-containing metals to combine to produce low melting temperature salts. In Northern hemisphere coals, the base to acid ratio is the most frequently used parameter for correlating ash fusibility with its composition.

Base/Acid = $(Fe_2O_3+CaO+MgO+K_2O+Na_2O) / (Al_2O_3+SiO_2+TiO_2)$

Iron Index = Fe_2O_3 / *(Base/Acid ratio)*

Silica is more likely to form lower melting species (silicates) with basic constituents than are other ash properties. The silica factor is calculated as follows:

Silica factor = $SiO_2 / (SiO_2 + Fe_2O_3 + CaO + MgO)$

Dolomite ratio = $(CaO + MgO) / (Fe_2O_3 + CaO + MgO + K_2O + Na_2O)$

Acidity = $(SiO_2 + Al_2O_3) / (Fe_2O_3 + CaO + MgO + Na_2O + K_2O)$

The Attig and Duzy factor is used as a slagging indicator for bituminous ash type fuels and was developed for eastern US coals.

Slagging factor = *(% Base / %Acid) x % dry Sulphur*

Fouling factor = *(% Base / %Acid)* x Na_2O

Acid flux factor = $(SiO_2 + TiO_2 + P_2O_5) / (Al_2O_3 + Fe_2O_3)$

Basic flux factor = $(Na_2O + K_2O) / (CaO + MgO)$

SiO_2*CaO = SiO_2 x CaO

*CaO*MgO* = $CaO \times MgO$

CaO+MgO = $CaO + MgO$

Dolomite ratio squared = $[(CaO + MgO) / (Fe_2O_3+CaO+MgO+K_2O+Na_2O)]^2$

Silica module = $SiO_2 / (Al_2O_3 + Fe_2O_3)$

Alumina module = Al_2O_3 / Fe_2O_3

Hydraulic module = $CaO / (SiO_2 + Al_2O_3 + Fe_2O_3)$

Basic module = $(CaO + MgO) / (SiO_2 + Al_2O_3)$

The indices were mostly developed for Northern hemisphere coals. Juniper (1996) did not agree that the Attig and Duzy slagging factor was applicable to Australian coals, since the slagging factor uses the sulphur content as a surrogate for iron, which is present as pyrite in US coals. Iron is sometimes in the form of pyrite in Australian coals, but more often as siderite, making the use of sulphur in the index inappropriate for Australian coals.

Juniper (1996) found reasonable correlations when using a modified slagging factor as well as a ratio that had previously been proposed for Australian coals.

New Slagging index = $(\%\ Base / \%Acid) \times Fe_2O_3$

New Australian index = $Fe_2O_3 + CaO$

2.5 CORRELATIONS BETWEEN CHEMICAL PROPERTIES AND ASH FUSION TEMPERATURE

Many authors have looked at correlations between chemical properties and ash fusion temperatures. However, better correlations are found with respect to a specific geological region and most indices have been developed using US coals.

Winegartner and Rhodes (1975) used stepwise regression analysis to determine the effect of the chemical constituents of eastern and western US coal ash on their ash fusibility. Looking at the combined eastern and western data, they found that SiO_2, CaO and MgO had high correlations with ash fusion temperature. Na generally showed an effect to reduce AFT. The relationship SiO_2*CaO best predicted oxidising AFT values. For the eastern data alone, CaO had high correlations. The western data alone had poor correlations.

Lolja *et al.* (2002) looked at Albanian coals from 17 operating coal mines located in three geological regions. They found correlations with different indices for the three regions and applying the indices for all mines together, did not produce any significant correlation.

Vassilev *et al.* (1995) studied the relationships between AFT and mineral and chemical composition of coals and coal ashes. They found that coals with low AFT are lower rank with increased concentrations of S, Ca, Mg, Fe, and Na and, respectively, sulphates, carbonates, sulphides, oxides, montmorillonite, and feldspars. While coals with high AFT have an advanced rank and increased contents of Si, Al, and Ti and, respectively, quartz, kaolinite, illite, and rutile, as well as some Fe oxides and siderite. Lower AFT is related to increased proportions of the fluxing sulphate, silicate and oxide minerals and higher AFT is a result of decreased concentrations of the fluxing minerals and increased concentrations of the refractory minerals such as quartz, metakaolinite, mullite and rutile.

2.6 CHAPTER SUMMARY

During Sasol-Lurgi Fixed Bed Dry Bottom coal gasification, the mineral matter in coal undergoes various transformations. Heat induced transformation due to low ash fusion temperatures leads to agglomeration of the ash particles (slagging or fouling) to sizes varying from tiny particles to lumps larger than 100mm. Channel burning and instability in the ash bed can occur as a result.

From the above literature studies, low ash fusion temperatures may be attributed to increased proportions of Ca, Mg, Fe, and Na and low SiO_2/Al_2O_3 ratios.

This study will investigate the significance and interaction of mineral elements with respect to the thermal properties of coal. Ash fusion temperature will be used, amongst others, as a measure of the expected behaviour of the ash bed during gasification. The correlations between mineral elements and ash fusion temperatures will then be examined. Finally, empirical equations to calculate the ash fusion temperatures from the chemical compositions of coal will be determined.

CHAPTER 3

EXPERIMENTAL APPROACH

In this chapter the sample acquisition and preparation are discussed. The samples were analysed by standard coal characterisation methods such as XRD and petrographic analysis, as well as by the latest techniques such as Mössbauer and Computer Controlled Scanning Electron Microscopy (CCSEM). Chemical fractionation tests were also conducted in order to produce coals with different mineral properties which could be used to explain the effect of specific minerals and mineral phases on ash fusion temperature.

The information obtained from the sample characterisation (**Section 3.1**) will be evaluated statistically in order to identify correlations between minerals and ash fusion temperature.

3.1 SAMPLE CHARACTERISATION

The reasons for performing each analysis were provided in **Chapter 2 Sections 2.3 and 2.4**.

3.1.1 Sample acquisition and preparation

Coals from six seams in the Secunda area (Mpumalanga, South Africa) are blended and used for gasification at the Sasol Synthetic Fuels Operation. The coals are screened at 6mm. The -6mm fraction is used at the power station for steam generation and thus not included in this study. The -100+6mm fraction (gasification fraction) is blended and fed to the Sasol-Lurgi fixed bed gasifiers. The feed to gasification is referred to as the SCS (Sasol coal sources) blend.

For the laboratory tests, representative samples of run-of-mine coal from Twistdraai and Middelbult were acquired, as well as the SCS blend to gasification. Twistdraai was selected due to its high vitrinite content, Middelbult for its medium vitrinite content and the SCS blend for being a combination of coals being fed to gasification.

The coals were prepared to the gasification particle size of -100+6.7mm then density separated by Coal and Mineral Technologies laboratory according to standard ISO method 7936. Relative densities ranging from 1.4g/cm^3 to 2.2g/cm^3 in increments of 0.05 were used. The gasification fraction was used in order to simulate gasifier conditions.

3.2 Sample analysis and characterisation

The original coal, as well as the density separated fractions, were comprehensively characterised according to standard coal characterisation methods. The coals were crushed and prepared as required by each method. The quarter-and-cone method was used to split and homogenise the samples.

3.2.1 Ash fusion temperature

The Coal and Mineral Technologies laboratory used standard ISO method 1171 to ash the coal. The standard ISO method 540 was then followed to demonstrate the fusion properties of the laboratory prepared coal ash. Ash melting properties were determined under oxidising conditions to 1600°C. The temperatures recorded were initial deformation temperature (DT), softening temperature (ST), hemisphere temperature (HT) and flow temperature (FT).

3.2.2 Proximate analysis

The proximate analysis was conducted by the Coal and Mineral Technologies laboratory and used standard methods to measure the percentage of moisture (SABS 924), ash content (ISO 1171), volatile matter (ISO 562) and fixed carbon by difference.

3.2.3 Ultimate analysis

The Coal and Mineral Technologies laboratory determined the carbon, hydrogen, and nitrogen content using ASTM D5373. Total sulphur was determined using ASTM D4239 and oxygen was calculated by difference.

3.2.4 Ash composition

Coal and Mineral Technologies laboratory conducted ASTM D3682 to express the ash composition in terms of its oxides of Si, Al, Fe, Ti, P, Ca, Mg, Na, K, and S.

3.2.5 X-ray diffraction (XRD)

The density fractions were analysed at the Council for Geoscience Laboratory with a Siemens D500 X-ray goniometer equipped with Cu tube, variable slit and secondary graphite monochromator to determine the mineral composition.

3.2.6 Fischer assay

The Fischer Assay, according to SABS 1073, determined the char, liquid hydrocarbon, water and gas (by difference).

3.2.7 Petrographic analyses

The coals were assessed in terms of their petrographic properties by the Coal and Mineral Technologies laboratory.

Analyses were conducted on four composites and the sink for each coal source. The composites comprised 1.40-1.55, 1.60-1.75, 1.80-1.95 and 2.00-2.20 density fractions. A petrographic block of each sample was prepared in accordance with the ISO Standard 7404-2, 1985 and then examined under the microscope.

3.2.7.1 Maceral analysis

The maceral analysis, ISO 7404-3, 1994, is obtained by the microscopic examination of coal and is a volumetric distribution of macerals in a coal sample.

3.2.7.2 Microlithotype analysis

Microlithotype, carbominerite and minerite analyses, to determine the organic/inorganic associations, were carried out in accordance with ISO method 7404-4, 1988.

3.2.7.3 Mineral group analysis

A mineral group analysis was carried out on each sample following the method used by Falcon Research and Consulting Services.

3.2.7.4 Rank

The rank of the coal is determined by means of reflectance analysis of the vitrinite macerals in the sample, according to ISO method 7404-5.

3.2.7.5 Weathering (general condition)

For the general condition, the constituents are quantified on the basis of a 500 point-count per sample according to the method set out in the ISO standard 7404-3.

3.2.8 CCSEM analysis

CCSEM analysis was conducted on composites (prepared as discussed in **Section 3.2.7**) of the density separated samples, according to the method developed by Van Alphen Consultancy. In order to accommodate the coarse size of the coal samples, the method was modified by milling the samples to 100% passing 1mm, a low magnification setting of 40X and particles that touched the frame boundary were included in the analysis.

The principal requirement of this investigation is to establish the association characteristics of mineral matter with coal.

3.2.9 Mössbauer analysis

All Mössbauer spectra were obtained with the aid of a Halder Mössbauer spectrometer, capable of operating in conventional constant acceleration mode using a proportional counter filled with Xe-gas to 2 atm. The samples were placed between Perspex plates and then irradiated with γ-rays from a 50 mCi ^{57}Co(Rh) radioactive source to obtain a room temperature Mössbauer spectrum. The data was collected in a multi-channel analyser (MCA) to obtain a spectrum of count rate against source velocity. A least-squares fitting program was used and by superimposing Lorentzian line shapes, the isomer shifts, quadrupole splitting and/or hyperfine magnetic field of each constituent

was determined with reference to the centroid of the spectrum of a standard α-iron foil at room temperature. The amount of each constituent present, was determined from the areas under the relevant peaks.

3.3 Chemical fractionation tests

Chemical fractionation tests were conducted on specific fractions of the density separated SCS blend coal in order to provide further information on the significance and interaction of mineral elements with respect to the thermal properties of coal. The experimental procedure, obtained from Baxter (2002) and adjusted to fit Sasol's needs, uses selective extraction of elements, based on solubility, which reflects their association in the coal.

3.3.1 Leaching

The leaching agents used were de-ionised water, 1M ammonium acetate (NH_4OAc), 1M hydrochloric acid (HCl), and 1M nitric acid (HNO_3). Each coal sample was crushed to <150μm in order to be completely permeated by the leaching agents. Samples were then homogenised by the quarter-and-coning technique before representative sub-samples are taken from the original sample. A coal sample of ±20g (dry basis) was taken from the original prepared coal sample. This sample was sealed for analyses as the reference and labeled *original*.

3.3.1.1 H_2O leaching

One 20g sample and 60 ml of de-ionised H_2O was used. The mixture was stirred for 24 hours at room temperature. After mixing, it was filtered and rinsed with 100ml distilled H_2O. The weights of the total sample before and after water washing were noted. From this information and the initial dry weight of the sample (taking into account the total moisture of the sample), the change in the dry weight induced by water washing can be calculated. The coal, leaching agent and wash water were each labeled *After H_2O* and set aside for further analyses.

3.3.1.2 NH_4OAc leaching

One 20g sample and 60 ml of NH_4OAc was used. The mixture was stirred for 24 hours at room temperature. After mixing, it was filtered and rinsed with 100ml distilled H_2O. The weights of the total sample before and after water washing were noted. From this information and the initial dry weight of the sample (taking into account the total moisture of the sample), the change in the dry weight induced by water washing can be calculated. The effect of the rinsing step with distilled H_2O is not evaluated again, as this will have a similar effect as an H_2O wash. The coal, leaching agent and wash water were each labeled *After NH_4OAc* and set aside for further analyses.

3.3.1.3 HCl leaching

One 20g sample and 60 ml of HCl was used. The mixture was stirred for 24 hours at room temperature. After mixing, it was filtered and rinsed with 100ml distilled H_2O. The weights of the total sample before and after water washing were noted. From this information and the initial dry weight of the sample (taking into account the total moisture of the sample), the change in the dry weight induced by water washing can be calculated. The coal, leaching agent and wash water were each labeled *After HCl* and set aside for further analyses.

3.3.1.4 HNO_3 leaching

One 20g sample and 60 ml of HNO_3 was used. The mixture was stirred for 24 hours at room temperature. After mixing, it was filtered and rinsed with 100ml distilled H_2O. The weights of the total sample before and after water washing were noted. From this information and the initial dry weight of the sample (taking into account the total moisture of the sample), the change in the dry weight induced by water washing can be calculated. The coal, leaching agent and wash water were each labeled *After HNO_3* and set aside for further analyses.

3.3.2 Ash chemistry and analyses

The five coal samples labeled *Original*, *After H_2O*, *After NH_4OAc*, *After HCl* and *After HNO_3* were submitted for ash composition and ash fusion

temperature (oxidising to 1600°C) analyses. The leaching agents and wash water were submitted for an ICP (inductively coupled plasma) analysis to determine the elemental composition.

3.4 STATISTICAL EVALUATION

Two statistical software packages were employed to analyse the analytical data obtained.

3.4.1 Calculation of correlation coefficients

The correlation coefficients between two data sets (ash elements and ash fusion temperatures) were calculated using the Data Analysis Tool Pack in Microsoft Excel. More detail was provided in **Chapter 2 Section 2.3.3.1**.

3.4.2 Development of a model to predict ash fusion temperature

The Design Expert (version 6) package was utilised to derive empirical equations to calculate ash fusion temperatures from chemical compositions of coal. More detail was provided in **Chapter 2 Section 2.3.3.2**.

CHAPTER 4

RESULTS AND DISCUSSION: COAL CHARACTERISATION

Representative samples of run-of-mine coal from three sources were acquired: Twistdraai, Middelbult and the SCS blend to gasification. The samples were analysed by standard characterisation methods such as XRD and petrographic analysis, as well as by the latest techniques such as Mössbauer and Computer Controlled Scanning Electron Microscopy (CCSEM).

This chapter presents the results obtained from the sample characterisation of the Twistdraai, Middelbult and SCS blend coal.

The statistical evaluation of the results will be discussed in **Chapter 6**.

4.1 DENSITY SEPARATION

The -100+6.7mm fraction of the coals were density separated using relative densities (RD) ranging from 1.4g/cm^3 to 2.2g/cm^3 in increments of 0.05 (**Appendix Table 4.1**).

The mass % distribution of all three coals are higher for the low relative densities, with a cumulative mass of 49% from 1.40-1.55 g/cm^3 for Middelbult (**Figure 4.1**), 61% for Twistdraai (**Figure 4.2**) and 50 % for SCS (**Figure 4.3**). The maceral analysis in **Section 4.2.7.1** shows higher concentrations of vitrinite with a very low density, hence the higher mass distribution at lower densities. The different values of 49% for Middelbult and 61% for Twistdraai is to be expected since, as mentioned in **Chapter 3 Section 3.1.1**, Middelbult is a low vitrinite coal and Twistdraai is a high vitrinite coal. SCS falls within the range since it's a blend of coals.

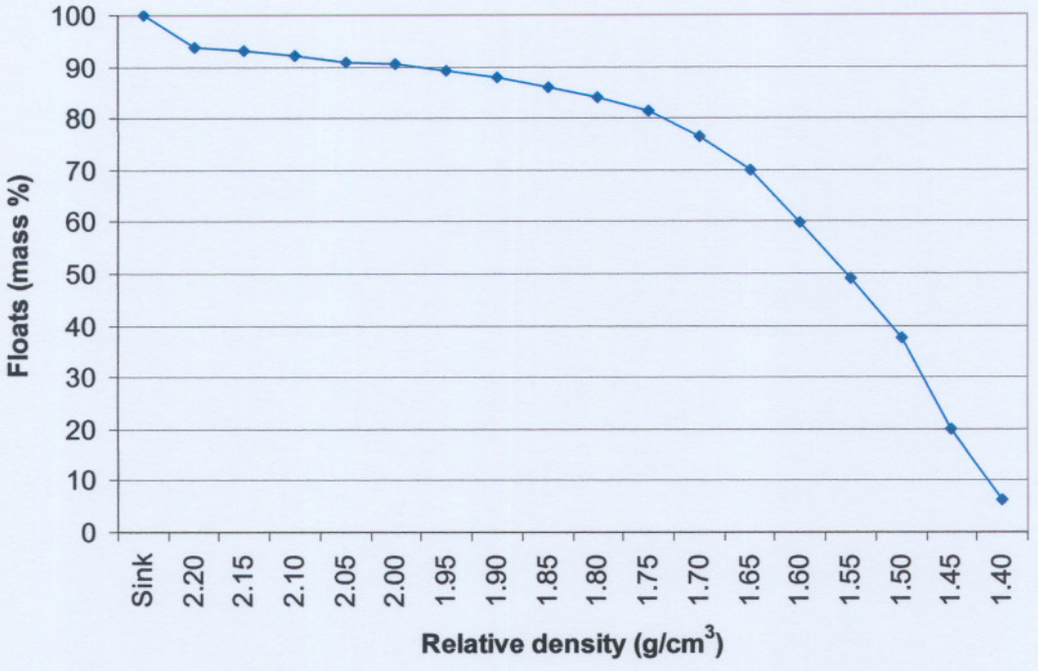

Figure 4.1 Densimetric curve for Middelbult coal

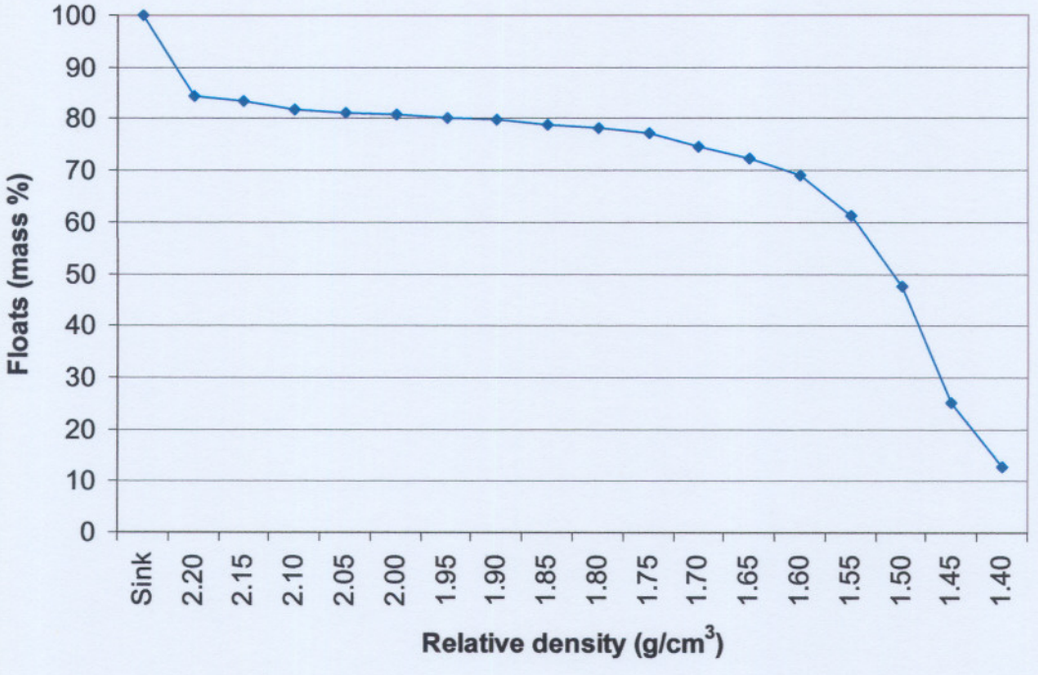

Figure 4.2 Densimetric curve for Twistdraai coal

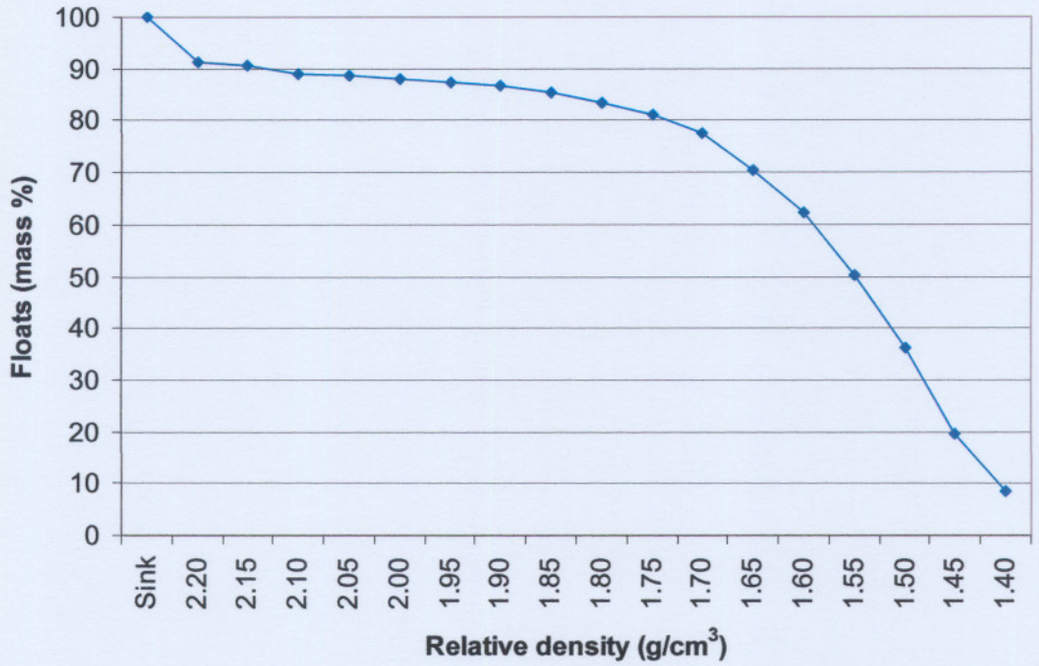

Figure 4.3 Densimetric curve for SCS coal

4.2 SAMPLE ANALYSIS AND CHARACTERISATION

The original coal, as well as the density separated fractions, were comprehensively characterised according to standard coal characterisation methods, as discussed in **Chapter 3**.

4.2.1 Ash fusion temperature

Ash fusion temperature (under oxidising conditions to 1600°C) was determined to serve as a measure of the expected behaviour of the ash in coal during gasification (**Appendix Table 4.2**). Middelbult (**Figure 4.4**) and the SCS blend (**Figure 4.6**) showed a trend of increasing AFT's at lower densities and then decreasing at higher densities. The results for Twistdraai (**Figure 4.5**) fluctuated and did not indicate any trend from low to high densities. The Middelbult and SCS blend sinks had high AFT's whereas Twistdraai's sink had low AFT's. These trends will be discussed further in terms of ash composition in **Section 4.2.4**.

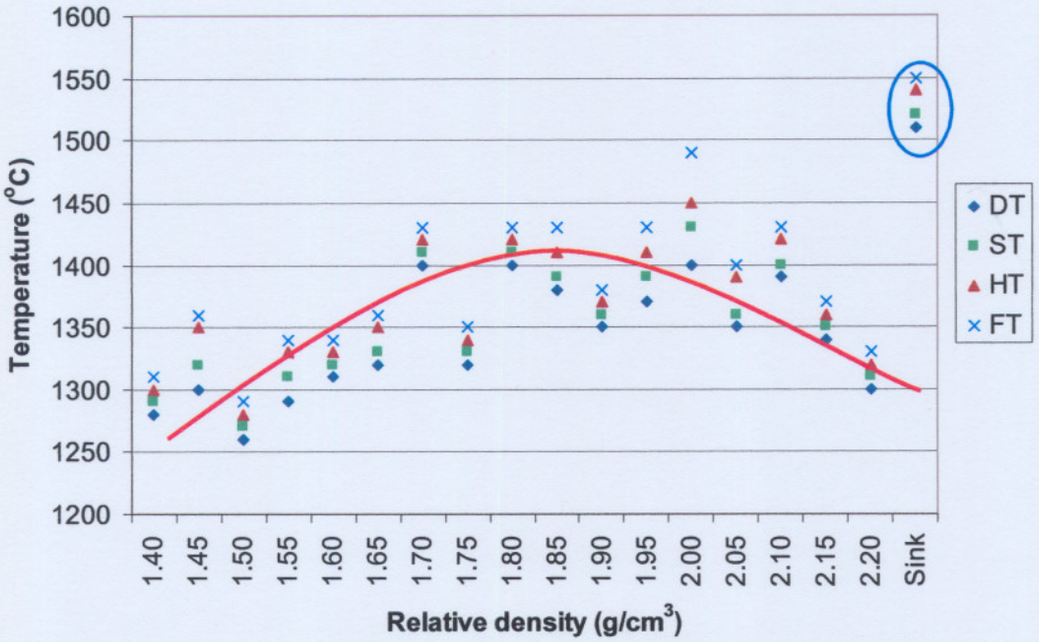

Figure 4.4 AFT's of density separated Middelbult coal

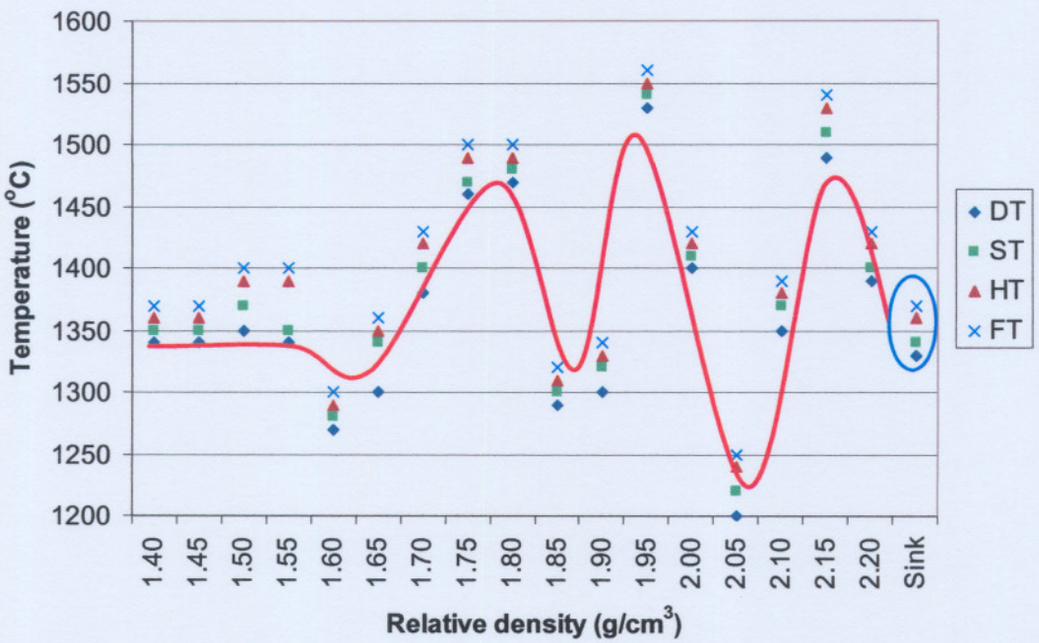

Figure 4.5 AFT's of density separated Twistdraai coal

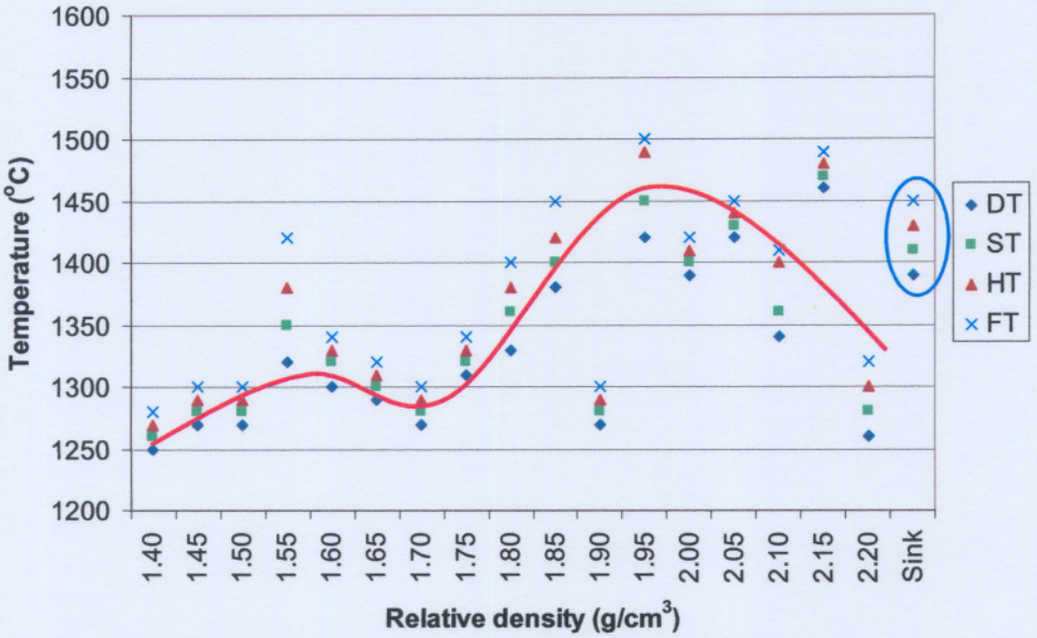

Figure 4.6 AFT's of density separated SCS coal

4.2.2 Proximate analysis and Fischer assay

The proximate analyses (**Appendix Table 4.3**) on the three coals showed a similar decrease in fixed carbon and increase in ash content when moving towards higher densities (**Figures 4.7, 4.8** and **4.9**). The sinks have the highest ash content with little fixed carbon and moisture.

According to the Fischer assay (**Appendix Table 4.4**), the char % (which includes mineral and ash) increased with increasing densities (**Figures 4.10, 4.11** and **4.12**). This indicates that although the density separation was performed on lump coal, the separation of organic and inorganic material did still occur, with the main proportion of minerals present at higher densities.

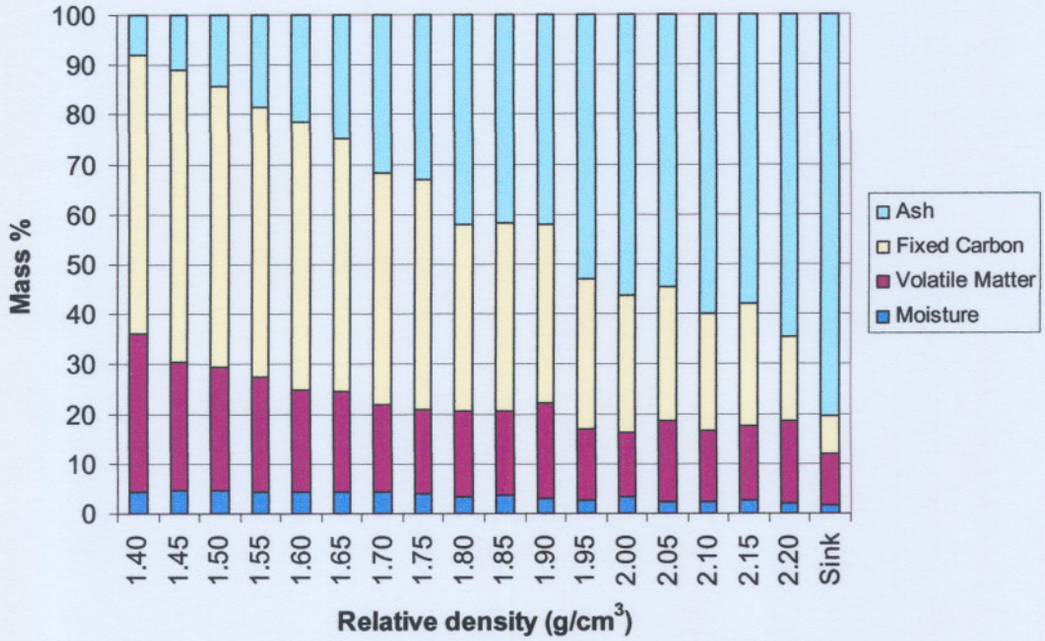

Figure 4.7 Proximate analysis on density separated Middelbult coal

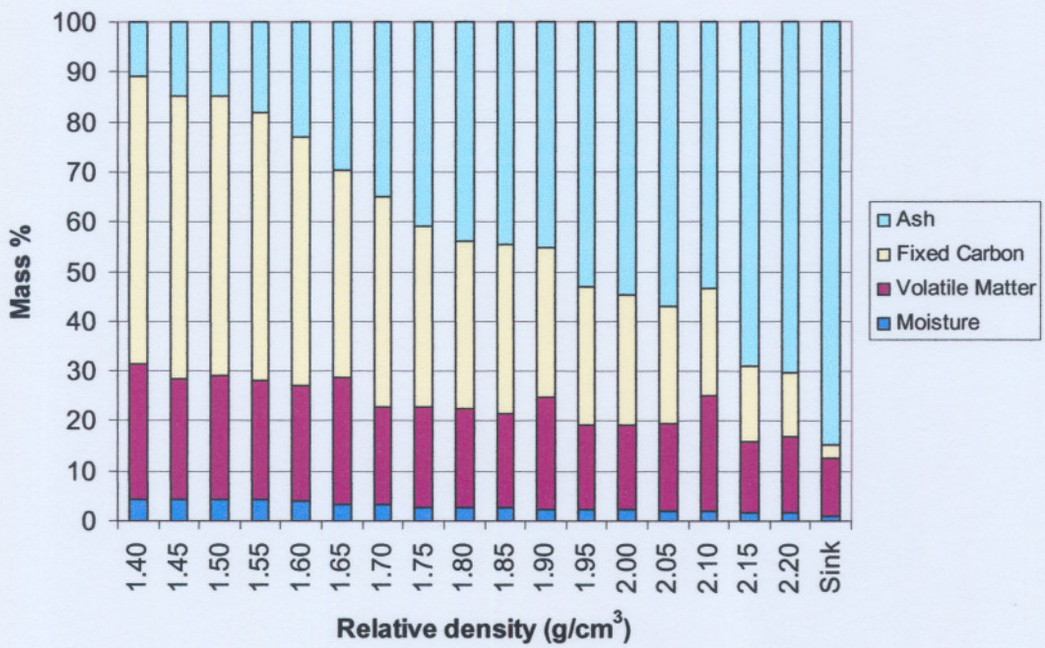

Figure 4.8 Proximate analysis on density separated Twistdraai coal

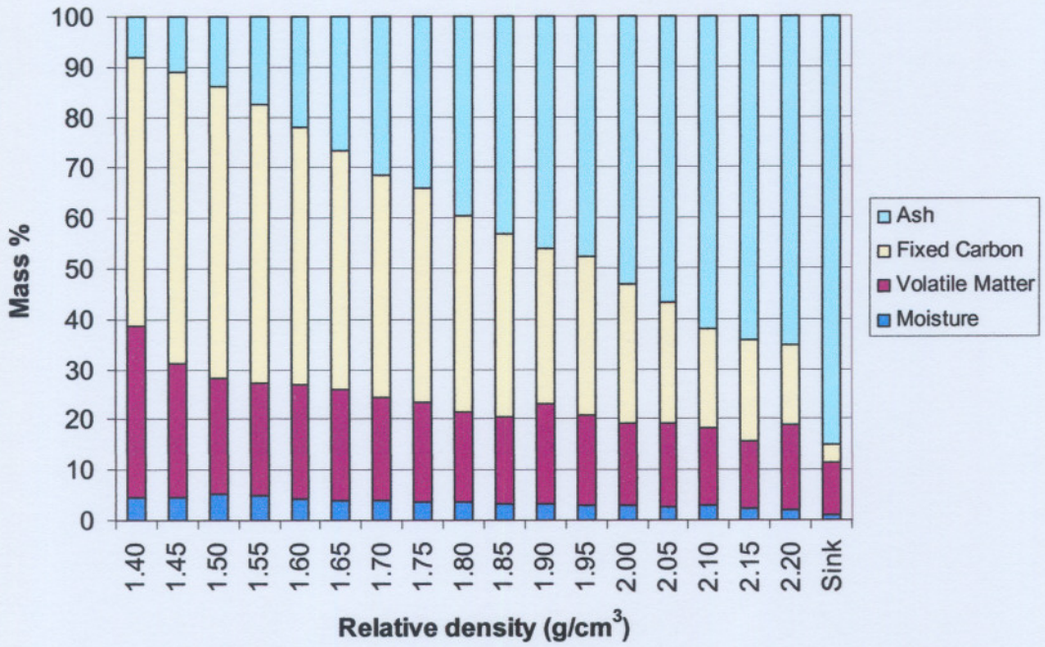

Figure 4.9 Proximate analysis on density separated SCS coal

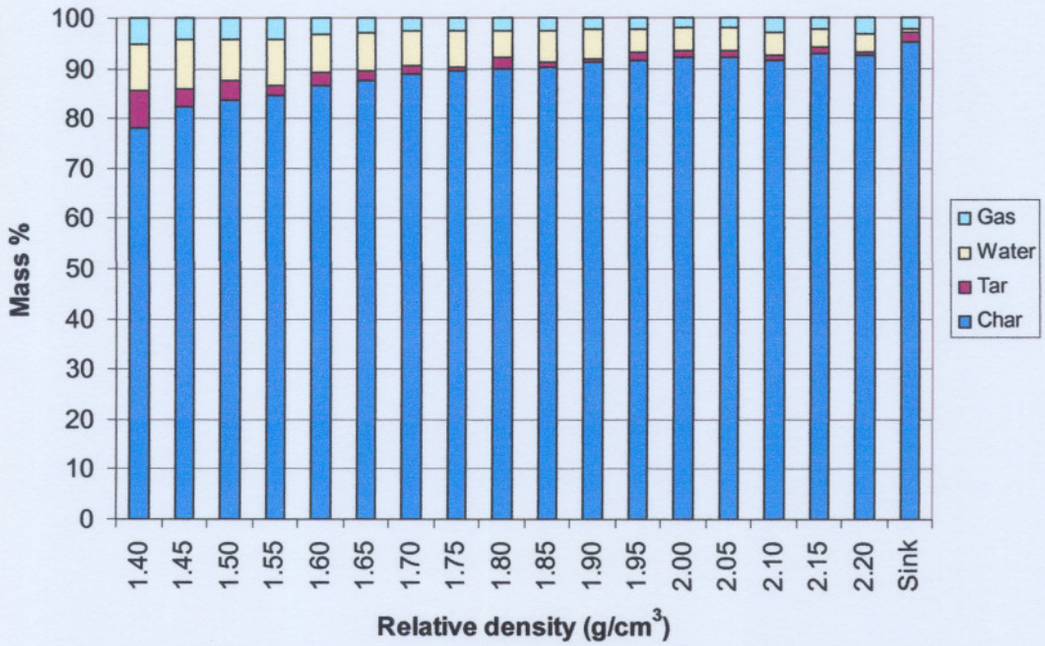

Figure 4.10 Fischer assays on density separated Middelbult coal

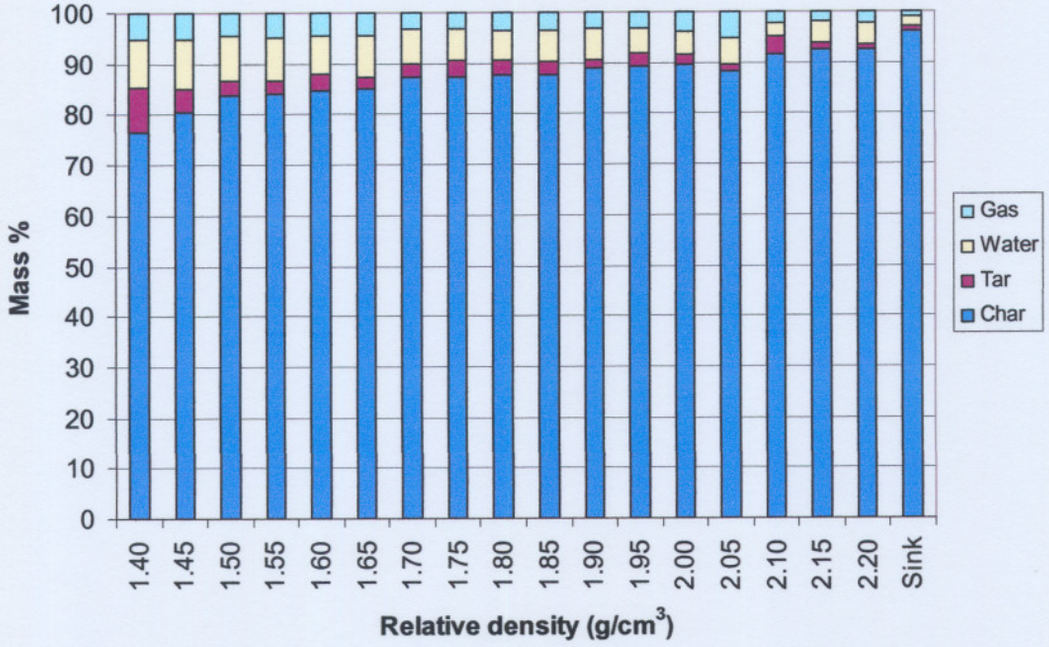

Figure 4.11 Fischer assays on density separated Twistdraai coal

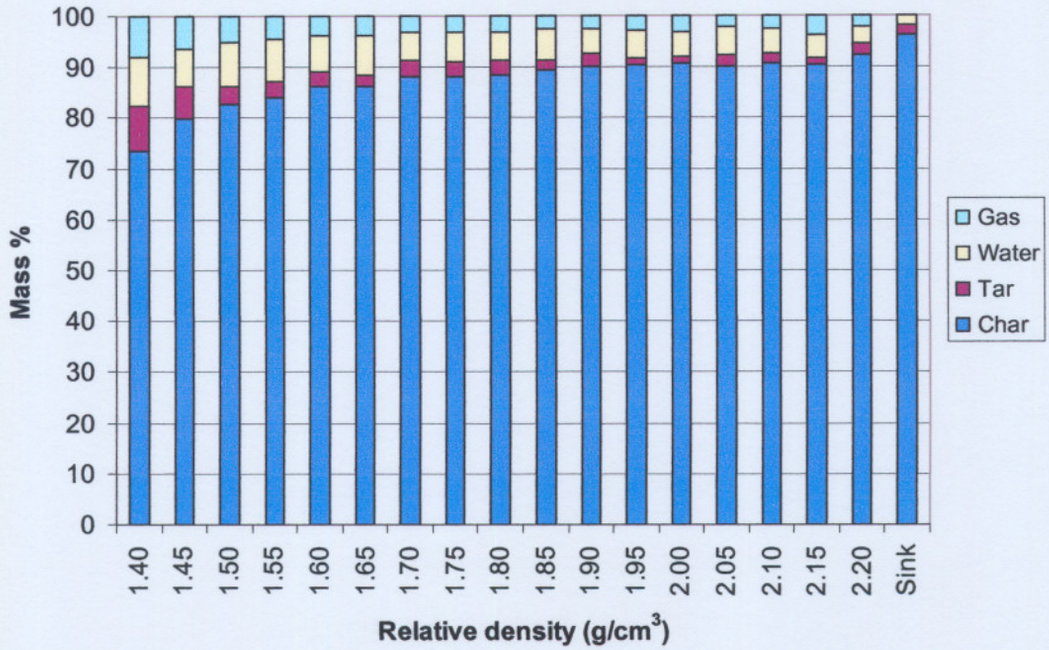

Figure 4.12 Fischer assays on density separated SCS coal

4.2.3 Ultimate analysis

The ultimate analysis (**Appendix Table 4.5**) shows that the carbon content of the coal fractions decreased with increasing density (**Figure 4.13, 4.14** and **4.15**). This is in keeping with the observation from the density separation

(**Section 4.1**) that showed the predominant concentration of the organic matter in the lower densities.

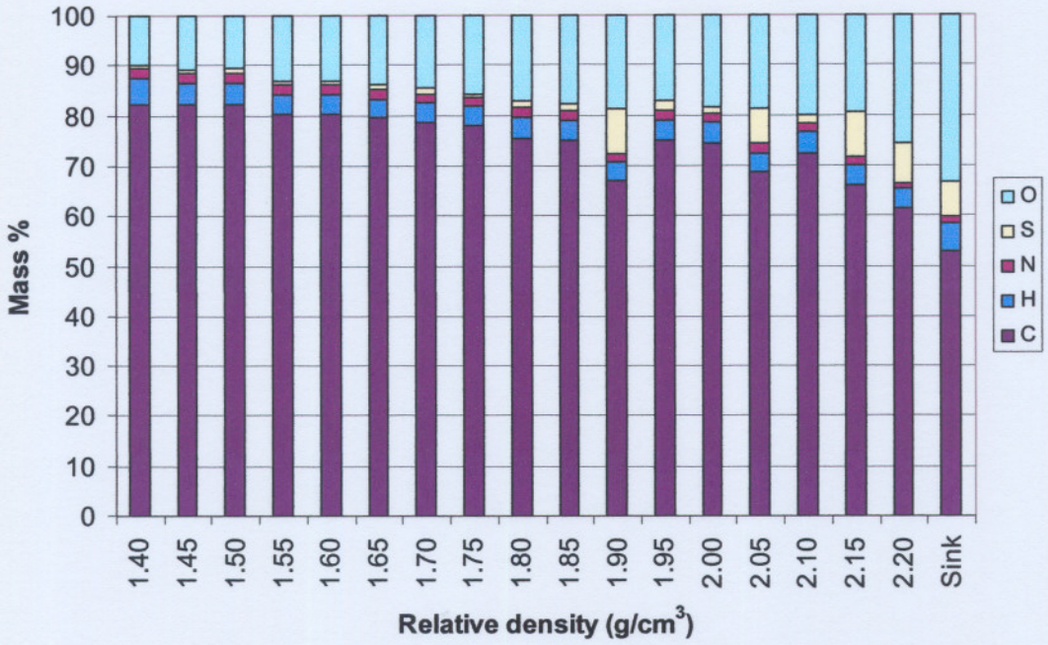

Figure 4.13 Ultimate analysis on density separated Middelbult coal

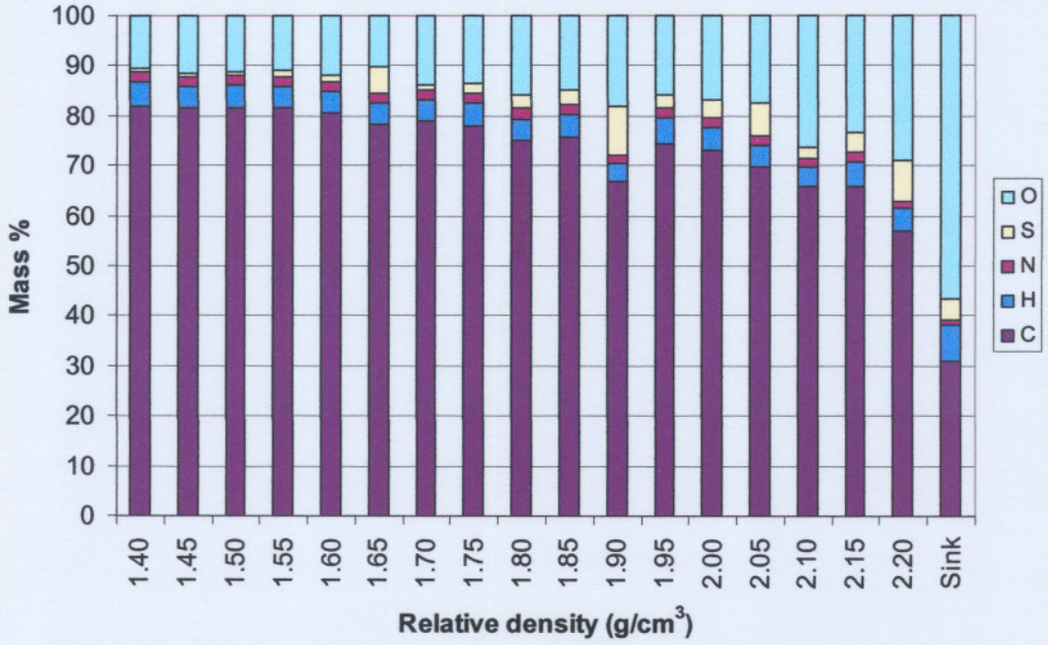

Figure 4.14 Ultimate analysis on density separated Twistdraai coal

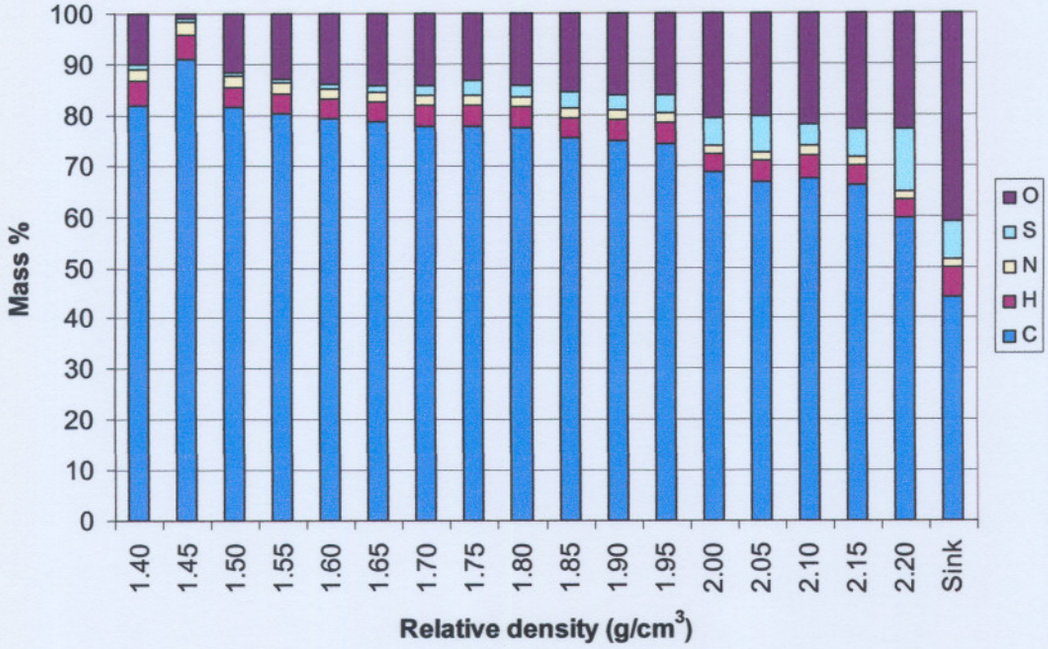

Figure 4.15 Ultimate analysis on density separated SCS coal

4.2.4 Ash composition

In **Chapter 2 Section 2.4.2.2**, it was mentioned from the literature, that the principal factors associated with coal ash melting were the SiO_2/Al_2O_3 ratio and basic oxide levels. The ash compositions of Middelbult (**Appendix Table 4.6**), Twistdraai (**Appendix Table 4.7**) and the SCS blend (**Appendix Table 4.8**) were determined.

The basic oxide distribution in Middelbult (**Figure 4.16**) shows an interesting trend that explains why the ash fusion temperature (**Figure 4.4**) first increases and then decreases over the density range investigated. The lower density fractions show high concentrations of CaO and MgO together with low concentrations of Fe_2O_3. The combined concentration of fluxing agents decreases as the densities increase, hence the AFT increases. But from RD 1.90 onwards, the Fe_2O_3 together with the CaO and MgO concentrations increase and this would once again push down the AFT. Therefore, it is the presence and interaction of a combination of minerals that results in lower ash fusion temperatures. A similar explanation will apply for SCS (**Figure 4.18**).

An interesting point to note is the significantly higher proportion of Fe present in the 1.90 RD samples of Middelbult and Twistdraai (**Figure 4.17**). Petrographic analysis sheds more light on this observation in **Section 4.2.6.3**.

Determination of the SiO_2/Al_2O_3 ratios explains why the Middelbult and SCS sinks have high AFT's whereas the Twistdraai sink has a low AFT (**Figure 4.4**). Middelbult and SCS are 2.85 and 2.84 respectively and Twistdraai is 1.79. The higher SiO_2/Al_2O_3 ratios of Middelbult and SCS also indicate that the sinks comprise predominantly of clays and quartz.

Chapter 6 will examine the correlation of the ash oxides to the AFT further.

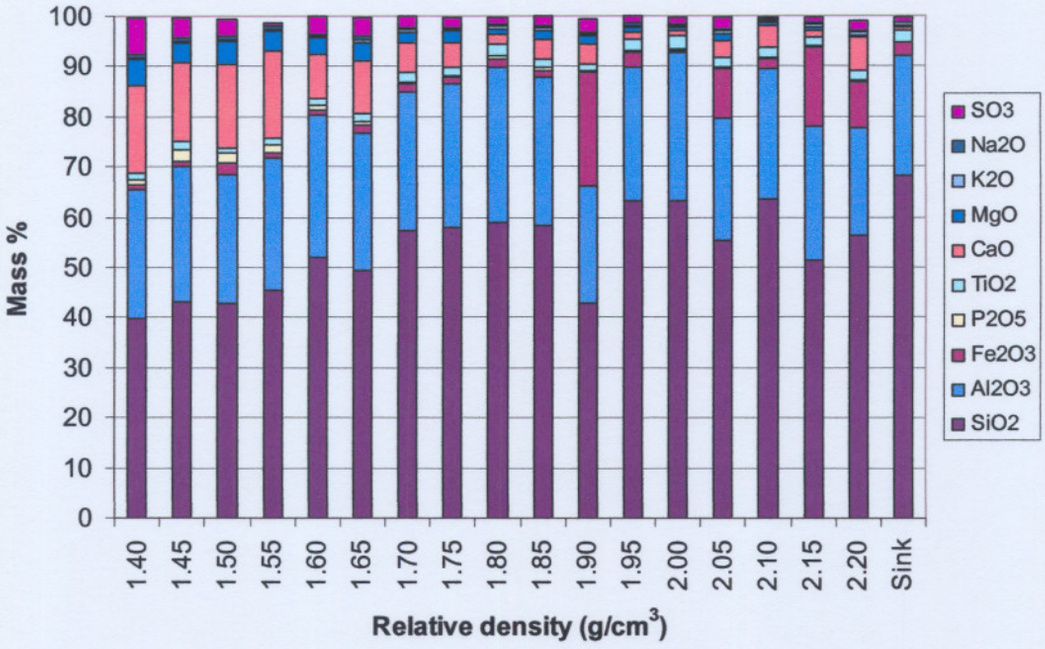

Figure 4.16 Ash composition of density separated Middelbult coal

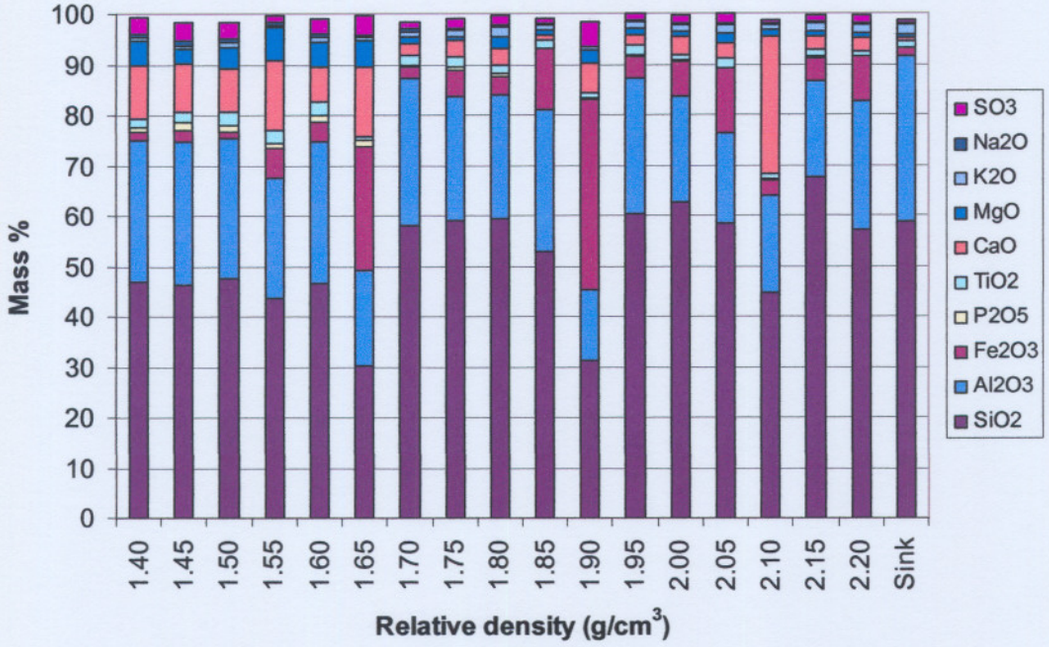

Figure 4.17 Ash composition of density separated Twistdraai coal

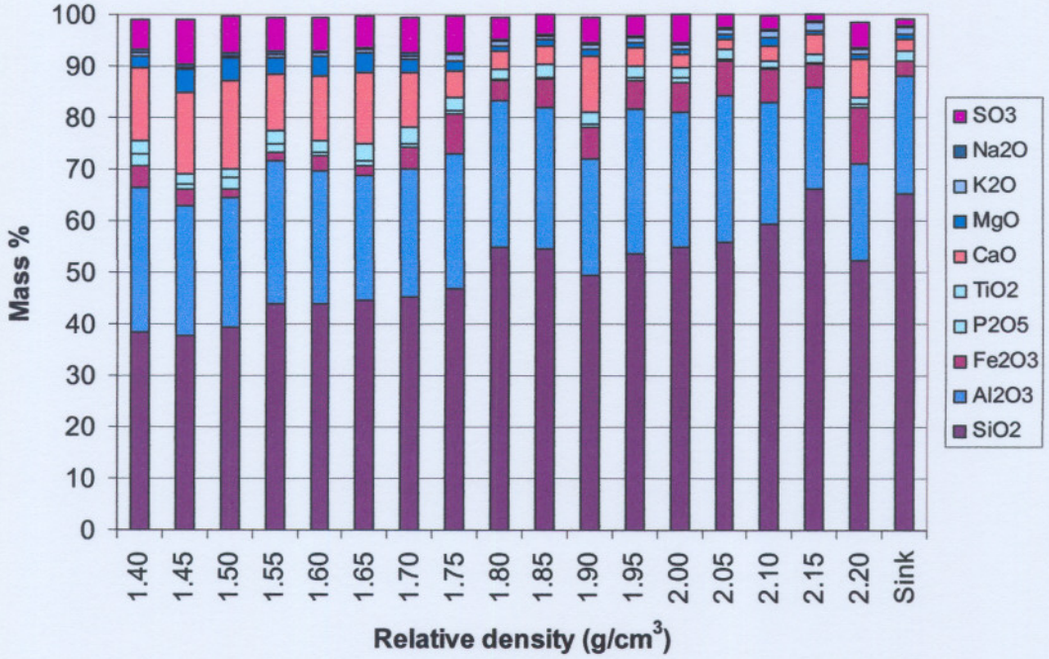

Figure 4.18 Ash composition of density separated SCS coal

4.2.5 X-ray diffraction (XRD) and Mössbauer

The distributions of minerals in the coals, as determined by X-ray diffraction (XRD), are given in **Appendix Tables 4.9, 4.10** and **4.11**.

Ca and Mg-bearing minerals such as calcite, dolomite, aragonite and smectite were identified. Iron minerals such as pyrite and siderite were also found. The Mössbauer results (**Appendix Figures 4.19-4.33**) identified pyrite as the abundant Fe-containing mineral in the Middelbult and SCS sink fractions (**Appendix Table 4.12**). The presence of silica and the clays; illite and montmorrillonite were also noted. This was consistent with the observation in **Section 4.2.4** regarding the higher SiO_2/Al_2O_3 ratios in the Middelbult and SCS sinks.

4.2.6 Petrographic analyses

The major petrographic properties of the coals are presented in **Appendix Tables 4.13, 4.14 and 4.15**. The characteristics of the coals are summarised below.

4.2.6.1 Maceral analysis (proportions of organic components)

The maceral analyses on a mineral matter-free basis (**Appendix Table 4.13**) revealed that the coals were all inertinite-rich, with higher total inertinite contents occurring in the higher relative density fractions in each of the three coal sources.

The total vitrinite and reactive maceral contents of the Twistdraai set of samples showed relatively less variation from the RD 1.40-1.55 sample to the 2.00-2.20 sample (percentages by volume, mineral matter-free basis); the variation was more marked in the case of the SCS blend set, but most marked in the Middelbult set, which reported 29% of vitrinite at 1.40-1.55 decreasing rapidly to around 5% in the other four samples in this set. The observation in **Section 4.1** about 49% of the sample reporting to the 1.40-1.55 density fractions can be explained by the higher concentration of vitrinite with a very low density.

In all fifteen samples, the liptinites, mainly sporinite with some cutinite, occurred in low quantities (1 to 5%, mineral matter-free basis). Alginite was seen only very occasionally.

As expected, visible mineral concentrations increased dramatically with increase in relative density.

4.2.6.2 Microlithotype analysis (organic/inorganic associations)

"Pure" vitrinite (vitrite) (**Appendix Table 4.14**) reported approximately 10% of the whole coal in the 1.40-1.55 sample in each set, reducing to <5% in the corresponding 2.00-2.20 sample.

"Pure" inertinite (inertite) (**Appendix Table 4.14**) reported approximately 40 to 50% of the whole coal in the 1.40-1.55 samples, reducing to 10 to 20% in the 2.00-2.20 samples.

Intermediate microlithotypes i.e. maceral/maceral associations (bi- and tri-macerite) (**Appendix Table 4.14**) reported approximately 30 to 40% in the 1.40-1.55 samples, reducing to around 10% or less in the 2.00-2.20 samples.

The visible minerals (**Appendix Table 4.14**) were found to be both finely dispersed and intimately associated with the coal macerals in carbominerite and occurring in mineral-rich particles, i.e., minerite.

Carbominerite analysis

Finely dispersed clay/maceral associations (as carbargilite) reached the highest concentrations in the 1.80-1.95 sample in each set (22 to 29%). Quartz/maceral associations (as carbosilicite) concentrated more noticeably in the 1.80-1.95 and 2.00-2.20 samples. Finely dispersed grains of syngenetic pyrite closely associated with organic matter (as carbopyrite) reported up to

2% across the suite of fifteen samples. Carbonate/maceral mixtures (as carbankerite) were relatively rather more common in the 1.60-1.75 samples in each of the three sets (5 to 6%).

Minerite analysis

Mineral-rich particles occurred in progressively increasing proportions with increasing relative density, as could be expected; clays and quartz group minerals together became more markedly predominant with increase in relative density.

4.2.6.3 Mineral group analysis

Particles in which clays and quartz represented less than 25% by volume (**Appendix Table 4.13**) tended to concentrate in the 1.60-1.75 samples in each set (26% in the Twistdraai set, and 38 and 34% in the Middelbult and SCS blend sets). Particles in which clays and quartz accounted for 25 to 50% concentrated in the 1.80-1.95 and the 2.00-2.20 samples. Particles composed of >50% of these minerals reported the highest concentrations in the sink fractions, as could be expected.

Finely dispersed syngenetic pyrite accounting for <25% of the particles (**Appendix Table 4.13**) occurred a little more noticeably in the Twistdraai and SCS blend samples than in the Middelbult samples. Relatively more massive replacement forms of pyrite tended to occur rather more noticeably in the 1.80-1.95 samples of Middelbult and Twistdraai. This is compatible with the earlier observation of a significantly higher proportion of Fe present in the 1.90 RD samples of Middelbult and Twistdraai.

Finely dispersed syngenetic carbonates (mainly siderite) accounting for <25% of the particles (**Appendix Table 4.13**) presented rather more significantly in the 1.40-1.55 and 1.60-1.75 composites. Overall, total carbonate/organic matter mixtures appeared to be most common in the 1.60-1.75 samples.

Particles which were clean from inorganic matter (clean coal) (**Appendix Table 4.13**) represented around 60% of the whole coal in the 1.40 - 1.55

Twistdraai and SCS blend composites, and around 70% in the corresponding Middelbult sample.

4.2.6.4 Rank

Reflectance measurements were conventionally taken on the vitrinite sub-maceral, Collotelinite (**Appendix Table 4.15**). These samples are recognised as ortho-bituminous (Medium rank C) coals. The mean random reflectance values fell within quite a narrow range of between 0.60 and 0.71%.

4.2.6.5 Weathering (general condition)

The particles in these samples often displayed some form of cracking (**Appendix Table 4.15**). However, at least some cracks probably developed during handling and preparation, due to the brittle nature of the organic constituents (particularly vitrinites) at this level of rank. Signs of severe weathering or pronounced thermal effects were only very occasionally observed. The pyrite present had retained its "fresh" bright yellow colour and no oxidised forms were seen.

4.2.7 CCSEM analysis

CCSEM analysis was conducted on composites of the density separated samples, according to the method developed by Van Alphen Consultancy. Mineral variations across the size fractions are summarised in **Appendix Table 4.16**.

4.2.7.1 Twistdraai

Twistdraai is characterised by large extraneous pyrite, calcite, quartz, sandstone and mudstone rock fragments (**Figure 4.34**).

Pyrite is present in cleats in coal, attached to extraneous quartz grains, fine included pyrite in coal and attached to extraneous calcite particles. The large extraneous calcite and probably pyrite particles common in Twistdraai are derived from liberation of calcite and pyrite which occur in large cleats transecting coal seam (**Figure 4.35**).

Kaolinite commonly occurs as fine included grains in coal ranging in size from sub-micron to as coarse as 50 µm. Kaolinite is also a common constituent of the mudstone and sandstone rock fragments (**Figure 4.34**). Quartz in the sandstone rock fragments range in size form 45 to 150 µm (**Figure 4.36**). Quartz has similar association characteristics as kaolinite with the exception that there are a larger proportion of quartz associated with extraneous quartz particles and rock fragments. Due to the size of these quartz grains it is surmised that they are fragments of coarse grained sandstone.

Orthoclase is commonly associated with the sandstone rock fragments or occurs as included grains commonly associated with quartz and kaolinite. Dolomite predominately occurs in cleats in coal fragments (**Figure 4.36**).

The occurrence of rock fragments and extraneous large particles in Twistdraai, will account for the higher total ash content (31 %) and the high mass proportion in the >2.2 sink fraction (15.6 %).

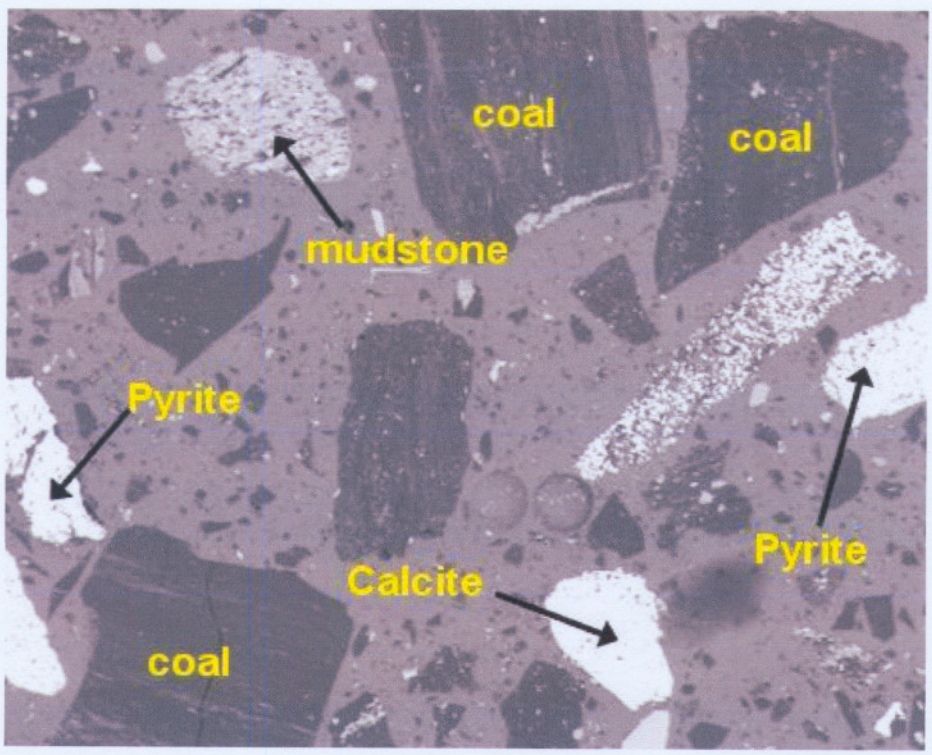

Figure 4.34 Layered coal, extraneous calcite and pyrite, mudstone and fine included pyrite – Twistdraai (width of image is 2.7mm)

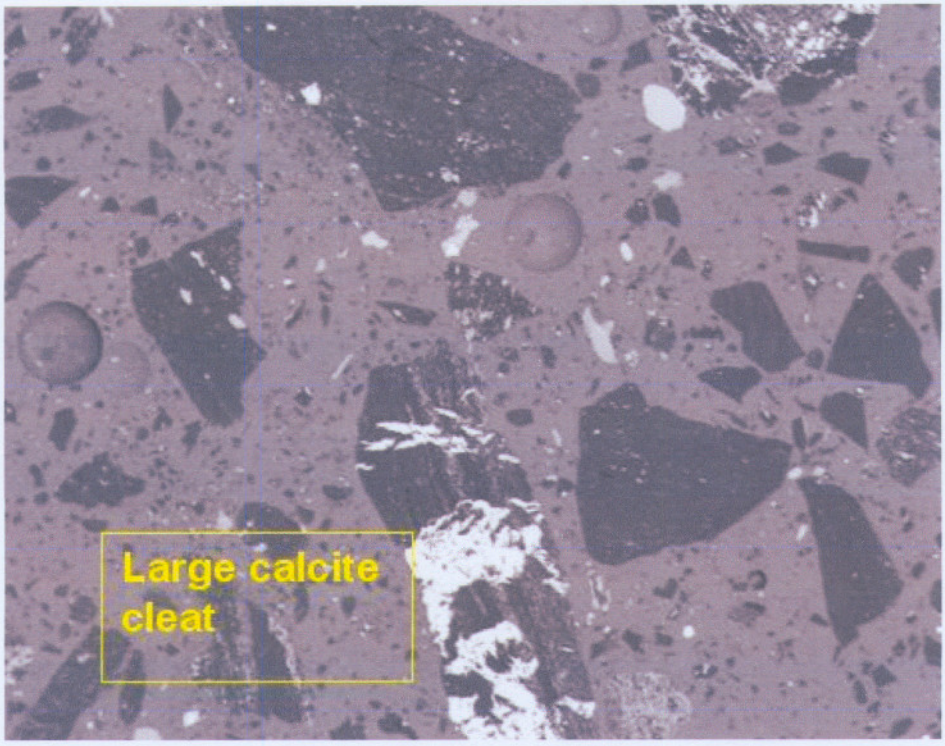

Figure 4.35 Calcite-rich cleat (381 µm long) transecting coal. Probable source of large extraneous calcite fragments – Twistdraai (Width of image is 2.7 mm)

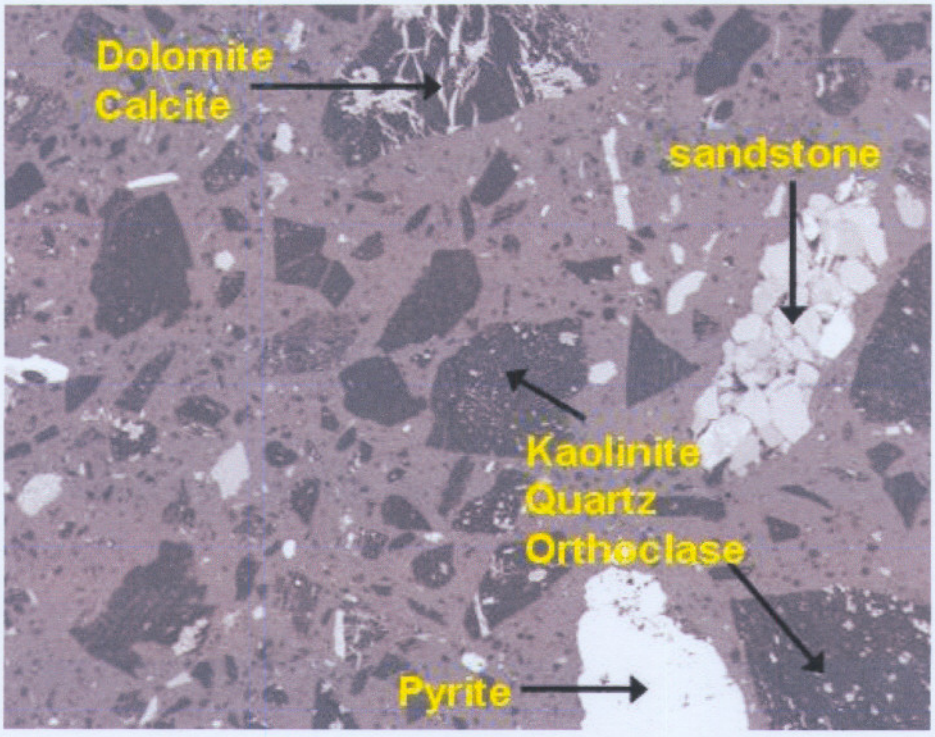

Figure 4.36 Fine-grained sandstone, large extraneous pyrite, dolomite and calcite cleats and included kaolinite/quartz/orthoclase – Twistdraai

4.2.7.2 SCS blend

The SCS blend is characterised by a significantly lower proportion of large extraneous calcite, pyrite, quartz, sandstone and mudstone rock fragments than Twistdraai. Any extraneous calcite and pyrite particles present are significantly finer ranging in size from 30 to 180 µm. The calcite and pyrite are predominately fine included grains or associated with finer cleats either attached to coal particles or transecting coal particles (**Figure 4.37**). The grain size of the fine included calcite and pyrite grains range from sub-micron to 60 µm and the width of the cleats are 50-125 µm. The coarse included calcite and dolomite grains give the coal fragment a patchy appearance (**Figures 4.37** and **4.38**). Pyrite can be intimately associated with calcite and forming complex included grains (**Figure 4.38**).

Kaolinite and quartz are predominately included grains ranging in size from a few microns to 165 µm. The proportion of kaolinite and quartz associated with extraneous rock fragments is significantly less than Twistdraai. Large included kaolinite and calcite/dolomite filling cell cavities and occurs in SCS coals.

A noted feature of SCS (blend) is the significantly high proportion of coarse extraneous Fe-oxide/hydroxide/siderite (26.1 mass-%) particles in the >2.2 sink and in the original sample.

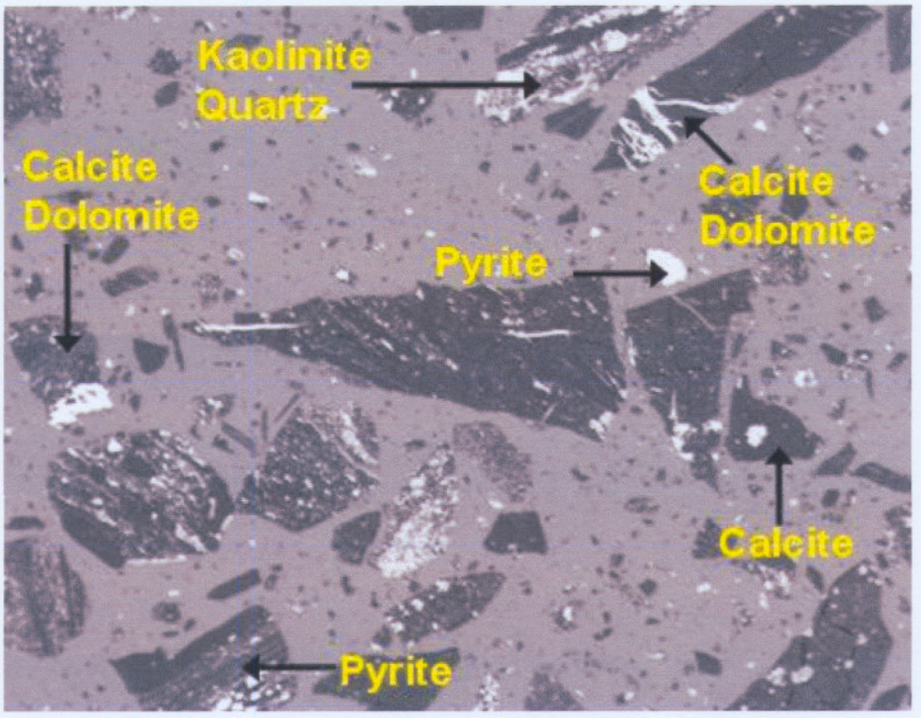

Figure 4.37 Calcite/dolomite cleats attached to coal or transecting coal, small extraneous pyrite, large included pyrite, kaolinite/quartz grains and calcite – SCS blend (width of image is 2.7mm)

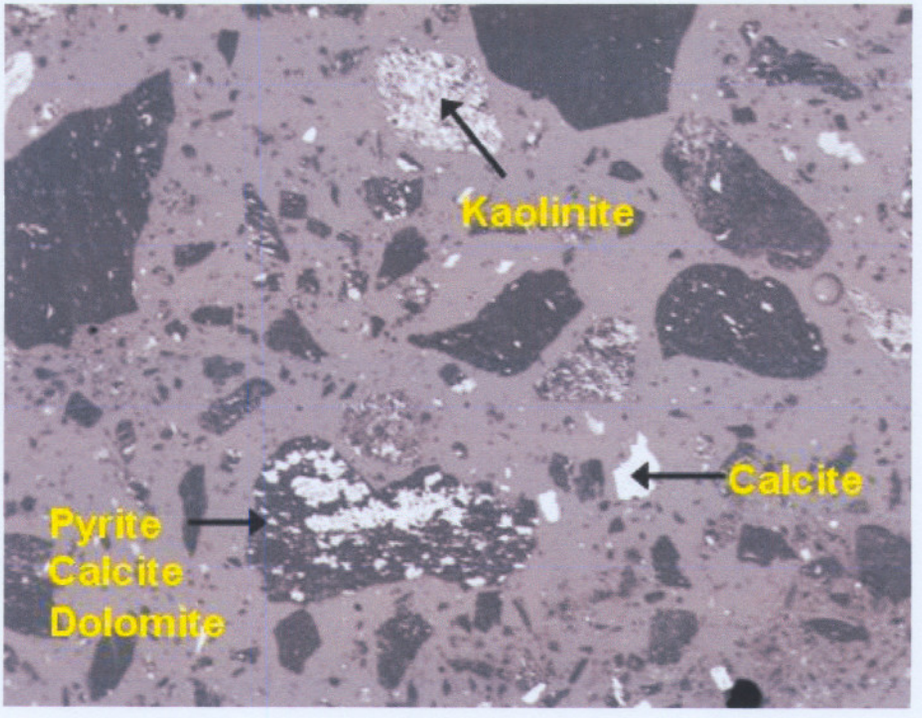

Figure 4.38 Complex association of included pyrite and calcite/dolomite ("patch" appearance), kaolinite-rich mudstone and extraneous calcite - SCS blend (width of image is 2.7mm)

4.2.7.3 Middelbult

Middelbult is similar to SCS except that there are probably a larger proportion of mudstone, siltstone and sandstone rock fragments, and large extraneous calcite particles (**Figure 4.39**). Extraneous calcite can exceed 500 µm in size. The "patchy" appearance of coarse calcite and pyrite inclusions observed in SCS blend are also present. The size of these included calcite/dolomite inclusions can reach 150 µm. Dolomite is common in cleats transecting coal.

Pyrite commonly occurs as large grains attached to coal or in cleats transecting coal. Large extraneous pyrite (>500 µm) grains common in Twistdraai are not common in Middelbult. Kaolinite occurs as fine included grains, infilling cell cavities, large included grains and associated with mudstone and siltstone (**Figure 4.40**). Kaolinite included in or attached to coal can reach sizes of 300 µm. It seems if there is a relatively higher proportion of extraneous mudstone and siltstone fragments in Middelbult than in Twistdraai or SCS. It is feasible that the high proportion of extraneous kaolinite rich mudstone and siltstone fragments are derived from the large included kaolinite common in Middelbult.

Quartz has similar association characteristics as kaolinite except that there are a higher proportion of larger extraneous quartz grains. Extraneous quartz grains on average finer than in Twistdraai and invariably less than 200 µm in size.

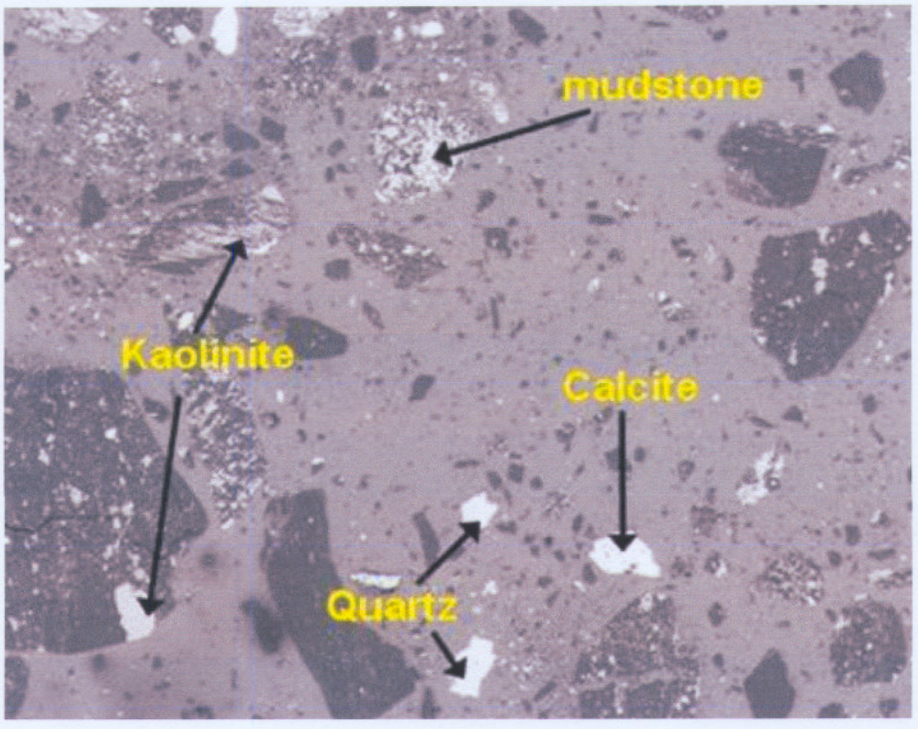

Figure 4.39 Large included kaolinite, extraneous quartz, extraneous calcite, kaolinite infilling cell cavities and mudstone – Middelbult (width of image is 2.7mm)

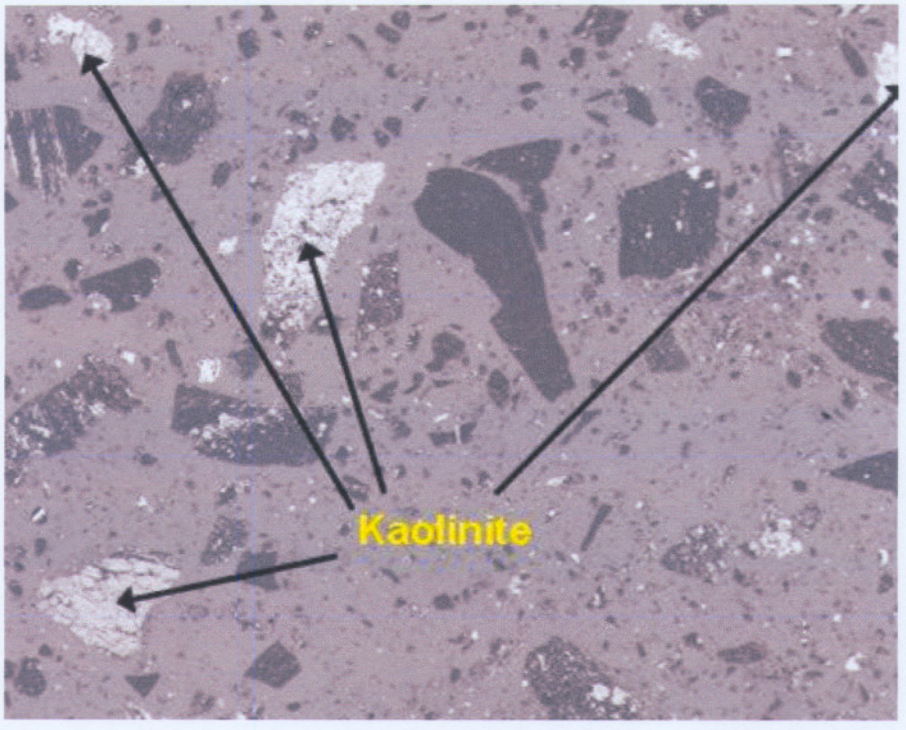

Figure 4.40 Large predominately kaolinite-rich fragments in Middelbult (width of image is 2.7mm)

4.2.7.4 Comparison of the three coals

The rock fragments identified were a fine-grained sub-arkosic sandstone, siltstone and mudstone. Quartz and to a lesser extent kaolinite, mica and feldspar are the major minerals present in the sub-arkosic sandstone and siltstone. Minor concentrations of calcite/dolomite, pyrite and coal fragments are also present in sandstone and the siltstone. Mudstone is predominately kaolinite with lesser proportions of quartz, mica and feldspar. The rock fragments are from footwall, hanging wall and in-seam partings.

Kaolinite, quartz, calcite, pyrite and dolomite are the major included minerals. For all samples, the relative proportion of kaolinite, quartz, mica/illite and orthoclase increase with an increase in the density fraction. This is comparable to the petrographic observations and variations in ash elemental SiO_2, Al_2O_3 and K_2O values. Compared to Twistdraai, calcite, dolomite and pyrite in the SCS blend and Middelbult commonly occurs in cleats with widths less than 150 μm intimately associated with coal. Kaolinite in Middelbult and the SCS blend also occurs infilling cell cavities. Middelbult has larger kaolinite grains (>300 μm) attached to coal or occurring as "mudstone" fragments. The high proportion of included fine kaolinite, calcite and dolomite would explain the high proportion of these minerals occurring in the 1.4-1.55 and 1.6-1.75 density fractions of Middelbult and the SCS blend. Unlike the other coals, the SCS blend has large Fe-oxide/Fe-hydroxide/siderite particles.

The relative proportion of pyrite is variable between the density fractions. Twistdraai has a high pyrite proportion (> 5 mass %), whereas Middelbult has a low pyrite proportion (0.5 mass %). The variation in pyrite content is validated by the petrographic results (**Section 4.2.6**).

Based on the CCSEM results, the SCS blend appears to have the highest proportion of calcite (4 mass-%) and dolomite (4 mass %), while Twistdraai has the lowest. Calcite relative proportions are variable between density fractions. For Middelbult and the SCS blend, the relative proportion of dolomite tends to decrease with the increase in the density fraction.

Without exception the P_2O_5 and SO_3 content tends to concentrate in the coal rich 1.4-1.65 density fractions. This suggests that apatite (main P-bearing phase) is principally associated with coal. It is proposed that the SO_3 in the ash is no reflection on the pyrite content, but controlled by the proportion of CaO and MgO in the ash that reacts with the volatile SO_3 and forms stable Ca-sulphates.

4.3 CHAPTER SUMMARY

The principal factors affecting ash fusion temperatures are the SiO_2/Al_2O_3 ratio and basic oxide levels.

High SiO_2/Al_2O_3 ratios mean higher AFT's. The presence of silica and the clays; illite and montmorrillonite contributed to the higher SiO_2/Al_2O_3 ratios in the Middelbult and SCS sinks, hence the higher AFT's.

The predominant basic oxides present in Middelbult, Twistdraai and SCS blend coals are Ca, Mg and Fe. At a sufficient combined level, they lower the ash fusion temperature. Ca and Mg-bearing minerals identified in the coals were calcite, dolomite, aragonite and smectite. The Fe minerals were pyrite and siderite with pyrite identified as the abundant Fe-containing mineral. This finding implies that the AFT could be manipulated to higher levels by removing combinations of fluxing agents.

CHAPTER 5

RESULTS AND DISCUSSION: CHEMICAL FRACTIONATION

This chapter will deal with the results obtained from the chemical fractionation (leaching) tests conducted on three density separated fractions of the SCS blend coal in order to alter the mineral properties of the coal thereby providing further information on the effect of specific minerals on ash fusion temperature. **Chapter 6** will discuss correlations of the minerals to ash fusion temperatures in the chemical fractionated SCS blend coal.

More detail on the reasons and method for performing the analysis was provided in **Chapter 2 Sections 2.3.2** and **Chapter 3 Section 3.3.**

Twelve samples were analysed – 3 density separated fractions (1.55, 1.95 and the 2.20 sink) in each of 4 leaching agents. The leached coals were submitted for ash composition and ash fusion temperature (oxidising to 1600°C) analyses. These were then compared against the unleached coal to determine the changes. The leachates were submitted for ICP (inductively coupled plasma) analysis to determine the elemental composition.

5.1 ANALYSES ON LEACHATE

The type and amount of elements washed from the different densities by specific leaching agents are given in **Appendix Table 5.1** and graphically illustrated in **Figure 5.1.**

Figure 5.1 shows that the acid washes with HCl and HNO_3 removed the highest concentrations of elements. Al, Ca, Mg, Na and Fe were removed in higher concentrations by the acids than the other leaching agents. The main elements removed by the acids were Ca and Mg in the 1.55 and 1.95 densities and Ca and Fe in the sink. H_2O and NH_4OAc removed mainly Ca and Na. Different mineral elements and combinations of elements are removed by different leaching agents.

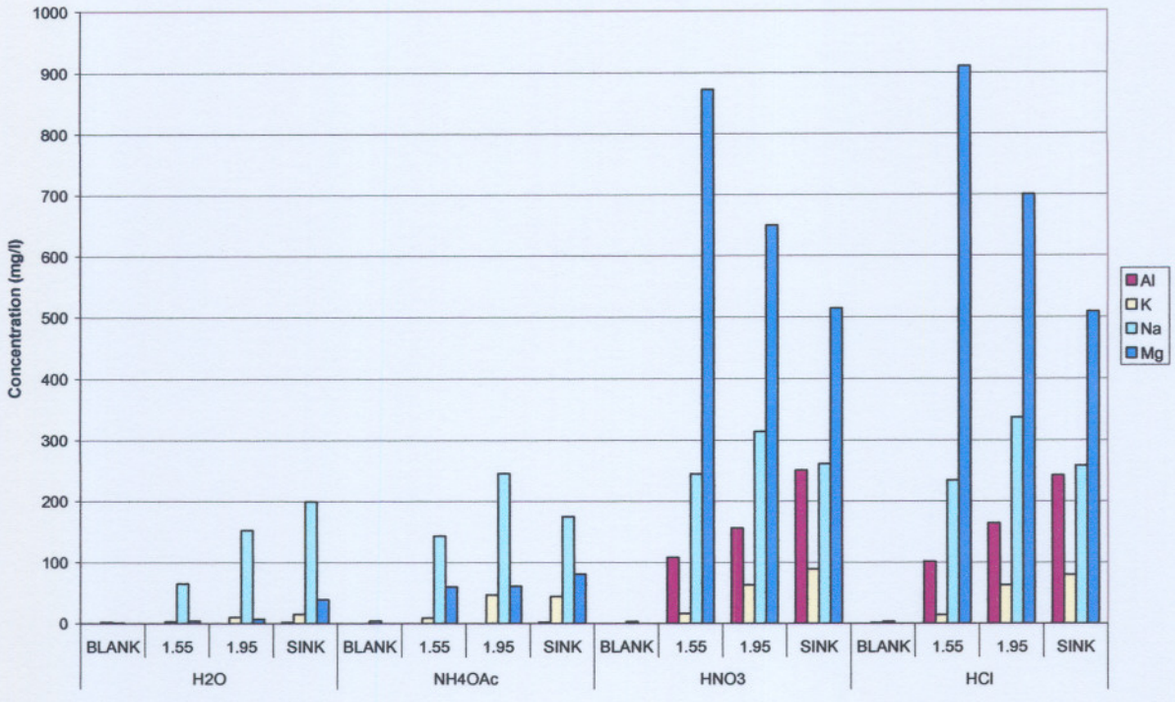

Figure 5.1(a) **Mineral element type and concentration in leaching agents after leaching**

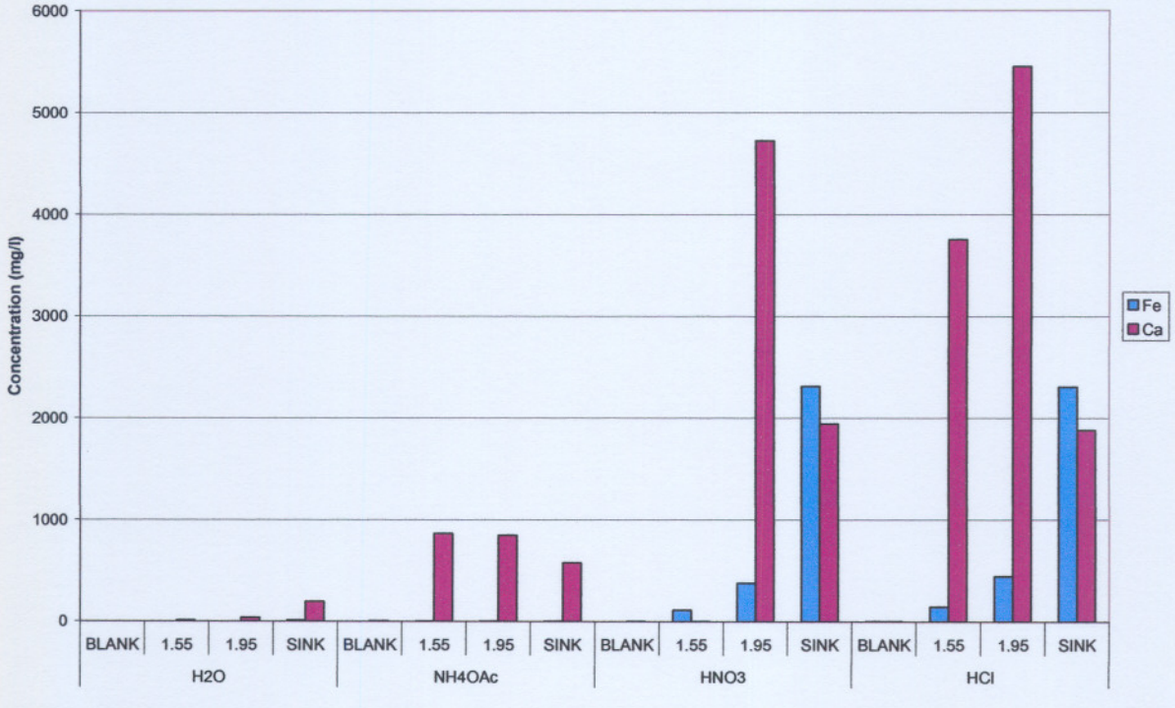

Figure 5.1(b) **Mineral element type and concentration in leaching agents after leaching**

5.2 ANALYSES ON LEACHED COAL

It is necessary to evaluate the coals to determine which mineral elements remained in order to confirm the results seen in **Figure 5.1**. The ash composition of the original coals as well as those of the leached coals (**Appendix Table 5.2**) is illustrated in **Figure 5.2**.

Ca and Mg significantly decreased after the acid wash. It is only in the sink that a decrease in Fe is noted. An interesting finding is that the SO_3 concentration decreased after acid leaching of the 1.55 and 1.95 densities was not proportional with that of Fe. Since a large portion of S is normally associated with Fe in the form of pyrite, this implies that the S removed during the acid wash was possibly also from other minerals as well as from the coal structure.

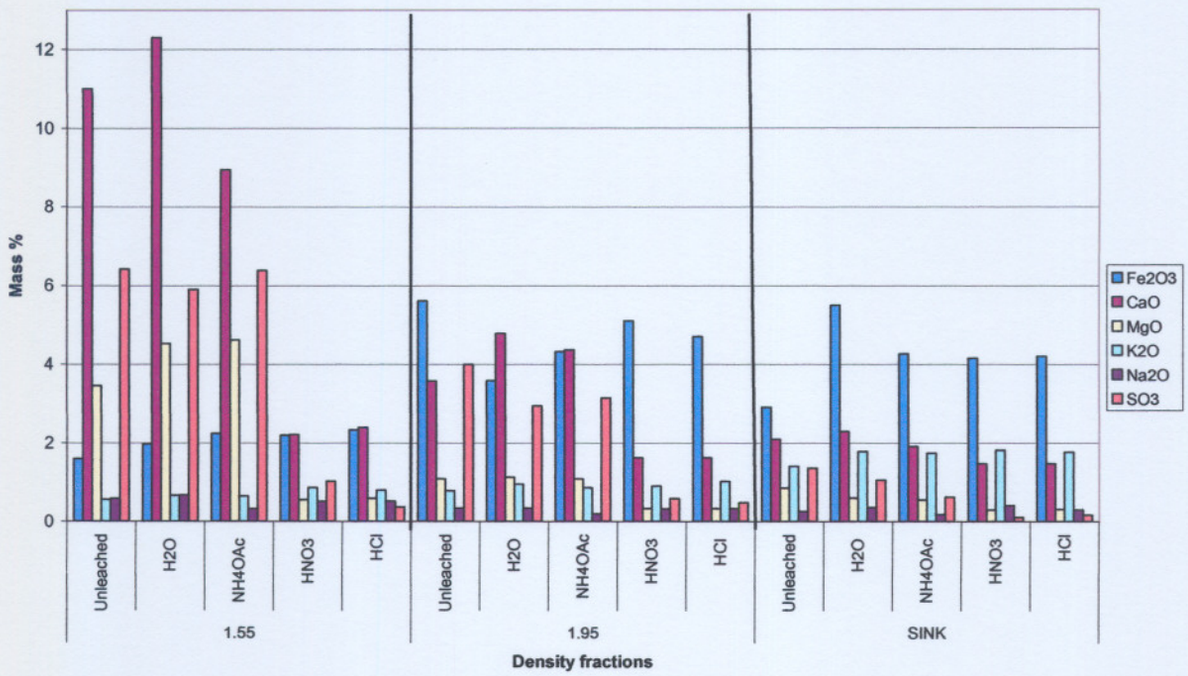

Figure 5.2 Ash composition of original coal and after leaching

5.3 ASH FUSION TEMPERATURE OF LEACHED COAL

Figure 5.3 (**Appendix Table 5.3**) shows significantly higher ash fusion temperatures for the acid-leached coals. This indicates that removal of some mineral types from the coal by acid leaching caused the AFT to increase to >1500°C. In **section 5.1.2**, it was noted that Ca and Mg were mainly removed in RD 1.55 and RD 1.95 but that changed

to Ca and Fe in the sink. Therefore, it was the removal of a combination of elements that resulted in an increase in AFT.

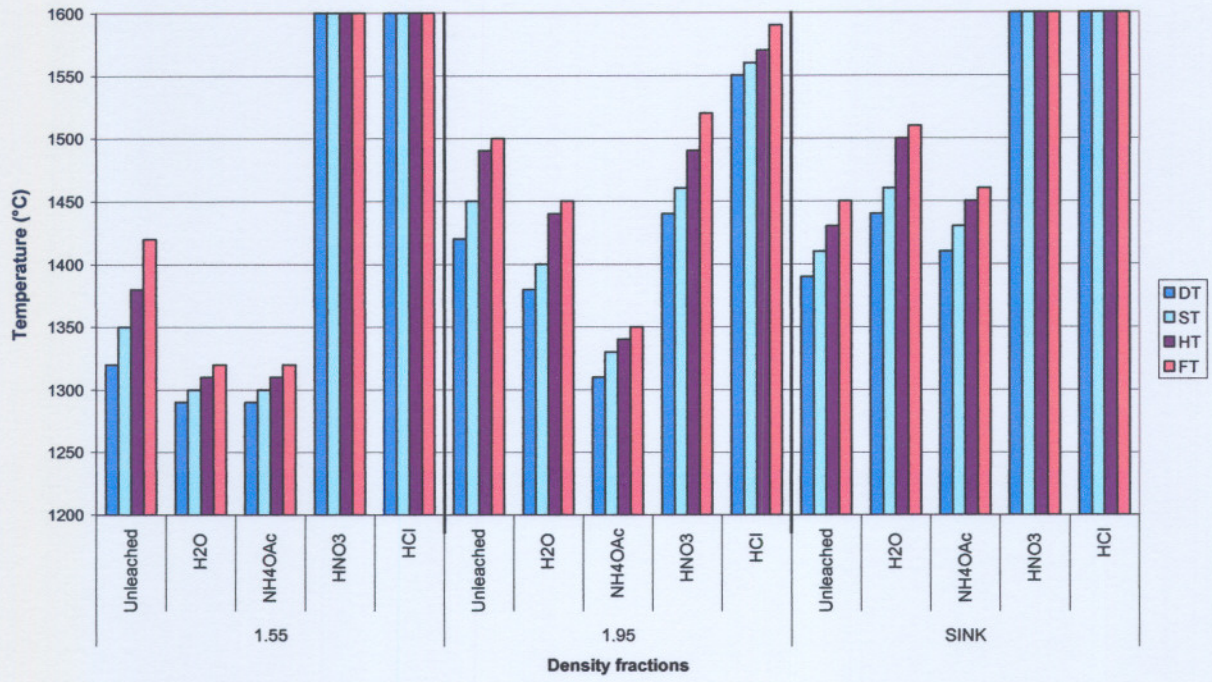

Figure 5.3 AFT of original coal and after leaching

5.4 CHAPTER SUMMARY

Chemical fractionation tests resulted in coal with different mineral properties which can be used to explain the effect of specific minerals on ash fusion temperature. Different mineral elements and combinations of elements were removed by different leaching agents. It was the removal of combinations of elements that resulted in an increase in AFT.

The AFT of coal after acid leaching increased to >1500°C. Since Ca, Mg and Fe were removed in the highest concentrations, it suggests that the presence of combinations of these minerals had resulted in lower AFT's.

CHAPTER 6

STATISTICAL EVALUATION

In this chapter, the results discussed in **Chapter 4** will be statistically evaluated to confirm the results from the chemical fractionation tests (**Chapter 5**).

The purpose of this chapter is to examine the correlations between mineral elements and ash fusion temperatures. Also, empirical equations to calculate the ash fusion temperatures from the chemical compositions of coal will be determined. This will also highlight which variables in ash composition affect ash properties.

6.1 MINERAL COMPOSITION

The ash fusion temperatures (DT, ST, HT and FT) were evaluated with coal characteristics using a linear regression method. As mentioned in **Chapter 2 Section 2.3.3.1**, if *r* has a value between +0.8 and +1 it indicates that there is a strong positive correlation while *r* values of -0.8 and -1 indicate a strong negative correlation.

6.1.1 Correlation coefficients

The correlation coefficients of the ash fusion temperature (dependent variable) associated with each ash oxide (independent variable) are given in **Appendix Table 6.1**.

In the Middelbult sample, the highest positive correlations were obtained with SiO_2 (0.81) and TiO_2 (0.70) while the highest negative correlations were obtained with CaO (-0.73) and MgO (-0.71). **Figure 6.1** graphically illustrates the relationships of SiO_2 and CaO to the melting temperature. Increasing the Si concentration in the coal would result in a higher AFT. There was no data for CaO > 20 mass %. The trend suggests that if the concentration of Ca could be increased, at some point the minimum AFT would be reached and the curve would then move upwards towards higher AFT.

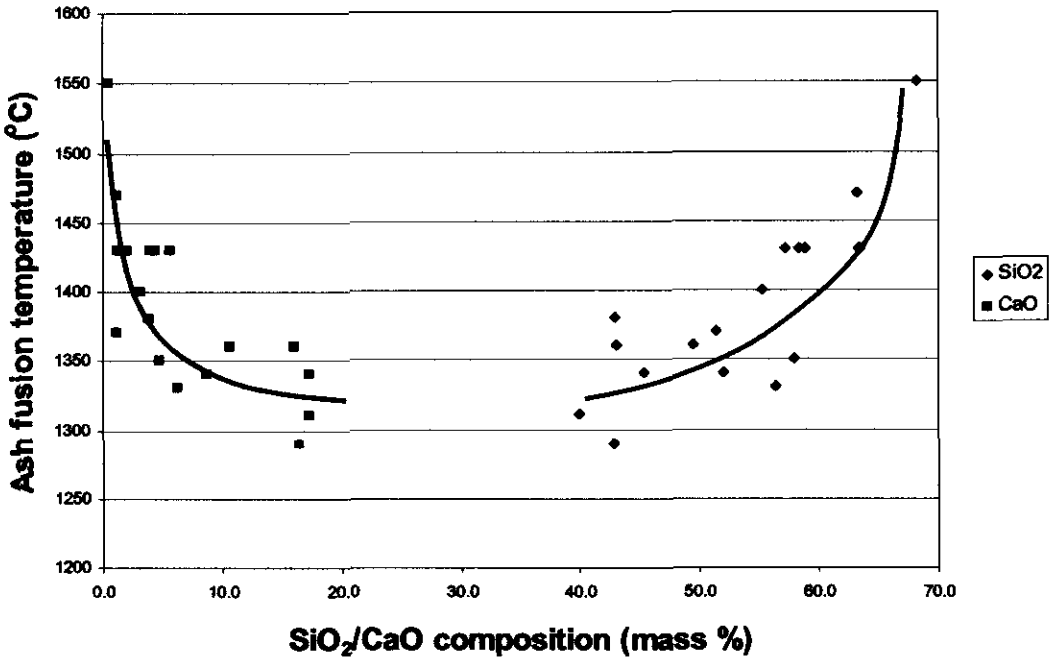

Figure 6.1 Correlations between AFT and SiO_2 and CaO

Twistdraai coal showed very low correlations with the highest correlation being 0.52 for SiO_2.

Similarly to Middelbult coal, the highest correlations for the SCS blend coal were for SiO_2 (0.78) and CaO (-0.80). These results reflect those obtained for the leached SCS blend coal.

The correlations coefficients of the DT, ST, HT and FT with mineral composition are similar. This implies that individual minerals do not affect the difference between the ash fusion temperatures. The temperature range from deformation temperature to flow temperature was calculated and also compared with the ash composition (**Appendix Table 6.1**) in order to determine if the mineral composition had any effect on the deformation rate. There were no significant correlations for any of the coals.

From **Appendix Table 6.1**, it is interesting to note the low correlation coefficients for Fe. This is important due to the oxidation state of Fe. Reduced Fe lowers AFT much better than the oxidized form (Hatt, 2001).

6.1.2 Model to predict ash fusion temperature

The analysis of variance (ANOVA) results indicating the effect of ash oxides on the deformation temperature are presented in **Table 6.2**. In order for a specific effect to be statistically significant, the "Prob > F" (p-value) should be smaller than 0.05. From the values in **Table 6.2**, it is clear that Fe_2O_3 and CaO have a significant effect on the initial deformation temperature. The model F-value of 14.87 implies the model is significant. There is only a 0.03% chance that a model F-Value this large could occur due to chance.

Table 6.2 ANOVA results indicating the effect of ash oxides on DT

Source	Sum of Squares	DF	Mean Square	F Value	Prob > F
Model	53732	2	26866	14.87	0.0003
Fe_2O_3	*9579*	*1*	*9579*	*5.30*	*0.0360*
CaO	*53118*	*2*	*53118*	*29.41*	*<0.0001*
Residual	27095.43	15	1806		
Cor Total	80827	17			
R-squared	**0.66**				

The empirical model describing the relationship between the ash oxides and initial deformation temperature is:

$$DT = 1440 - 4.1*Fe_2O_3 - 9.8*CaO$$

Although Fe and Ca have a significant effect of DT, the model explains only 66% (R-squared) of the variability in the data. The prediction of DT with the empirical model will therefore not be very accurate. A larger model is required in order to improve the variability.

Empirical models were similarly derived for Middelbult, Twistdraai, the SCS blend and the leached SCS coal, for a p-value<0.05. These are summarised in **Table 6.3**. The p-value was then changed to <0.10 in an attempt to improve the R-squared value. However, the model remained unchanged. The models appear to be specific to each coal source. Their application would be in determining the effect of changing the concentrations of various ash constituents on the slagging characteristics of a coal.

The unleached coals once again show no significant differences between the DT, ST, HT and FT. However, the leached SCS blend coal has more significant minerals in the model and the R-squared value is higher than for the other coals. In addition, the models obtained for DT and ST are different to those obtained for HT and FT. The clear difference between the model for the SCS blend and leached SCS blend confirms the previous conclusion (**Chapter 5**) that chemical fractionation tests result in coal with different mineral properties which can be used to explain the effect of specific minerals on ash fusion temperature. By altering the mineral composition while monitoring the AFT, it is possible to gain a clearer picture of which mineral interactions affect AFT.

Table 6.3 Empirical models describing relationships between mineral composition and AFT (p-value<0.05)

	Equation		F value	R-squared
Middelbult	DT =	1440 – 4.1 * Fe_2O_3 – 9.8 * CaO	14.87	0.66
	ST =	1454 – 4.4 * Fe_2O_3 – 9.9 * CaO	13.45	0.64
	HT =	1472 – 4.6 * Fe_2O_3 – 9.9 * CaO	12.23	0.62
	FT =	1490 – 5.1 * Fe_2O_3 – 10.5 * CaO	11.96	0.61
Twistdraai	DT =	1136 + 4.4 * SiO_2	6.60	0.29
	ST =	1170 + 4.0 * SiO_2	5.47	0.25
	HT =	1180 + 4.1 * SiO_2	5.85	0.27
	FT =	1190 + 4.1 * SiO_2	5.85	0.27
SCS blend	DT =	755 + 7.0 * SiO_2 + 8.7 * Al_2O_3	23.97	0.76
	ST =	727 + 7.4 * SiO_2 + 9.8 * Al_2O_3	28.22	0.79
	HT =	694 + 7.9 * SiO_2 + 10.8 * Al_2O_3	29.55	0.80
	FT =	683 + 8.0 * SiO_2 + 11.4 * Al_2O_3	28.10	0.79
Leached SCS blend	DT =	8870 - 75.8 * SiO_2 - 74.2 * Al_2O_3 - 92.6 • Fe_2O_3 - 180.2 * TiO_2 - 152.3 • CaO - 127.6 * MgO + 947.2 • Na_2O	19.16	0.95
	ST =	8391 - 70.9 * SiO_2 - 70.4 * Al_2O_3 - 83.8 * Fe_2O_3 - 152.3 • TiO_2 - 140.95 * CaO - 124.1 * MgO + 889.8 * Na_2O	22.54	0.95
	HT =	1422 - 33.7 * CaO + 508.4 • Na_2O	49.36	0.89
	FT =	1435 - 32.2 * CaO + 489.9 * Na_2O	45.11	0.88

6.2 MINERAL RATIOS

The discussion so far has highlighted the significance of mineral interactions. Mineral ratios provide a means of looking at various combinations of mineral interactions.

6.2.1 Correlation coefficients

The mineral ratios (**Chapter 2 Section 2.4.2.4**) were calculated for Middelbult (**Appendix Table 6.4**), Twistdraai (**Appendix Table 6.5**), the SCS blend (**Appendix Table 6.6**), and the leached SCS blend (**Appendix Table 6.7**).

The AFT (dependant variable) was then compared with each mineral ratio (independent variable) on a one-to-one basis (**Appendix Table 6.8**).

The highest correlation coefficients (DT, ST, HT, FT) for each of the coals were as follows:

Middelbult coal (0.88, 0.90, 0.90, 0.92) and leached SCS blend coal (0.84, 0.85, 0.83, 0.82):

Acidity $= (SiO_2 + Al_2O_3) / (Fe_2O_3 + CaO + MgO + Na_2O + K_2O)$

Twistdraai coal (0.59, 0.57, 0.59, 0.59):

Silica module $= SiO_2 / (Al_2O_3 + Fe_2O_3)$

SCS blend coal (0.87, 0.88, 0.88, 0.88:

% Acid $= Al_2O_3 + SiO_2 + TiO_2$

The correlation coefficients for Twistdraai coal were poor. The other coals had stronger coefficients. The three mineral ratios have SiO_2 and Al_2O_3 as common factors, confirming the significance of the SiO_2/Al_2O_3 ratio (**Chapter 4 Section 4.2.4**).

6.2.2 Model to predict ash fusion temperature

The models derived from multiple correlations with mineral ratios (**Table 6.9**) have good R-squared values, with the exception of Twistdraai. The models are dependant on the mineral composition of the coal. As discussed in **Chapter 4**, the mineral compositions of the three coals differ as they come from different origins. Therefore, the models differ for each of the coals. It is not possible to propose a single model that would explain the AFT of every coal. The model would be source specific.

The model for the leached SCS blend coal especially, with R-squared values from 0.94 to 0.97, shows the highly complex range of mineral interactions that occur.

Table 6.9 Empirical models describing relationships between mineral ratios and AFT (p-value<0.05)

	Equation		F value	R-squared
Middelbult	DT =	1320 + 6.3 * Acidity – 188.3 * Basic module	39.70	0.84
	ST =	1289 + 6.7 * Acidity – 66.8 * Basic flux factor	45.56	0.86
	HT =	1307 + 8.4 * Acidity	65.05	0.80
	FT =	1312 + 9.2 * Acidity	83.21	0.84
Twistdraai	DT =	1196 + 94.7 * Acid flux factor	8.49	0.35
	ST =	1220 + 89.5 * Acid flux factor	7.63	0.32
	HT =	1231 + 91.9 * Acid flux factor	8.21	0.34
	FT =	1241 + 91.9 * Acid flux factor	8.21	0.34
SCS blend	DT =	881 + 582.1 * Si factor	39.59	0.71
	ST =	874 + 611.6 * Si factor	45.17	0.74
	HT =	858 + 654.3 * Si factor	46.59	0.74
	FT =	861 + 669.3 * Si factor	44.68	0.74
Leached SCS blend	DT =	61967 + 46.4 * % Acid -65320.9 * Silica value +31.0 • SiO_2*CaO -2991.4 * CaO+MgO +34055.5 * Base/Acid -1317.5 • new Australian index +1.0E+005 * Basic module	34.10	0.97

	ST =	58467 + 42.1 * % Acid -61376.0 • Silica value +29.2 • SiO_2*CaO -2824.4 * CaO+MgO +31562.6 • Base/Acid -1232.0 * new Australian index +1.0E+005 * Basic module	42.17	0.98
	HT =	41119 + 102.6 • Acidity +375.0 * % Base -42179.5 * Silica value +21.2 • SiO_2*CaO -2027.5 * CaO+MgO -854.9 * new Australian index +69881 • Basic module	15.02	0.94
	FT =	37334 + 239.7 * % Base +56.1 * % Acid -41602.9 • Silica value +19.4 • SiO_2*CaO -2031.8 • CaO+MgO -786.6 • new Australian index +80171 * Basic module	16.98	0.94

6.3 CHAPTER SUMMARY

Middelbult, the SCS blend and the leached SCS blend coals showed high correlations with SiO_2 and CaO. The trend suggested that if the concentration of Ca was increased, at some point this would result in higher AFT's.

The leaching of the SCS blend coal altered the mineral composition, which then made it possible to gain a clearer picture of the complex mineral interactions.

The models developed can be applied in determining the effect of changing the concentrations of various ash constituents on the slagging characteristics of a coal.

CHAPTER 7

SUMMARY AND CONCLUSIONS

The principal aims of this study were to investigate the changes in coal characteristics brought about by density separation and the subsequent effect on the ash fusion temperature of the coal. Ash fusion temperature was used as a measure of the expected behaviour of the ash bed during gasification. Chemical fractionation tests were conducted on the density separated coal from the SCS blend in order to alter the chemical properties of the coal and provide further information on the effect on the thermal properties. The correlations between mineral elements and ash fusion temperatures were then examined. Finally, empirical equations to calculate the ash fusion temperatures from the chemical compositions of coal were determined.

Density separation reduced the heterogeneity of the coal particles and allowed the preparation of series of samples that covered a range of mineral contents in raw coal particles. The study of the density separated samples allowed the gathering of information on the influence of mineral matter composition and distribution within the particles on the behaviour of the whole coal. Although density separation is usually performed on coal crushed to -1mm, it was shown that the density separation of lump coal (100+6.7mm) did still separate organic and inorganic material. The organic matter tended to concentrate in the lower densities and the mineral matter in the higher densities. The minerals that did occur in the lower density fractions were included fine kaolinite, calcite and dolomite.

Representative samples of run-of-mine coal from three sources; Twistdraai, Middelbult and the SCS blend to gasification were analysed by standard characterisation methods such as XRD and petrographic analysis, as well as by other techniques such as Mössbauer and Computer Controlled Scanning Electron Microscopy (CCSEM).

The predominant basic oxides present were Ca, Mg and Fe. Ca and Mg-bearing minerals identified in the coals were calcite, dolomite, aragonite and smectite. The Fe minerals were pyrite and siderite with pyrite identified as the abundant Fe-containing

mineral. The results confirmed that low ash fusion temperatures may be attributed to increased basic oxide levels and low SiO_2/Al_2O_3 ratios.

The chemical fractionation of the SCS blend coal altered the mineral composition, which then made it possible to gain a clearer picture of the complex mineral interactions that affect AFT. Different mineral elements and combinations of elements were removed by different leaching agents. It was the removal of combinations of elements, mainly Ca, Mg and Fe, that resulted in an increase in AFT.

The correlations between mineral elements and ash fusion temperatures were then examined. Twistdraai had very poor correlations in all instances. The Middelbult, SCS blend and leached SCS blend coals showed high correlations with SiO_2 and CaO. However, when correlations were determined using mineral ratios, each coal correlated with a different ratio.

The models developed for the calculation of AFT were specific to the coal source. An interesting phenomenon occurred in the models of the leached SCS blend coal. DT and ST showed different relationships to those HT and FT. All the other models showed the similar relationships for DT, ST, HT and FT. These models allow basic studies of variance of different coal ash constituents on slagging potential.

REFERENCES

BAXTER L.L., 2002. Coal Characterisation Techniques for Slagging and Fouling, *Proceedings of 19th Pittsburgh Coal Conference*, Pittsburgh, USA.

BRYANT G.W., BROWNING G.J., EMANUEL S.K., GUPTA S.K., GUPTA R.P., LUCAS J.A., WALL T.F., 2000. The Fusibility of Blended Coal Ash. *Energy and Fuels*, Vol. 14, pp. 316-325.

BRYERS R.W., TAYLOR T.E., 1976. An examination of the relation between ash chemistry and ash fusion temperatures in various coal size and gravity fractions using polynomial regression analysis. *Journal of Engineering for Power*, Vol. 98, pp. 528-539.

COHEN R.L., 1976. Applications of Mössbauer spectroscopy. New York:Academic Press. 349 p.

CREELMAN R.A., POHL J.H., DEVIR G.P., SU S., 2000. The Heterogeneous Nature of Mineral Matter, Fly-ash and Deposits. *Proceedings of 9th Biennial Coal Science Conference: Solutions for Industry*, Qld, Australia.

DEMARIS P.J., READ R.B., CAMP L.R., 1988. The effects of advanced physical coal cleaning on mineral matter and ash composition and its relationship to boiler slagging and fouling potential. *Prepr. Symp. - Am. Chem. Society, Div. Fuel Chem.*, 33(2), pp.13-18.

FALCON L.M., FALCON R.M.S., 1987. The Petrographic Composition of Southern African coals in relation to friability, hardness, and abrasive indices. *Journal of the South African Institute of Mining and Metallurgy*, Vol. 87, No. 10, pp. 323-336.

FALCON R.M.S., SNYMAN C.P., 1986. An Introduction to Coal Petrography: Atlas of Petrographic Constituents in the Bituminous Coals of Southern Africa. pp. 3-4, 19.

GOVENDER A., 2004. Gasification Handbook. Sasol internal report.

GRAINGER L., GIBSON J., 1981. Coal Utilization: Technology, Economics and Policy. pp 1-8.

GRAY V.R., 1987. Prediction of ash fusion temperature from ash composition for some New Zealand coals. *Fuel*, Vol. 66, pp 1230-1239.

GUPTA S.K., GUPTA R.P., BRYANT G.W., WALL T.F., 1998. The effect of potassium on the fusibility of coal ashes with high silica and alumina levels. *Fuel*, Vol. 77, pp 1195-1201.

HATT R., 2001. Influence of coal quality and boiler operating conditions on slagging of utility boilers. *Proceedings of Power Production in the 21st century: Impacts of Fuel Quality and Operators*, Utah.

HUGGINS F.E., 2002. Overview of analytical methods for inorganic constituents in coal. *International Journal of Coal Geology*, Vol. 50, pp. 169-214.

JUNIPER L., 1996. Ash deposition indices revisited. *Workshop on Impact of Coal Quality on Thermal Coal Utilisation*, Brisbane.

KAHRAMAN H., REIFENSTEIN A.P., COIN C.D.A., 1999. Correlation of ash behaviour in power stations using the improved ash fusion test. *Fuel*, Vol. 78, pp. 1463-1471.

LOLJA S.A., HAXHI H., DHIMITRI RO., DRUSHKU S., MALJA A., 2002. Correlation between ash fusion temperatures and chemical composition in Albanian coal ashes. *Fuel*, Vol. 81, pp. 2257-2261.

MACK C., 1975. *Essentials of statistics for scientists and technologists.* Plenum Publishing Corporation, New York. pp. 118-119.

MAGASINER N., VAN ALPHEN C., INKSON M.B., MISPLON B.J., 2001. Characterising fuels for biomass – Coal fired cogeneration. *Proceedings of 75th Annual Congress of the S.A. Sugar Technologists Association*, South Africa.

MENDEZ L.B., BORREGO A.G., MARTINEZ-TARAZONA M.R., MENENDEZ R., 2002. Influence of petrographic and mineral matter composition of coal particles on their combustion reactivity. *Fuel*, 82, pp. 1875-1882.

PATTERSON J.H., HURST H.J., 2000. Ash and slag qualities of Australian bituminous coals for use in slagging gasifiers. *Fuel*, 79, pp. 1671-1678.

SANDERS D, 1996. Coal Characterisation in Marketing - an Elementary Approach. *Workshop on Coal Characterisation - for Existing & Emerging Technologies*, CRC for Black Coal Utilisation, Newcastle, Australia.

SLAGHUIS J.H., 1993. *Coal Gasification: A Study Guide for the National Diploma in Fuel Technology, Coal Processing III, Part A*. Sasolburg: Sasol Technology R&D.

STEVENS J.G., KHASANOV A.M., POLLAK J.W., LI Z., 1998. *Mössbauer Mineral Handbook*. Mössbauer Effect Data Centre, University of North Carolina, USA.

TOMECZEK J., PALUGNIOK H., 2002. Kinetics of mineral matter transformation during coal combustion. *Fuel*, 81, pp. 1251-1258.

VAN ALPHEN C., 2003. Sasol Feedstock Characterisation by CCSEM. Full analysis Report to Sasol Technology R&D.

VAN DYK J.C., KEYSER M.J., VAN ZYL J.W., 2001. Suitability of feedstocks for the Sasol-Lurgi Fixed Bed Dry Bottom Gasification Process. *Gasification Technologies Conference*, San Francisco, USA.

VASSILEV S. V., KITANO K., TAKEDA S., TSURUE T., 1995. Influence of mineral and chemical composition of coal ashes on their fusibility. *Fuel Processing Technology*, Vol. 45, pp. 27-51.

WALL T.F., GUPTA S.K., GUPTA R.P., SANDERS R.H., CREELMAN R.A., BRYANT G.W., 1999. False deformation temperatures for ash fusibility associated with the conditions for ash preparation. *Fuel*, Vol. 78, pp.1057-1063.

WARD C.R., 2002. Analysis and significance of mineral matter in coal seams. *International Journal of Coal Geology*, Vol. 50, pp. 135-168.

WINEGARTNER E.C., RHODES B.T., July 1975. An empirical study of the relation of chemical properties to ash fusion temperatures. *Journal of Engineering for Power*, pp.395-406.

APPENDIX

Table 4.1 Mass % distribution of density fractionated Middelbult, Twistdraai and SCS coals

	MIDDELBULT		TWISTDRAAI		SCS	
Relative density (g/cm^3)	**Fraction mass %**	**Cumulative mass %**	**Fraction mass %**	**Cumulative mass %**	**Fraction mass %**	**Cumulative mass %**
1.40	6.1	6.1	12.6	12.6	8.5	8.5
1.45	13.8	19.9	12.4	25.0	11.1	19.6
1.50	17.6	37.5	22.4	47.4	16.5	36.1
1.55	11.5	49.0	14.0	61.4	14.1	50.2
1.60	10.9	59.9	7.6	69.0	11.9	62.1
1.65	10.0	69.9	3.2	72.2	8.1	70.2
1.70	6.7	76.6	2.4	74.6	7.5	77.7
1.75	4.8	81.4	2.7	77.3	3.4	81.1
1.80	2.6	84.0	0.8	78.1	2.1	83.2
1.85	1.9	85.9	0.8	78.9	2.1	85.3
1.90	2.1	88.0	0.9	79.8	1.4	86.7
1.95	1.1	89.1	0.3	80.1	0.6	87.3
2.00	1.3	90.4	0.6	80.7	0.7	88.0
2.05	0.6	91.0	0.3	81.0	0.5	88.5
2.10	1.0	92.0	0.8	81.8	0.6	89.1
2.15	1.1	93.1	1.5	83.3	1.5	90.6
2.20	0.6	93.7	1.1	84.4	0.6	91.2
Sink	6.3	100.0	15.6	100.0	8.8	100.0

Table 4.2 Ash fusion temperatures (°C) on original and density fractionated Middelbult, Twistdraai and SCS coals

	MIDDELBULT				TWISTDRAAI				SCS			
Relative density (g/cm^3)	DT	ST	HT	FT	DT	ST	HT	FT	DT	ST	HT	FT
Original	1330	1360	1380	1400	1330	1340	1350	1370	1310	1340	1350	1360
1.40	1280	1290	1300	1310	1340	1350	1360	1370	1250	1260	1270	1280
1.45	1300	1320	1350	1360	1340	1350	1360	1370	1270	1280	1290	1300
1.50	1260	1270	1280	1290	1350	1370	1390	1400	1270	1280	1290	1300
1.55	1290	1310	1330	1340	1340	1350	1390	1400	1320	1350	1380	1420
1.60	1310	1320	1330	1340	1270	1280	1290	1300	1300	1320	1330	1340
1.65	1320	1330	1350	1360	1300	1340	1350	1360	1290	1300	1310	1320
1.70	1400	1410	1420	1430	1380	1400	1420	1430	1270	1280	1290	1300
1.75	1320	1330	1340	1350	1460	1470	1490	1500	1310	1320	1330	1340
1.80	1400	1410	1420	1430	1470	1480	1490	1500	1330	1360	1380	1400
1.85	1380	1390	1410	1430	1290	1300	1310	1320	1380	1400	1420	1450
1.90	1350	1360	1370	1380	1300	1320	1330	1340	1270	1280	1290	1300
1.95	1370	1390	1410	1430	1530	1540	1550	1560	1420	1450	1490	1500
2.00	1500	1530	1550	1590	1400	1410	1420	1430	1390	1400	1410	1420
2.05	1350	1360	1390	1400	1200	1220	1240	1250	1420	1430	1440	1450
2.10	1390	1400	1420	1430	1350	1370	1380	1390	1340	1360	1400	1410
2.15	1340	1350	1360	1370	1490	1510	1530	1540	1460	1470	1480	1490
2.20	1300	1310	1320	1330	1390	1400	1420	1430	1260	1280	1300	1320
Sink	1510	1520	1540	1550	1330	1340	1360	1370	1390	1410	1430	1450

Table 4.3 Proximate analysis on original and density fractionated Middelbult, Twistdraai and SCS coals (% air dried basis)

	MIDDELBULT				TWISTDRAAI				SCS			
Relative density (g/cm^3)	Moisture	Volatile matter	Fixed carbon	Ash	Moisture	Volatile matter	Fixed carbon	Ash	Moisture	Volatile matter	Fixed carbon	Ash
Original	4.2	22.6	47.5	25.7	3.0	25.3	46.2	25.5	4.4	24.6	23.1	47.9
1.40	4.2	31.8	56.2	7.8	4.2	27.1	57.7	11.0	4.6	8.2	34.1	53.1
1.45	4.6	25.9	58.6	10.9	4.4	24.0	56.9	14.7	4.6	10.9	26.6	57.9
1.50	4.7	24.7	56.5	14.1	4.3	24.8	56.0	14.9	5.3	14.0	22.9	57.8
1.55	4.4	23.2	53.7	18.7	4.2	24.0	53.5	18.3	4.8	17.6	22.6	55.0
1.60	4.2	20.5	53.9	21.4	3.9	23.3	49.7	23.1	4.3	22.2	22.7	50.8
1.65	4.3	20.3	50.5	24.9	3.3	25.3	41.7	29.7	4.0	26.7	22.0	47.3
1.70	4.2	17.8	46.2	31.8	3.2	19.7	42.2	34.9	3.9	31.4	20.4	44.3
1.75	4.1	16.8	45.9	33.2	2.8	20.1	36.3	40.8	3.7	34.2	19.8	42.3
1.80	3.4	17.0	37.5	42.1	2.8	19.8	33.6	43.8	3.5	39.6	18.0	38.9
1.85	3.7	16.8	37.7	41.8	2.7	18.7	34.0	44.6	3.2	43.3	17.4	36.1
1.90	3.1	19.1	35.8	42.0	2.3	22.3	30.1	45.3	3.2	46.2	19.8	30.8
1.95	2.7	14.2	30.0	53.1	2.3	16.7	27.7	53.3	3.0	47.6	17.9	31.5
2.00	3.4	12.9	27.4	56.3	2.2	17.0	26.1	54.7	3.0	53.4	16.0	27.6
2.05	2.4	16.0	26.8	54.8	2.1	17.4	23.3	57.2	2.7	56.8	16.3	24.2
2.10	2.4	14.3	23.3	60.0	1.9	23.2	21.4	53.5	3.0	61.9	15.3	19.8
2.15	2.5	15.0	24.7	57.8	1.8	14.0	15.3	68.9	2.2	64.2	13.4	20.2
2.20	2.1	16.3	16.9	64.7	1.7	15.0	13.1	70.2	2.0	65.4	16.8	15.8
Sink	1.7	10.1	7.9	80.3	1.0	11.5	2.7	84.8	1.0	85.2	10.4	3.4

Table 4.4 Fischer assay analysis on original and density fractionated Middelbult, Twistdraai and SCS coals (% as received basis)

	MIDDELBULT				TWISTDRAAI				SCS			
Relative density (g/cm^3)	Char*	Tar	Water**	Gas***	Char*	Tar	Water**	Gas***	Char*	Tar	Water**	Gas***
Original	85.0	3.5	8.3	3.3	83.7	5.2	7.4	3.7	84.4	3.5	8.4	3.7
1.40	78.2	7.4	9.1	5.3	76.7	8.8	9.4	5.0	73.4	8.9	9.7	8.1
1.45	82.2	3.9	9.6	4.3	80.3	4.7	9.7	5.3	79.7	6.4	7.4	6.6
1.50	83.7	3.8	8.1	4.4	83.6	3.1	8.7	4.6	82.7	3.5	8.8	5.0
1.55	84.7	2.0	9.2	4.2	83.9	2.9	8.3	4.9	84.1	3.0	8.4	4.6
1.60	86.5	2.7	7.4	3.4	84.8	3.1	7.7	4.5	86.2	3.0	7.1	3.7
1.65	87.6	1.8	7.5	3.0	84.9	2.3	8.1	4.6	86.1	2.4	7.5	4.0
1.70	88.9	1.7	6.7	2.7	87.3	2.5	6.9	3.3	88.1	3.1	5.5	3.3
1.75	89.7	0.5	7.3	2.6	87.3	3.2	6.3	3.2	88.3	2.8	5.7	3.3
1.80	89.9	2.2	5.3	2.6	87.7	2.8	5.8	3.8	88.6	2.9	5.4	3.0
1.85	90.3	0.9	6.3	2.5	87.7	2.4	6.4	3.5	89.5	2.0	5.8	2.7
1.90	91.1	0.8	5.9	2.3	89.0	1.5	6.2	3.3	90.0	2.6	4.9	2.5
1.95	91.5	1.7	4.4	2.4	89.3	2.7	4.8	3.3	90.3	1.5	5.3	2.9
2.00	92.2	1.4	4.6	1.8	89.6	1.9	4.5	4.0	90.8	1.1	4.8	3.4
2.05	92.3	1.1	4.6	1.9	88.4	1.1	5.3	5.1	90.2	2.0	5.4	2.4
2.10	91.4	1.1	4.4	3.0	91.5	3.5	2.8	2.2	90.7	1.9	4.7	2.6
2.15	92.7	1.3	3.8	2.2	92.5	1.3	4.3	2.0	90.5	1.2	4.6	3.7
2.20	92.4	0.7	3.6	3.2	92.4	1.0	4.3	2.2	92.4	2.0	3.2	2.4
Sink	95.2	1.8	0.7	2.4	96.1	1.1	1.7	1.2	96.1	2.0	1.8	0.2

* Includes minerals and ash

** Includes moisture and chemical water

*** Includes experimental losses

Table 4.5 Ultimate analysis on original and density fractionated Middelbult, Twistdraai and SCS coals (% dry ash-free basis)

	MIDDELBULT					TWISTDRAAI					SCS				
Relative density (g/cm^3)	C	H	N	S	O*	C	H	N	S	O*	C	H	N	S	O*
Original	81.5	4.1	2.1	1.0	11.3	78.6	4.4	2.0	1.9	13.1	80.3	4.3	2.0	1.4	12.0
1.40	82.3	5.1	2.2	0.6	9.8	82.0	4.7	2.1	0.7	10.5	81.8	5.0	2.1	0.8	10.2
1.45	82.1	4.4	2.1	0.6	10.8	81.5	4.3	2.0	0.7	11.5	90.8	5.1	2.3	0.8	1.0
1.50	82.2	4.3	2.1	0.7	10.7	81.7	4.3	2.0	0.6	11.3	81.6	4.0	2.1	0.7	11.7
1.55	80.3	3.9	2.1	0.6	13.1	81.5	4.3	2.0	1.3	10.9	80.2	4.1	2.1	0.7	12.9
1.60	80.2	3.9	2.0	0.6	13.3	80.5	4.3	2.0	1.3	11.9	79.2	4.1	1.9	0.9	13.9
1.65	79.4	3.9	2.0	0.8	13.9	78.3	4.2	1.9	5.3	10.2	78.7	4.0	1.9	1.1	14.4
1.70	78.5	3.9	1.9	1.2	14.5	78.8	4.4	1.9	1.1	13.7	77.8	4.0	1.9	2.0	14.3
1.75	78.0	3.7	1.8	0.6	16.0	78.0	4.7	1.9	1.9	13.5	77.8	4.2	1.9	2.9	13.2
1.80	75.2	4.3	1.9	1.4	17.3	74.9	4.5	2.0	2.8	15.8	77.5	4.1	1.8	2.2	14.4
1.85	75.0	3.9	1.9	1.4	17.8	75.7	4.6	2.0	3.1	14.7	75.6	3.9	1.8	3.3	15.5
1.90	67.0	3.5	1.8	8.8	18.9	66.7	3.8	1.6	10.0	18.0	74.7	4.4	1.9	2.9	16.2
1.95	74.9	4.1	1.9	2.1	17.0	74.5	5.0	1.9	2.6	15.9	74.0	4.4	1.8	3.6	16.1
2.00	74.4	4.0	1.9	1.1	18.6	73.0	4.6	1.9	3.7	16.7	68.5	3.6	1.9	5.4	20.7
2.05	68.5	3.8	1.8	7.2	18.8	69.9	4.3	1.8	6.6	17.4	66.6	4.3	1.7	7.0	20.4
2.10	72.4	4.1	1.7	1.8	20.1	65.9	3.9	1.6	2.3	26.3	67.4	4.6	1.8	4.4	21.9
2.15	66.1	3.8	1.7	8.9	19.5	65.9	4.8	1.9	4.1	23.3	65.9	4.1	1.5	5.5	22.9
2.20	61.3	3.9	1.2	8.0	25.6	56.8	4.7	1.5	8.3	28.8	59.5	3.6	1.4	12.5	22.9
Sink	52.9	5.4	1.4	6.9	33.3	30.8	7.3	1.0	4.2	56.7	44.1	5.9	1.3	7.8	40.9

* by difference

Table 4.6 Ash composition of original and density fractionated Middelbult coal (% dry ash-free basis)

Relative density (g/cm^3)	SiO_2	Al_2O_3	Fe_2O_3	P_2O_5	TiO_2	CaO	MgO	K_2O	Na_2O	SO_3
Original	53.6	27.1	2.17	0.63	1.62	6.87	2.37	0.53	0.60	3.52
1.40	39.9	25.6	1.02	0.86	1.35	17.3	5.26	0.36	0.93	7.02
1.45	43.0	27.0	1.13	2.35	1.43	16.0	3.89	0.32	0.76	3.90
1.50	42.8	25.5	2.34	1.97	1.23	16.5	4.64	0.28	0.63	3.56
1.55	45.3	26.4	0.95	1.68	1.32	17.3	4.12	0.32	0.60	0.55
1.60	52.0	28.3	1.05	0.78	1.49	8.79	3.15	0.36	0.53	3.42
1.65	49.4	27.4	1.50	0.50	1.69	10.6	3.79	0.50	0.62	3.52
1.70	57.2	27.8	1.54	0.46	1.98	5.62	2.26	0.41	0.45	2.21
1.75	57.9	28.7	1.39	0.10	1.73	4.81	2.45	0.27	0.39	1.77
1.80	58.8	30.9	1.87	0.52	2.34	2.01	0.91	0.74	0.37	1.30
1.85	58.3	29.5	1.42	0.55	1.74	4.00	1.47	0.59	0.35	2.05
1.90	42.9	23.3	22.5	0.34	1.43	3.86	1.74	0.41	0.23	2.59
1.95	63.3	26.6	2.82	0.28	2.54	1.28	0.72	0.62	0.51	1.34
2.00	63.2	29.4	0.41	0.28	2.65	1.12	0.63	0.45	0.34	1.11
2.05	55.2	24.3	9.89	0.30	2.21	3.27	1.24	0.61	0.34	2.34
2.10	63.4	26.1	1.85	0.41	1.86	4.40	0.50	0.47	0.29	0.54
2.15	51.4	26.4	16.0	0.37	1.68	1.17	0.52	0.66	0.35	0.96
2.20	56.4	21.1	9.28	0.31	2.17	6.31	0.64	0.50	0.27	2.04
Sink	68.2	23.9	2.68	0.01	2.25	0.50	0.35	0.67	0.27	0.80

Table 4.7 Ash composition of original and density fractionated Twistdraai coal (% dry ash-free basis)

Relative density (g/cm^3)	SiO_2	Al_2O_3	Fe_2O_3	P_2O_5	TiO_2	CaO	MgO	K_2O	Na_2O	SO_3
Original	50.1	25	5.9	0.8	1.29	7.8	2.01	1.04	0.47	5.53
1.40	46.8	28.3	1.68	1.08	1.45	10.6	4.74	0.73	0.75	3.33
1.45	46.2	28.6	2.28	1.56	2.00	9.41	3.13	0.73	0.70	3.64
1.50	47.5	28.0	1.31	1.32	2.43	8.68	4.24	0.99	0.71	3.30
1.55	43.7	23.8	6.10	0.89	2.43	13.9	6.51	0.53	0.61	1.22
1.60	46.4	28.4	3.97	1.34	2.59	6.73	4.84	1.13	0.52	3.16
1.65	30.2	19.1	24.5	1.19	0.86	13.6	5.30	0.66	0.36	3.81
1.70	57.9	29.4	2.10	0.51	2.04	2.17	1.35	1.05	0.41	1.50
1.75	58.9	24.8	5.19	0.67	2.05	3.13	0.81	1.25	0.31	2.07
1.80	59.4	24.6	3.66	0.58	1.44	3.41	2.24	1.89	0.33	2.05
1.85	52.9	28.2	11.9	0.27	1.34	1.27	0.75	1.07	0.26	1.20
1.90	31.2	14.0	37.9	0.30	0.73	6.11	2.68	0.50	0.13	4.78
1.95	60.2	27.1	4.23	0.25	1.98	2.04	1.24	1.25	0.35	1.29
2.00	62.5	21.2	6.87	0.18	0.90	3.76	0.84	1.44	0.25	1.62
2.05	58.2	18.1	12.8	0.18	1.72	2.97	1.99	1.68	0.24	2.00
2.10	44.5	19.3	2.93	0.49	1.03	27.2	1.28	0.97	0.31	0.54
2.15	67.4	19.3	4.61	0.08	1.35	2.62	1.11	1.63	0.14	1.40
2.20	57.2	25.3	8.89	0.05	0.86	2.73	0.97	1.66	0.24	1.89
Sink	58.8	32.7	1.62	0.10	1.17	0.83	0.62	1.83	0.39	0.77

Table 4.8 Ash composition of original and density fractionated SCS coal (% dry ash-free basis)

Relative density (g/cm^3)	SiO_2	Al_2O_3	Fe_2O_3	P_2O_5	TiO_2	CaO	MgO	K_2O	Na_2O	SO_3
Original	50.5	26.8	3.58	0.71	1.44	7.63	2.42	0.87	0.58	5.15
1.40	38.5	27.9	4.30	2.25	2.39	14.3	2.27	0.53	0.73	5.97
1.45	37.6	25.2	3.29	1.13	1.86	15.9	4.23	0.42	0.56	8.72
1.50	39.5	25.1	1.42	2.51	1.45	17.0	4.48	0.50	0.70	6.88
1.55	43.8	27.9	1.60	1.58	2.43	11.0	3.45	0.56	0.58	6.41
1.60	43.9	25.7	2.94	0.73	2.35	12.4	3.87	0.67	0.47	6.26
1.65	44.6	24.1	2.10	0.81	3.16	14.0	3.72	0.60	0.37	6.23
1.70	45.2	24.9	4.25	0.54	3.23	10.6	2.51	0.85	0.43	6.81
1.75	46.8	26.1	7.80	0.48	2.81	5.09	2.01	1.01	0.34	7.39
1.80	54.8	28.5	3.68	0.42	2.07	3.36	1.19	0.81	0.32	4.28
1.85	54.6	27.3	5.44	0.49	2.43	3.73	1.01	0.88	0.39	3.59
1.90	49.5	22.5	5.9	0.71	2.34	10.9	1.31	0.93	0.45	4.68
1.95	53.6	28.0	5.61	0.41	2.35	3.57	1.09	0.78	0.34	3.99
2.00	54.8	26.1	5.78	1.18	1.83	2.72	0.68	1.23	0.29	5.27
2.05	55.8	28.4	6.76	0.32	1.87	1.99	1.04	0.98	0.27	2.46
2.10	59.2	23.7	6.41	0.28	1.38	3.03	1.41	1.47	0.35	2.51
2.15	66.0	19.8	4.70	0.20	1.59	3.87	0.70	1.46	0.34	1.28
2.20	52.1	18.8	11.0	0.71	1.36	7.30	1.04	0.93	0.22	4.99
Sink	65.1	22.9	2.90	0.11	2.05	2.09	0.85	1.41	0.26	1.36

Table 4.9 Mineral distribution in original and density fractionated Middelbult coal (%)

Relative density (g/cm^3)	Calcite	Dolomite	Alunite	Pyrite	Quartz	Mica	Kaolinite	Siderite	Smectite
Original	3	9	5	4	20	-	59	-	-
1.40	5	9	9	-	12	-	65	-	-
1.45	5	13	-	-	7	-	57	4	14
1.50	5	18	-	-	12	-	54	-	10
1.55	5	23	-	-	8	-	56	-	7
1.60	-	9	-	-	24	-	58	-	10
1.65	5	12	9	2	14	-	59	-	-
1.70	2	5	9	-	16	5	58	-	6
1.75	2	10	-	-	22	-	60	-	6
1.80	1	3	7	-	23	13	53	-	-
1.85	-	-	16	-	34	-	50	-	-
1.90	3	2	11	-	27	-	58	-	-
1.95	-	-	7	-	52	-	40	-	-
2.00	1	3	5	-	47	-	44	-	-
2.05	-	-	5	1	48	-	46	-	-
2.10	2	-	5	2	51	-	41	-	-
2.15	1	4	6	10	51	-	28	-	-
2.20	-	2	-	-	55	-	43	-	-
Sink	-	-	-	1	52	10	36	-	-

Table 4.10 Mineral distribution in original and density fractionated Twistdraai coal (%)

Relative density (g/cm^3)	Calcite	Dolomite	Aragonite	K-feldspar	Alunite	Pyrite	Quartz	Mica	Kaolinite	Siderite
Original	3	8	-	-	-	6	19	8	54	-
1.40	-	3	-	-	7	2	19	-	53	15
1.45	5	15	-	-	-	-	18	-	62	-
1.50	3	23	-	-	-	-	17	-	56	-
1.55	6	21	-	-	9	3	9	-	31	21
1.60	-	2	-	-	5	2	20	-	71	-
1.65	1	9	6	-	16	3	5	-	60	-
1.70	5	16	25	-	-	2	9	-	44	-
1.75	2	-	-	54	-	1	14	-	29	-
1.80	-	-	-	5	4	1	46	8	37	-
1.85	2	4	-	-	6	-	10	11	68	-
1.90	1	5	-	-	-	5	36	-	53	-
1.95	2	5	-	8	7	2	41	-	37	-
2.00	-	1	3	-	4	1	18	15	59	-
2.05	4	2	-	5	-	1	28	15	44	-
2.10	1	2	36	-	-	3	8	15	35	-
2.15	1	1	-	-	-	-	16	20	62	-
2.20	-	4	-	-	-	1	14	24	56	-
Sink	-	-	-	5	-	-	42	7	46	-

Table 4.11 Mineral distribution in original and density fractionated SCS coal (%)

Relative density (g/cm^3)	Calcite	Dolomite	Aragonite	Hematite	K-feldspar	Alunite	Pyrite	Quartz	Mica	Kaolinite
Original	2	9	-	-	-	4	5	26	-	54
1.40	-	10	-	-	-	-	3	11	-	76
1.45	4	5	-	-	-	11	-	12	-	68
1.50	4	11	-	-	-	12	-	19	-	55
1.55	-	7	-	3	-	16	-	14	-	61
1.60	6	23	-	-	-	14	2	12	-	44
1.65	5	8	-	-	-	15	1	19	-	52
1.70	-	2	-	-	-	10	-	28	-	61
1.75	2	-	-	-	-	15	1	26	-	57
1.80	12	-	-	-	-	3	-	22	4	58
1.85	2	3	-	-	-	7	-	33	7	48
1.90	-	-	-	-	-	14	4	29	-	52
1.95	-	-	-	-	-	5	2	25	24	45
2.00	3	-	-	-	-	11	2	43	-	41
2.05	4	-	-	-	-	6	2	26	-	62
2.10	2	-	5	-	-	-	1	43	16	34
2.15	3	2	-	-	-	3	7	25	20	40
2.20	3	-	10	-	-	9	5	36	-	37
Sink	-	-	3	-	3	-	1	42	12	38

Table 4.12 Mössbauer parameters on original and density fractionated Middelbult, Twistdraai and SCS coals (mineral %)

	Relative density (g/cm^3)	Mineral	δ^* ($mm.s^{-1}$)	Δ ($mm.s^{-1}$)	Relative area (%)
Middelbult	Original	Pyrite	0.27	0.55	100
	1.40	Pyrite	0.25	0.56	100
	1.70	Pyrite	0.27	0.60	100
	2.20	Pyrite	0.27	0.61	100
	Sink	Pyrite	0.21	0.55	50
		Illite	0.89	2.33	22
		Montmorrillonite	0.38	0.57	28
Twistdraai	Original	Pyrite	0.23	0.55	100
	1.40	Pyrite	0.28	0.55	100
	1.70	Pyrite	0.26	0.64	100
	2.20	Pyrite	0.28	0.62	100
	Sink	Pyrite	0.26	0.66	100
SCS	Original	Pyrite	0.28	0.66	100
	1.40	Pyrite	0.28	0.57	100
	1.70	Pyrite	0.28	0.56	100
	2.20	Pyrite	0.27	0.61	100
	Sink	Pyrite	0.25	0.60	55
		Illite	1.05	2.21	18
		Montmorrillonite	0.38	0.57	27
Typical literature values for mineral identification (Stevens *et al.*, 1998)		Pyrite	0.25-0.30	0.57-0.62	
		Illite	0.92-1.10	2.02-2.55	
		Montmorrillonite (up to 3 doublets)	0.25-0.38	0.31-0.81	

* Note: Isomer shift relative to α-Fe

Table 4.13 Maceral and mineral group analyses on original and density fractionated Middelbult, Twistdraai and SCS coals (% by volume)

		MACERAL (% by volume mineral matter-free basis)				MACERAL (% by volume mineral matter basis)				MINERAL GROUP (% mineral matter basis)			
	Relative density (g/cm^3)	Vitrinite	Liptinite	Inertinite	Total reactive macerals	Vitrinite	Liptinite	Inertinite	Visible minerals	Clays and quartz	Pyrite	Carbonates	Clean coal
Middelbult	Original	21	4	75	47	18	3	64	15	44	5	15	36
	1.40-1.55	29	5	66	55	27	5	62	6	17	1	14	68
	1.60-1.75	5	2	93	40	4	2	77	17	52	3	22	23
	1.80-1.95	8	1	91	39	5	1	55	39	66	13	9	12
	2.00-2.20	5	1	94	33	2	<1	39	59	83	9	4	4
	Sink	5	2	93	30	0.2	0.1	3.7	96.0	88	10	1	1
Twistdraai	Original	31	5	64	55	27	5	55	13	39	8	10	43
	1.40-1.55	22	5	73	50	21	5	68	6	28	5	6	61
	1.60-1.75	24	5	71	48	19	4	55	22	43	12	10	35
	1.80-1.95	26	5	69	49	17	3	45	35	59	12	8	21
	2.00-2.20	17	2	81	41	7	1	33	59	79	11	5	5
	Sink	24	3	73	47	6	<1	19	75	70	19	6	5
SCS blend	Original	26	5	69	56	23	4	60	13	44	5	14	37
	1.40-1.55	36	5	59	60	34	5	54	7	23	6	12	59
	1.60-1.75	10	4	86	45	8	3	69	20	52	8	17	23
	1.80-1.95	13	3	84	44	8	2	50	40	70	12	5	13
	2.00-2.20	13	3	84	44	5	1	31	63	81	8	5	6
	Sink	3	3	94	29	0.2	0.2	5.6	94	88	3	8	1

Table 4.14 Microlithotype and visible minerals analyses on original and density fractionated Middelbult, Twistdraai and SCS coals (% by volume)

		MICROLITHOTYPE (MINERAL MATTER BASIS)			VISIBLE MINERALS: CARBOMINERITE				VISIBLE MINERALS: MINERITE			
	Relative density (g/cm^3)	Vitrite	Inertite	Intermediate	Carbagilite	Carbosilicite	Carbopyrite	Carbankerite	Clays	Quartz	Pyrite	Carbonates
Middelbult	Original	8	36	29	14	3	1	4	1	2	1	1
	1.40-1.55	11	42	37	5	1	<1	2	1	1	<1	<1
	1.60-1.75	6	52	12	14	3	1	6	2	1	<1	3
	1.80-1.95	4	28	11	29	6	2	4	7	3	4	2
	2.00-2.20	1	19	3	18	8	2	1	36	6	3	3
	Sink	<1	1	<1	3	5	1	<1	28	53	7	2
Twistdraai	Original	9	32	31	12	2	2	3	2	4	2	1
	1.40-1.55	10	48	29	7	1	1	2	<1	<1	<1	2
	1.60-1.75	7	31	27	15	3	2	5	1	4	4	1
	1.80-1.95	10	14	21	22	4	2	2	6	7	9	3
	2.00-2.20	3	9	12	15	5	2	2	19	21	7	5
	Sink	2	6	7	3	3	1	3	28	32	12	3
SCS blend	Original	10	33	30	13	2	2	3	2	2	2	1
	1.40-1.55	13	37	40	4	1	2	1	1	<1	<1	1
	1.60-1.75	4	50	17	14	3	1	5	2	2	1	1
	1.80-1.95	5	23	11	29	8	2	4	10	4	2	2
	2.00-2.20	4	8	5	20	10	2	3	22	18	6	2
	Sink	<1	<1	1	3	6	<1	<1	23	52	3	12

Table 4.15 Rank and general condition analyses on original and density fractionated Middelbult, Twistdraai and SCS coals

		RANK				WEATHERING			
	Relative density (g/cm^3)	Rank	ECE-UN in SEAM classification	Mean random reflectance (%)	Standard deviation	Cracks and fissures	Signs of severe weathering	Particles exhibiting oxidation rims	Heat altered
Middelbult	Original	Ortho-bituminous	Medium Rank C	0.66	0.066	Common	Occasional	None	None
	1.40-1.55	Ortho-bituminous	Medium Rank C	0.69	0.059	Common	Occasional	None	None
	1.60-1.75	Ortho-bituminous	Medium Rank C	0.71	0.088	Common	Occasional	None	None
	1.80-1.95	Ortho-bituminous	Medium Rank C	0.65	0.112	Common	Occasional	None	None
	2.00-2.20	Ortho-bituminous	Medium Rank C	0.65	0.103	Common	Occasional	None	None
	Sink	Ortho-bituminous	Medium Rank C	0.65	0.114	Common	Occasional	None	None
Twistdraai	Original	Ortho-bituminous	Medium Rank C	0.63	0.064	Common	Occasional	None	None
	1.40-1.55	Ortho-bituminous	Medium Rank C	0.63	0.057	Common	Occasional	None	None
	1.60-1.75	Ortho-bituminous	Medium Rank C	0.63	0.057	Common	Occasional	None	None
	1.80-1.95	Ortho-bituminous	Medium Rank C	0.64	0.060	Common	Occasional	None	None
	2.00-2.20	Ortho-bituminous	Medium Rank C	0.63	0.057	Common	Occasional	None	None
	Sink	Ortho-bituminous	Medium Rank C	0.67	0.069	Common	Occasional	None	None
SCS blend	Original	Ortho-bituminous	Medium Rank C	0.65	0.091	Common	Occasional	None	None
	1.40-1.55	Ortho-bituminous	Medium Rank C	0.60	0.065	Common	Occasional	None	None
	1.60-1.75	Ortho-bituminous	Medium Rank C	0.64	0.087	Common	Occasional	None	None
	1.80-1.95	Ortho-bituminous	Medium Rank C	0.62	0.094	Common	Occasional	None	None
	2.00-2.20	Ortho-bituminous	Medium Rank C	0.61	0.077	Common	Occasional	None	None
	Sink	Ortho-bituminous	Medium Rank C	0.63	0.076	Common	Occasional	None	None

Table 4.16 Mineral abundance as determined by CCSEM on original and density fractionated Middelbult, Twistdraai and SCS coals
(mass %)

	Relative density (g/cm^3)	Pyrite	Quartz	Feldspar	Muscovite/ Illite	Kaolinite	Fe-oxide/ hydroxide	Calcite	Dolomite	Ankerite/ Siderite	Apatite	Anatase/ Rutile	Other	Coal
Middelbult	Original	0.5	6.9	0.4	0.9	16.7	0.04	3.1	2.7	0.2	0.1	0.1	0.1	68.4
	1.40-1.55	0.8	1.8	0.5	1.3	7.0	0.0	3.1	2.5	0.1	0.2	0.1	0.1	82.3
	1.60-1.75	0.3	5.1	0.7	1.4	17.8	0.0	2.1	3.8	0.1	0.0	0.1	0.1	68.4
	1.80-1.95	4.6	9.9	1.6	3.9	25.9	0.0	3.4	1.2	0.1	0.0	0.3	0.1	48.9
	2.00-2.20	1.4	14.0	2.3	6.1	35.0	0.0	4.0	0.7	0.0	0.3	0.1	0.0	36.0
	Sink	9.6	29.4	3.4	6.0	38.1	0.0	3.3	0.2	0.1	0.0	0.2	0.0	9.4
Twistdraai	Original	5.1	5.3	0.4	1.3	12.7	0.1	3.4	1.9	0.1	0.0	0.1	0.3	69.2
	1.40-1.55	4.0	1.0	0.3	1.2	10.0	0.0	1.9	1.3	0.0	0.1	0.0	0.0	80.1
	1.60-1.75	14.7	4.5	0.8	2.0	15.1	0.0	0.7	2.0	0.0	0.0	0.1	0.1	59.9
	1.80-1.95	16.9	9.5	1.5	5.9	21.0	0.0	2.6	1.8	0.1	0.2	0.1	0.1	40.2
	2.00-2.20	9.2	19.3	3.5	7.1	28.0	0.0	7.0	1.5	0.1	0.1	0.3	0.1	23.8
	Sink	20.3	21.7	3.6	8.1	31.0	0.0	3.3	3.7	0.1	0.2	0.2	0.1	7.5
SCS blend	Original	1.4	5.9	0.4	0.9	16.5	0.4	4.1	4.7	0.2	0.2	0.03	0.0	65.3
	1.40-1.55	1.4	1.4	0.3	0.9	7.9	0.0	2.1	1.5	0.1	0.2	0.1	0.1	84.1
	1.60-1.75	1.7	5.4	1.1	2.4	16.8	0.0	3.7	1.1	0.1	0.1	0.1	0.1	67.5
	1.80-1.95	9.2	9.7	2.3	4.7	23.6	0.2	1.8	0.8	0.1	0.2	0.1	0.1	47.2
	2.00-2.20	6.8	19.7	3.9	7.4	28.4	0.1	2.9	1.0	0.0	0.1	0.2	0.4	29.0
	Sink	0.8	20.7	1.9	8.3	30.7	26.1	0.3	0.2	0.9	0.0	0.2	0.4	9.4

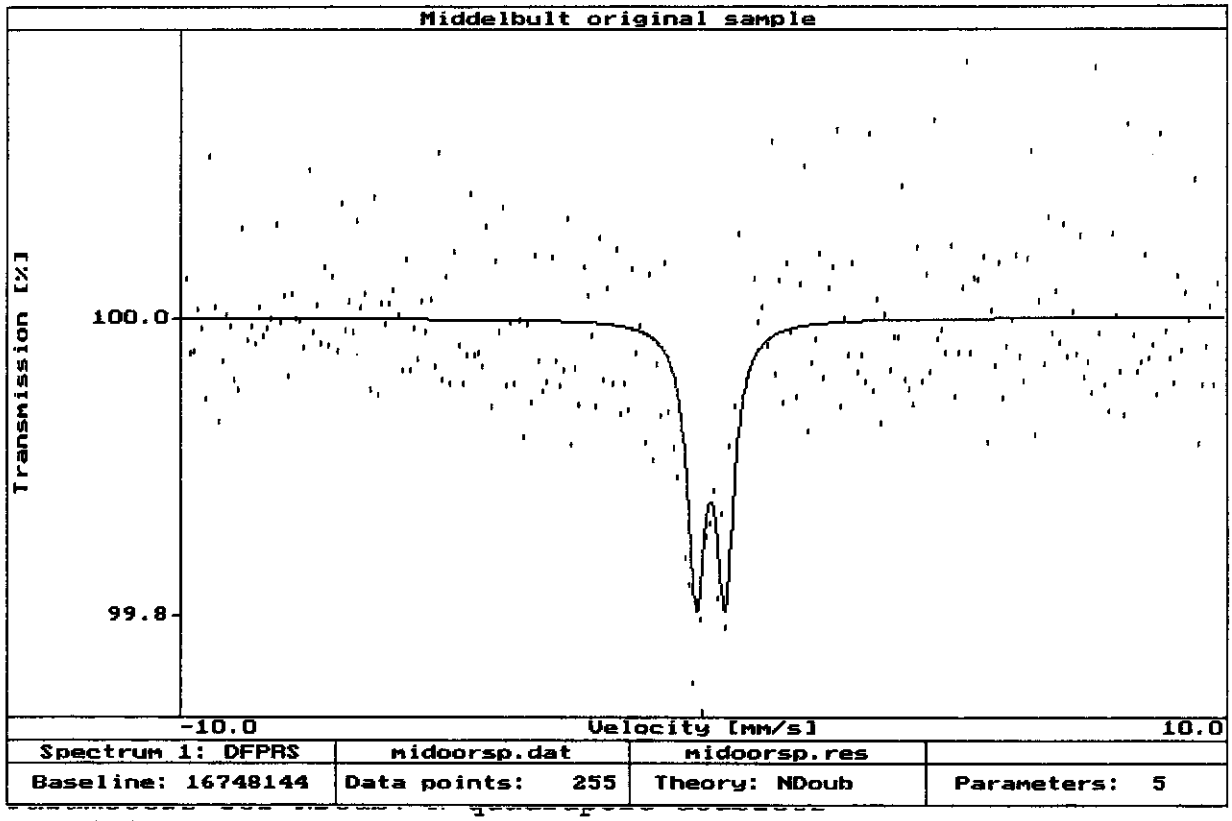

fitresults of data :
Middelbult original sample

foldingpoint	256.0				
geometryeffect	0.011 %				
theory	C:\PCMOS\NDoub.exe				
date	Tue Feb 22 22:32:57 2005				
flags	--PCE-				
fitspectra	1				
chi2	4.0935				
chi2-test	0.0000 %				
corr-test	0.0376 %				
fitcycles	3				
maxiter	25				
parasig	1				
chi2sig	1				
fitparameter	5				
Baseline	16752427	16748144	276.71645	0.999	0.996
Total Area	0.00130	0.00143	0.00008	1.017	0.950
Quad split 1	0.55000	0.55080	0.01890	1.000	0.958
Iso shift 1	0.16080	0.16008	0.01250	0.010	1.030
Width 1	0.45440	0.40562	0.04023	1.119	0.828

Figure 4.19 Mössbauer spectrum of original Middelbult coal

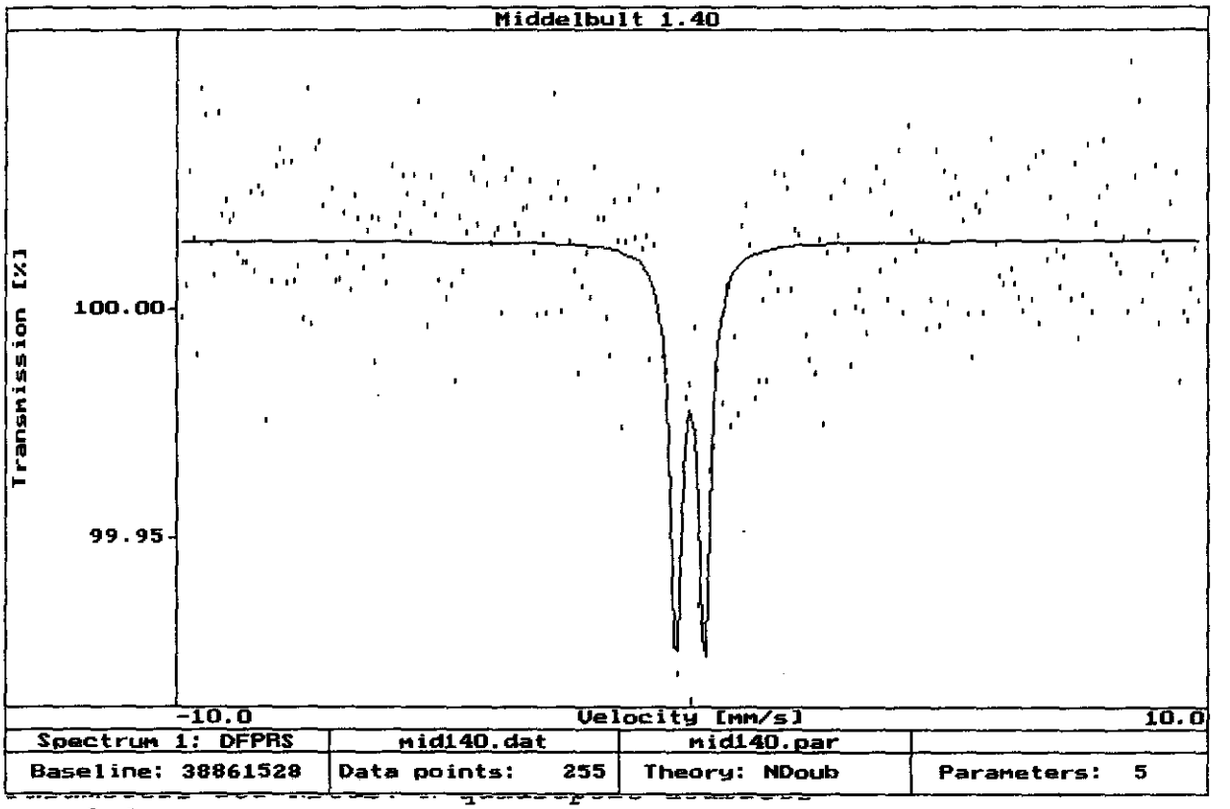


```
fitresults of data :
Middelbult 1.40
foldingpoint          256.0
geometryeffect          0.018 %
theory           C:\PCMOS\NDoub.exe
date             Tue Feb 22 22:40:53 2005
flags            ---CE-
fitspectra              1
chi2                    0.8788
chi2-test              91.6767 %
corr-test              68.6774 %
fitcycles               7
maxiter                25
parasig                 1
chi2sig                 1
fitparameter            5
Baseline            38855724      38861528      414.61029     0.993     0.997
Total Area            0.00053       0.00051        0.00005     0.985     0.930
Quad split 1          0.55582       0.55579        0.02894     1.007     0.984
Iso shift  1          0.14053       0.14356        0.01570     1.025     1.025
Width      1          0.45440       0.28444        0.04052     1.093     0.789
```

Figure 4.20 Mössbauer spectrum of 1.40 RD Middelbult coal

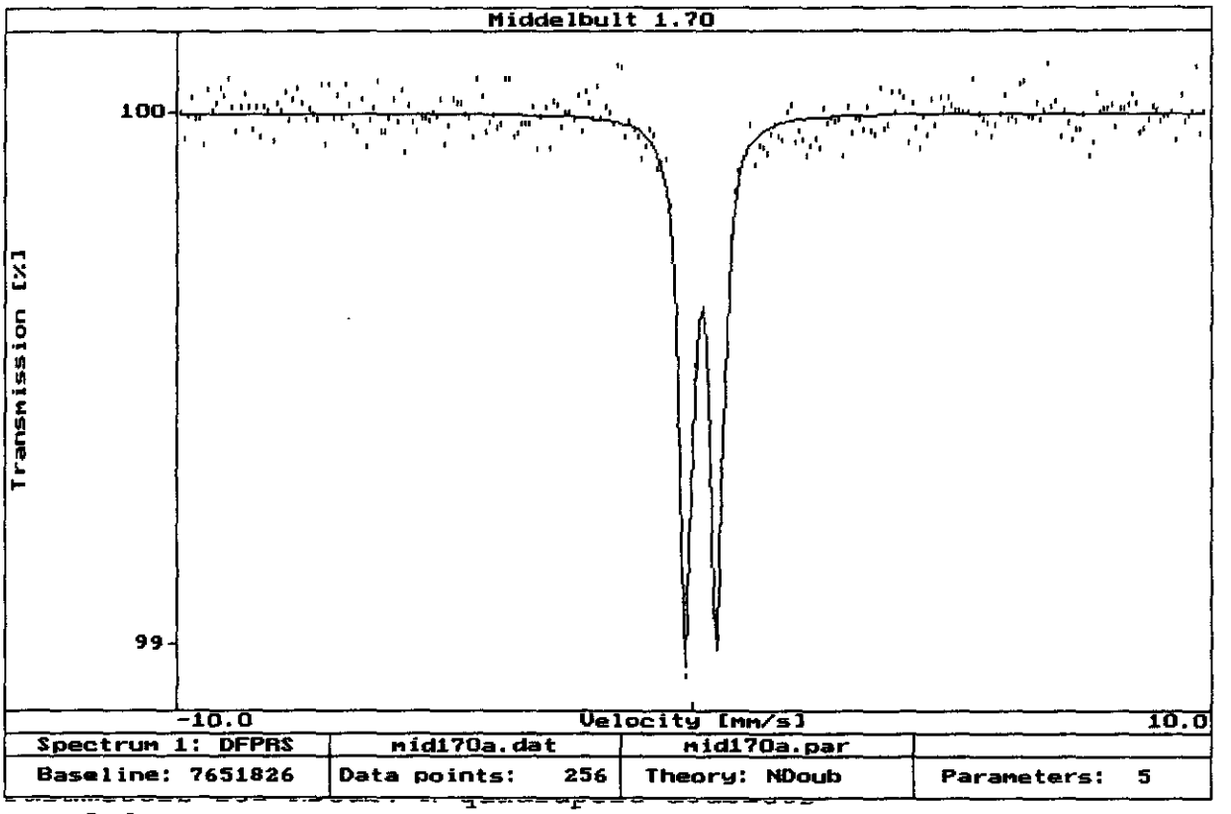

fitresults of data :
Middelbult 1.70

foldingpoint	255.5				
geometryeffect	0.012 %				
theory	C:\PCMOS\NDoub.exe				
date	Tue Feb 22 22:53:03 2005				
flags	--PCE-				
fitspectra	1				
chi2	0.8860				
chi2-test	90.2999 %				
corr-test	48.2374 %				
fitcycles	4				
maxiter	25				
parasig	1				
chi2sig	1				
fitparameter	5				
Baseline	7652012	7651826	183.93416	1.001	1.000
Total Area	0.00830	0.00570	0.00011	1.010	0.997
Quad split 1	0.61000	0.60524	0.00600	0.995	0.989
Iso shift 1	0.17030	0.16009	0.00321	0.993	0.993
Width 1	0.45440	0.28819	0.00821	1.045	0.979

Figure 4.21 Mössbauer spectrum of 1.70 RD Middelbult coal

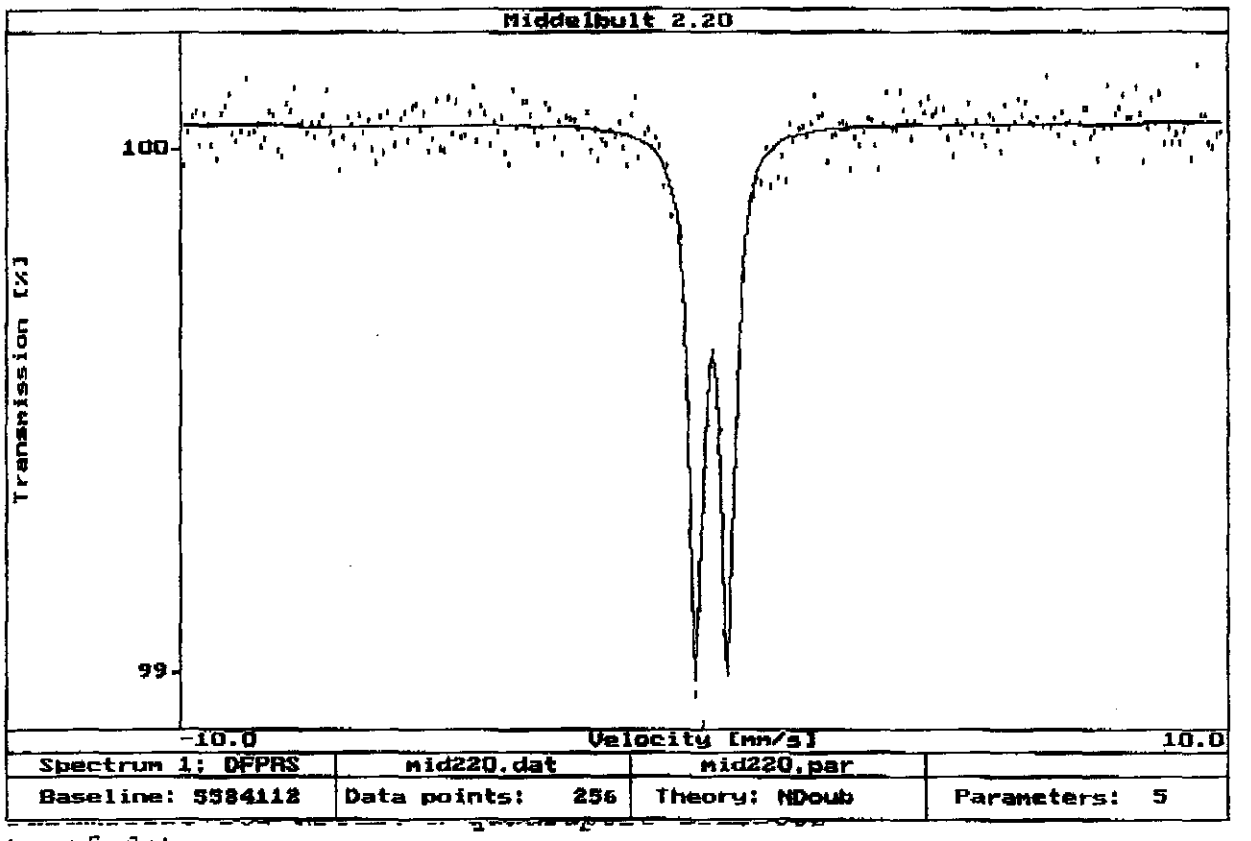

sults of data :
lbult 2.20
igpoint 255.5
:ryeffect 0.016 %
/ C:\PCMOS\NDoub.exe
Wed May 12 15:47:23 2004
--PCE-

ectra	1				
	0.7858				
:est	99.4856 %				
:est	59.7903 %				
:les	4				
er	25				
ig	1				
ig	1				
rameter	5				
ine	5581479	5584112	158.07240	0.999	0.999
Area	0.00830	0.00650	0.00013	1.001	0.985
split 1	0.61000	0.61453	0.00736	0.997	0.990
ift 1	0.17030	0.16501	0.00403	1.001	1.000
1	0.45440	0.32643	0.01027	1.032	0.954

Figure 4.22 Mössbauer spectrum of 2.20 RD Middelbult coal

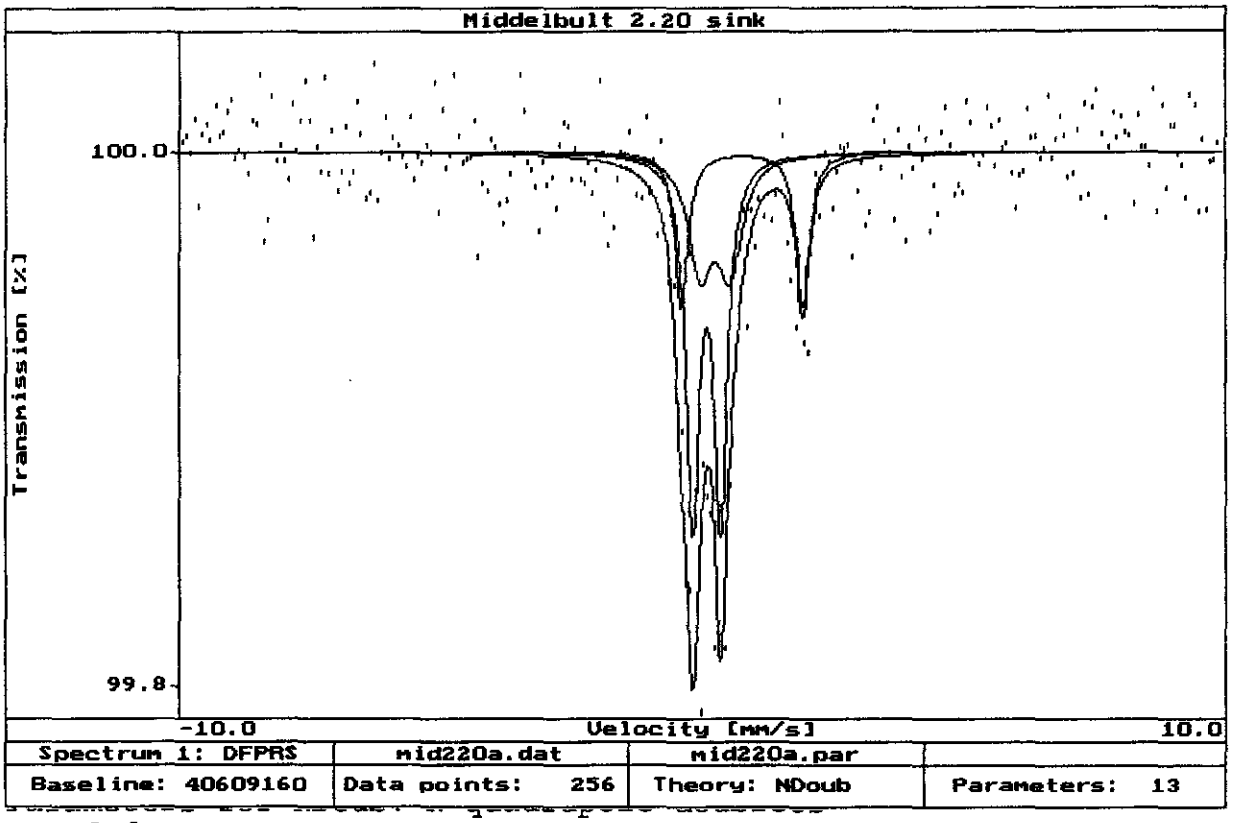

fitresults of data :
Middelbult 2.20 sink

foldingpoint	255.5				
geometryeffect	0.019 %				
theory	C:\PCMOS\NDoub.exe				
date	Tue Feb 22 22:48:27 2005				
flags	---CE-				
fitspectra	1				
chi2	0.9917				
chi2-test	52.4936 %				
corr-test	65.5687 %				
fitcycles	7				
maxiter	25				
parasig	1				
chi2sig	1				
fitparameter	13				
Baseline	40610612	40609160	445.75534	1.190	0.875
Total Area	0.00530	0.00163	0.00006	1.574	0.782
Quad split 1	0.56600	0.56600 F	0.00000	0.000	0.000
Iso shift 1	0.27030	0.27030 F	0.00000	0.000	0.000
Width 1	0.55440	0.55386	0.08264	3.322	0.746
Quad split 2	2.25000	2.32607	0.05108	0.698	0.813
Iso shift 2	0.98230	0.78336	0.02569	1.073	0.613
Width 2	0.55000	0.55000 F	0.00000	0.000	0.000
Area 2	0.27700	0.21634	0.02649	1.062	0.881
Quad split 3	0.59900	0.53425	0.02060	1.235	0.732
Iso shift 3	0.15230	0.10305	0.01601	1.714	0.709
Width 3	0.55000	0.55000 F	0.00000	0.000	0.000
Area 3	0.61700	0.50000	0.10169	3.117	0.516

Figure 4.23 Mössbauer spectrum of 2.20 SINK Middelbult coal

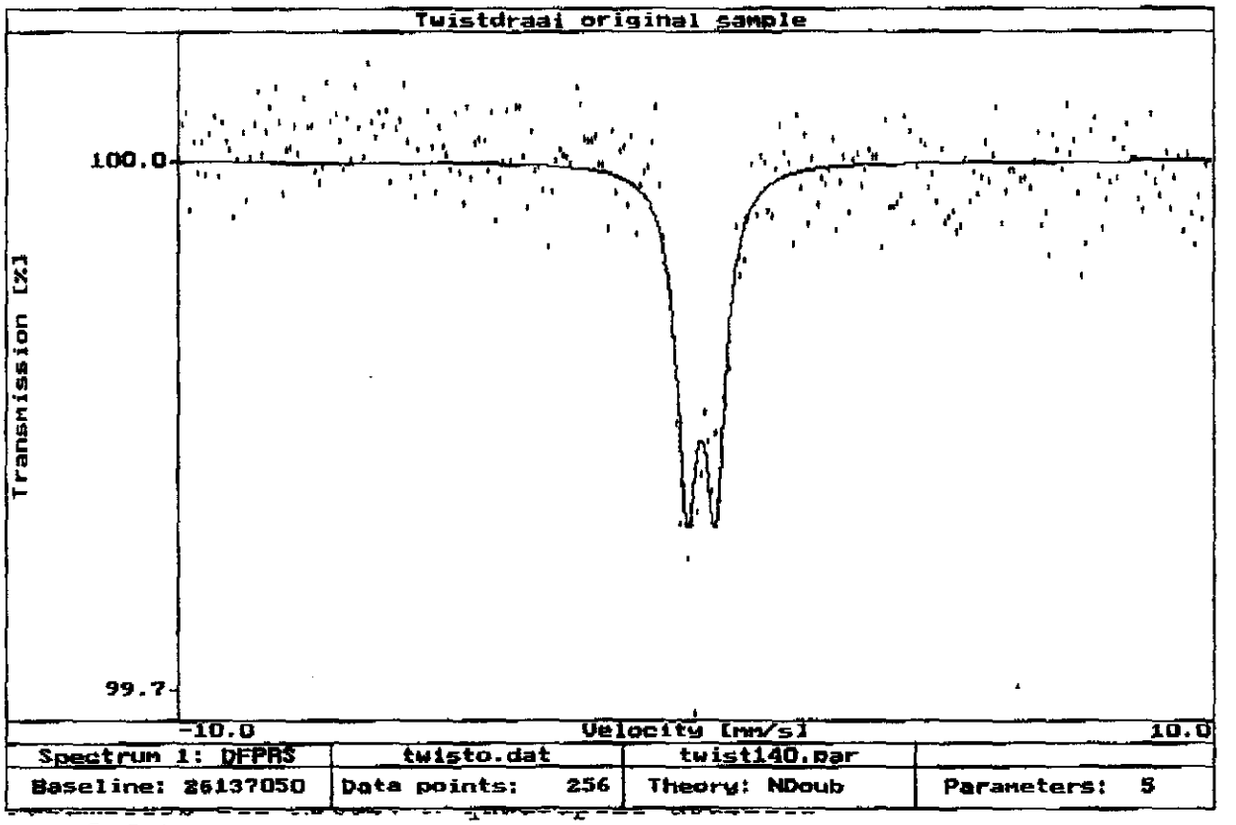


```
:esults of data :
;tdraai original sample
lingpoint          255.5
ietryeffect          0.009 %
)ry              C:\PCMOS\NDoub.exe
:                Fri Sep 24 21:19:04 2004
)s               ---CE-
spectra                1
?                      2.2126
?-test                 0.0000 %
:-test                 1.0826 %
:ycles                 4
iter                  25
asig                   1
?sig                   1
parameter              5
eline           26139476      26137050      350.69037     1.042     0.998
al Area             0.00130       0.00176       0.00007     1.212     1.037
i split 1           0.55000       0.55000 F     0.00000     0.000     0.000
 shift  1           0.07030       0.11870       0.01388     0.859     0.841
th      1           0.45440       0.49200       0.03762     1.501     1.072
```

Figure 4.24 Mössbauer spectrum of original Twistdraai coal

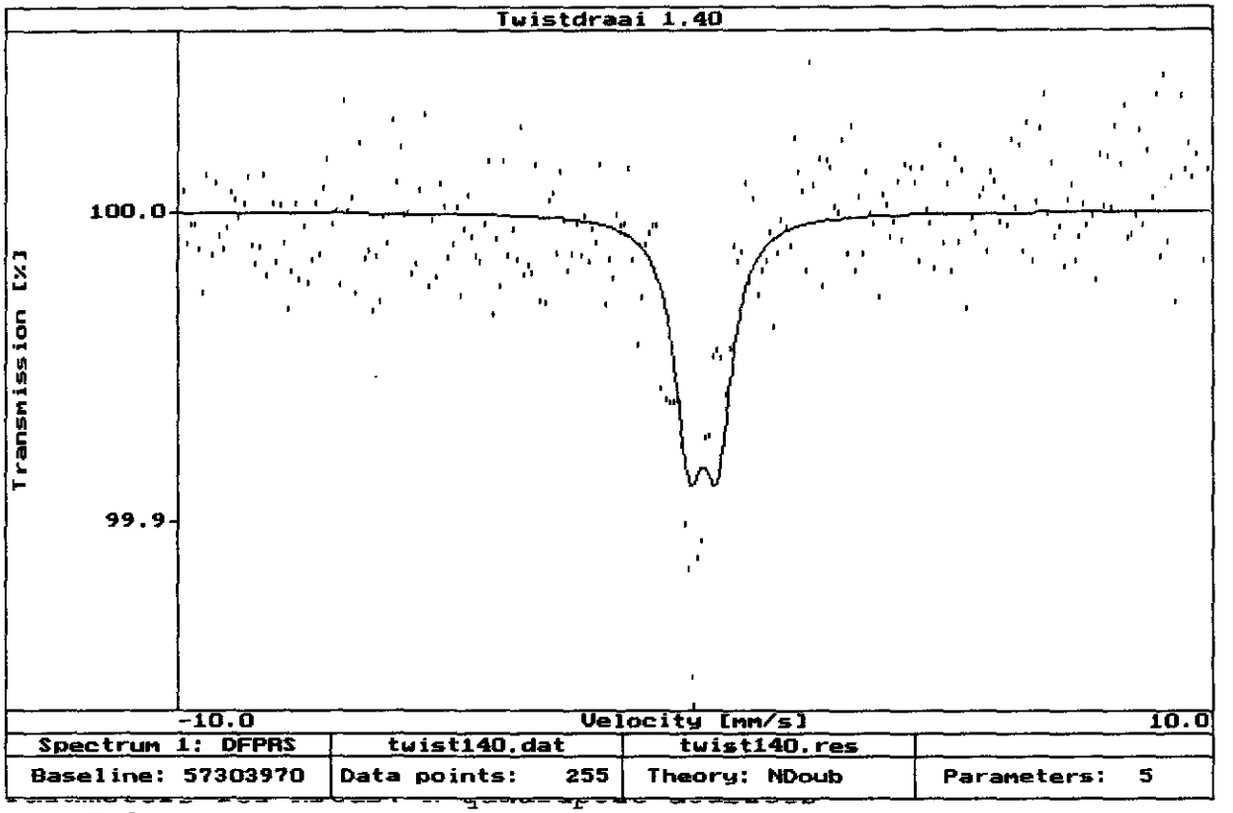


```
fitresults of data :
Twistdraai 1.40
foldingpoint          258.0
geometryeffect          0.018 %
theory              C:\PCMOS\NDoub.exe
date                Tue Feb 22 22:25:56 2005
flags               ---CE-
fitspectra              1
chi2                    1.8104
chi2-test               0.0000 %
corr-test              56.3551 %
fitcycles               4
maxiter                25
parasig                 1
chi2sig                 1
fitparameter            5
Baseline            57309870      57303970      544.47235     1.029     1.010
Total Area              0.00130       0.00093       0.00006     1.173     1.010
Quad split 1            0.55000       0.55000       0.00000     0.000     0.000
Iso shift  1            0.17030       0.17030       0.00000     0.000     0.000
Width      1            0.45440       0.68109       0.08600     1.365     0.995
```

Figure 4.25 Mössbauer spectrum of 1.40 RD Twistdraai coal

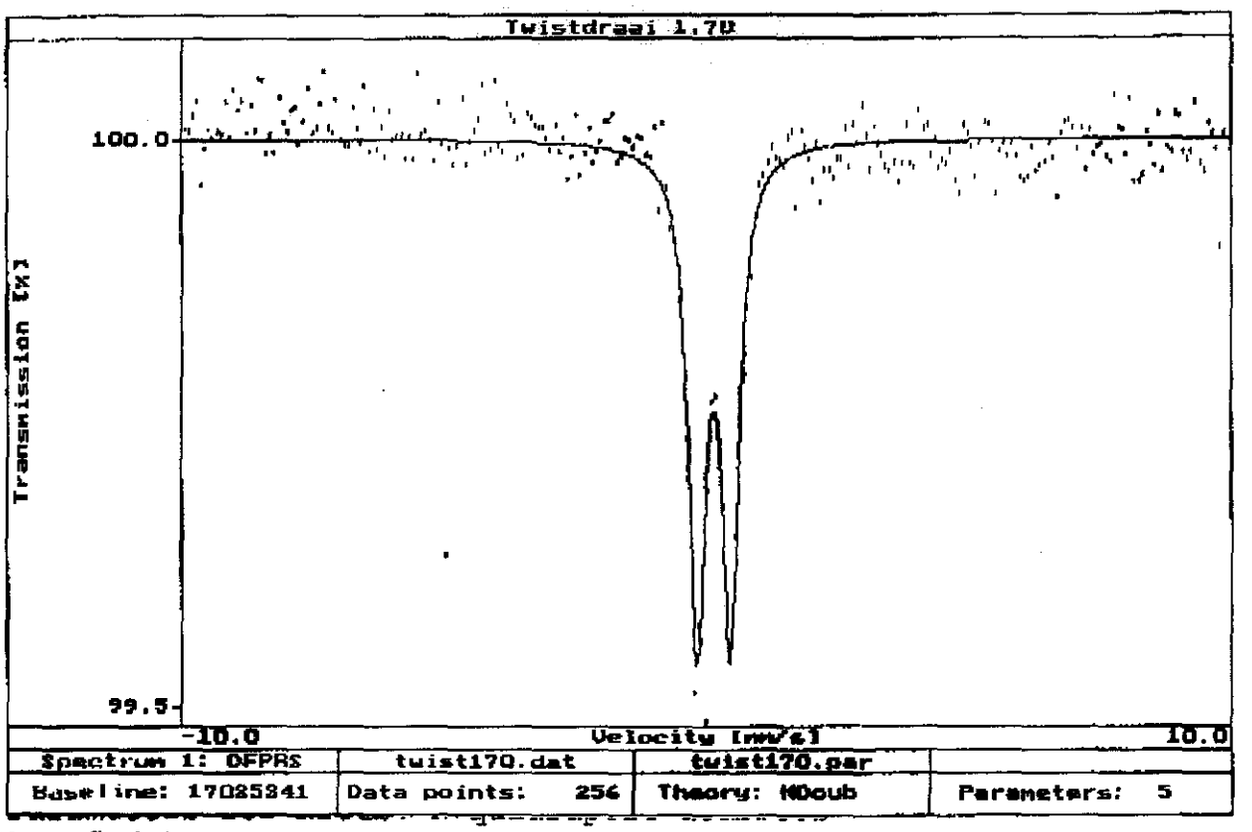

fitresults of data :
Twistdraai 1.70

foldingpoint	255.5				
geometryeffect	0.009 %				
theory	C:\PCMOS\NDoub.exe				
date	Thu Nov 04 15:53:09 2004				
flags	--PCE-				
fitspectra	1				
chi2	1.8734				
chi2-test	0.0000 %				
corr-test	33.0621 %				
fitcycles	6				
maxiter	25				
parasig	1				
chi2sig	1				
fitparameter	5				
Baseline	17026458	17025341	279.48912	1.002	1.000
Total Area	0.00130	0.00340	0.00008	1.020	0.995
Quad split 1	0.55000	0.63824	0.01082	0.986	0.980
Iso shift 1	0.07030	0.14881	0.00618	0.983	0.981
Width 1	0.45440	0.40122	0.01588	1.082	0.974

Figure 4.26 Mössbauer spectrum of 1.70 RD Twistdraai coal

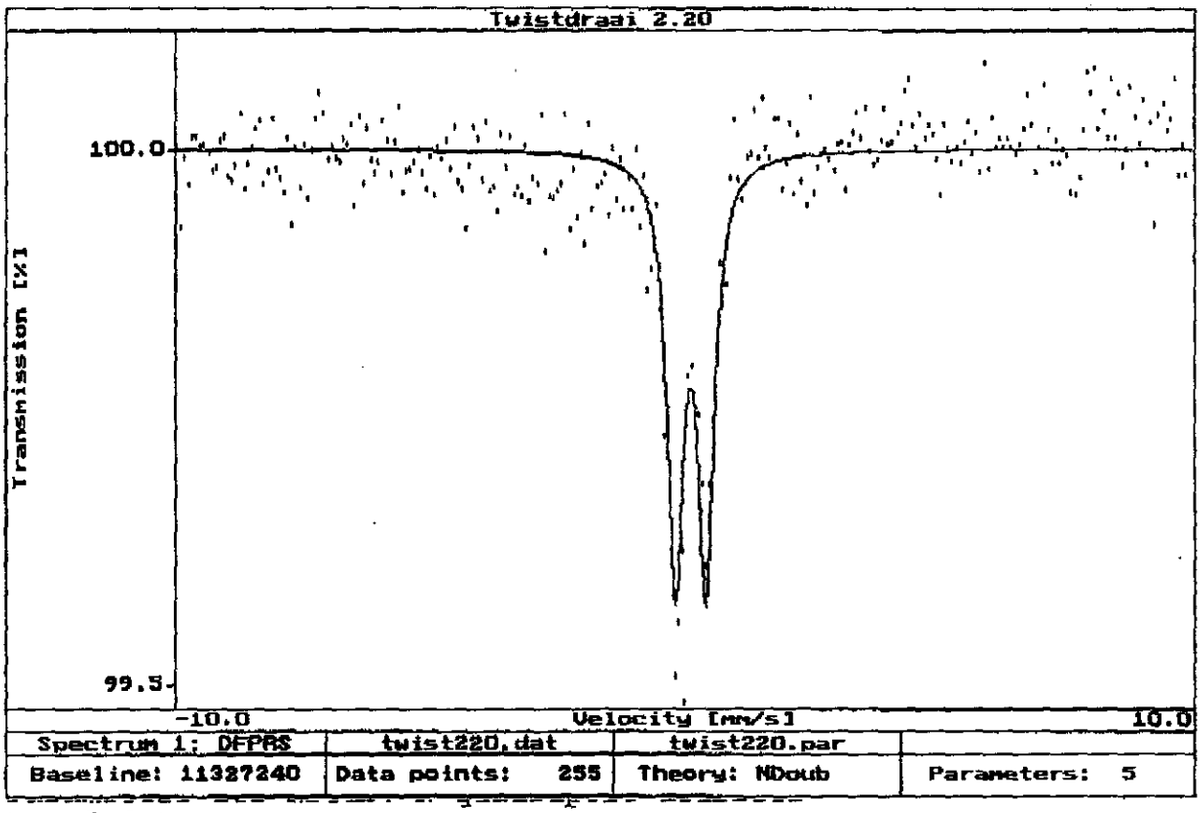


```
sults of data :
iraai 2.20
igpoint          256.0
:ryeffect          0.018 %
/             C:\PCMOS\NDoub.exe
              Wed May 12 16:07:05 2004
              ---CE-
actra                1
                     1.3441
:est                 0.0227 %
:est                 2.0046 %
:les                 5
er                  25
ig                   1
ig                   1
rameter              5
ine             11321635      11327240      227.92513     0.992     1.005
 Area               0.00830       0.00305       0.00010     0.988     0.995
split 1             0.61000       0.61504       0.01416     1.031     0.974
nift  1             0.17030       0.16617       0.00811     0.970     1.045
      1             0.45440       0.38993       0.02082     1.022     0.954
```

Figure 4.27 Mössbauer spectrum of 2.20 RD Twistdraai coal

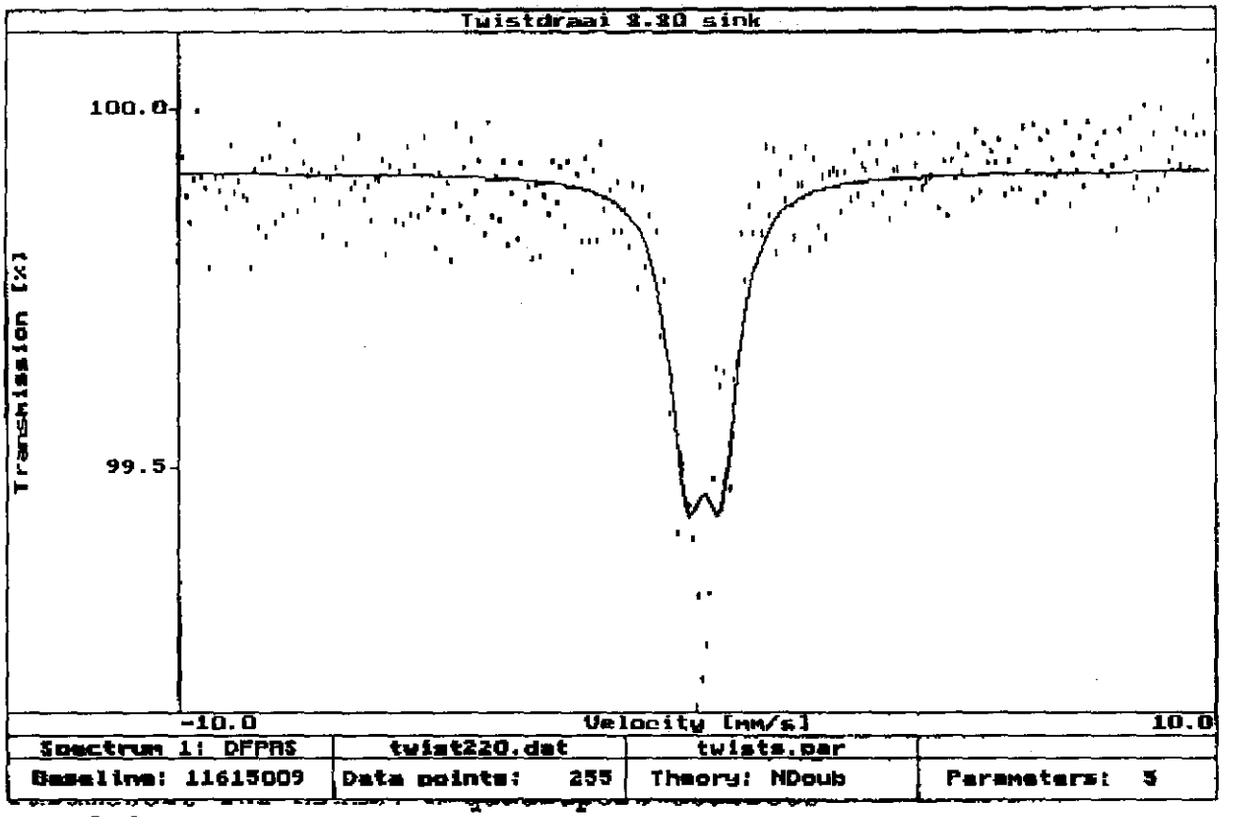

fitresults of data :
Twistdraai 2.20 sink

foldingpoint	258.5				
geometryeffect	0.018 %				
theory	C:\PCMOS\NDoub.exe				
date	Thu Nov 04 15:55:41 2004				
flags	---CE-				
fitspectra	1				
chi2	4.1546				
chi2-test	0.0000 %				
corr-test	25.3435 %				
fitcycles	6				
maxiter	25				
parasig	1				
chi2sig	1				
fitparameter	5				
Baseline	11625280	11615009	252.32924	1.794	0.465
Total Area	0.00130	0.00605	0.00016	2.808	0.164
Quad split 1	0.65820	0.65820 F	0.00000	0.000	0.000
Iso shift 1	0.14830	0.14830 F	0.00000	0.000	0.000
Width 1	0.45440	0.81898	0.03934	3.656	0.069

Figure 4.28 Mössbauer spectrum of 2.20 SINK Twistdraai coal

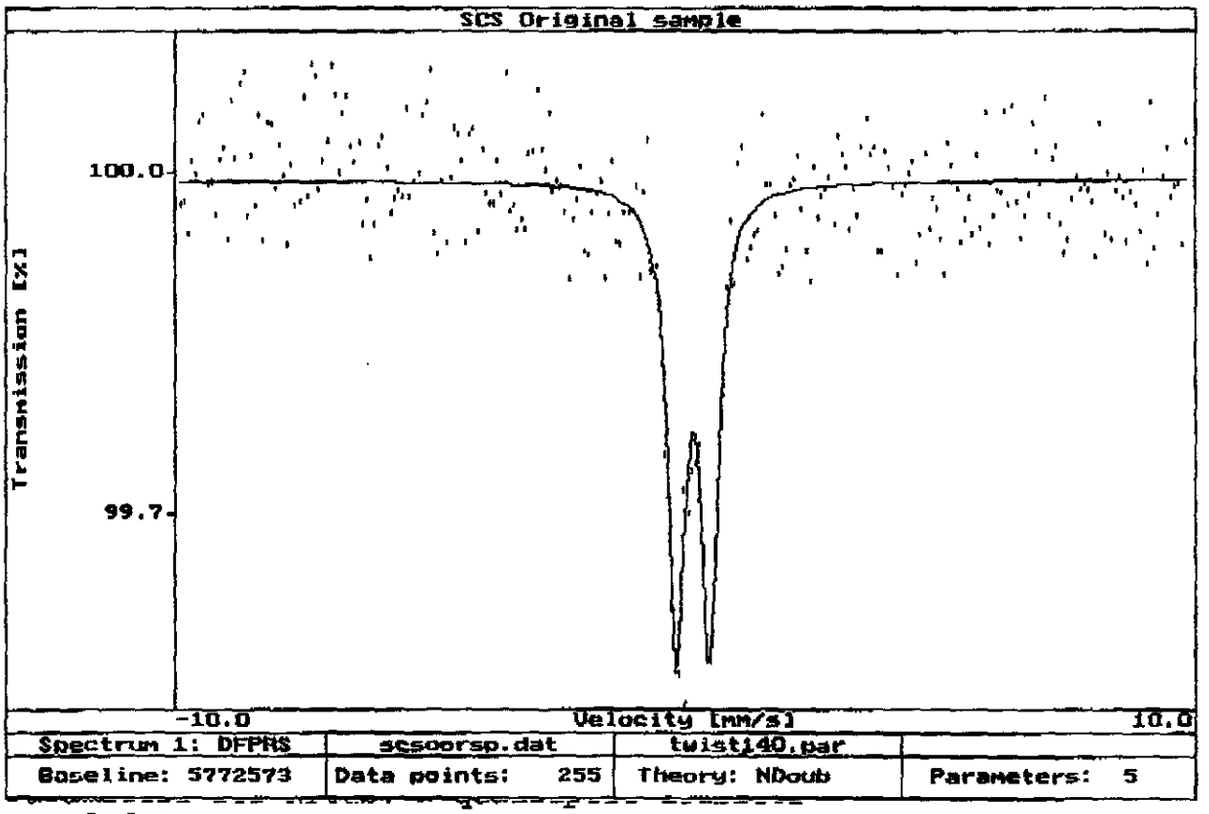


```
results of data :
 Original sample
lingpoint          256.0
metryeffect         -0.004 %
ory              C:\PCMOS\NDoub.exe
e                Fri Sep 24 21:23:45 2004
gs               --PCE-
spectra               1
2                     1.0350
2-test               33.8311 %
c-test               11.1856 %
cycles                7
iter                 25
asig                  1
2sig                  1
parameter             5
eline             5773040      5772573      163.15991    1.002    1.000
al Area            0.00130      0.00322        0.00014    1.029    0.987
d split 1          0.55000      0.65597        0.01961    1.017    1.006
 shift  1          0.07030      0.16883        0.01110    1.002    1.003
th      1          0.45440      0.39987        0.02852    1.103    0.917
```

Figure 4.29 Mössbauer spectrum of original SCS blend coal

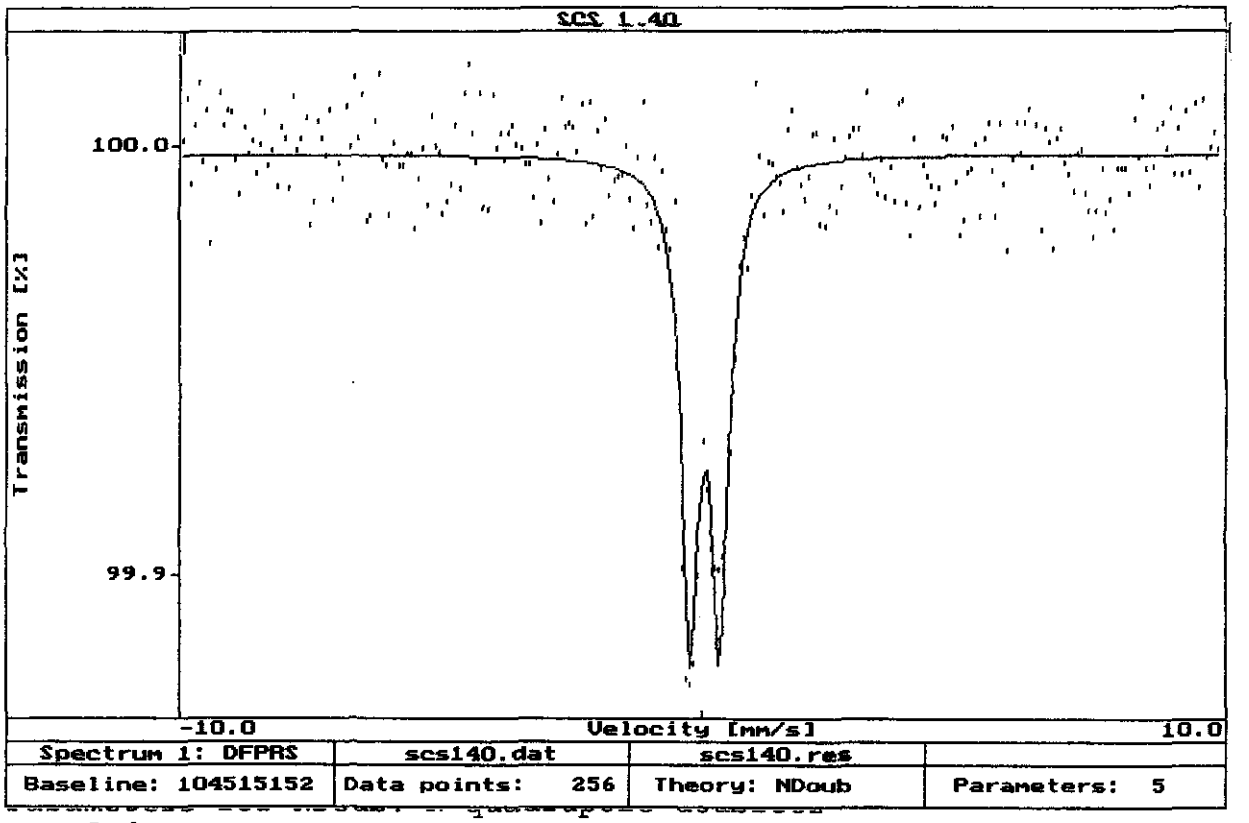

fitresults of data :
SCS 1.40

foldingpoint	255.5				
geometryeffect	0.014 %				
theory	C:\PCMOS\NDoub.exe				
date	Tue Feb 22 22:56:58 2005				
flags	---CE-				
fitspectra	1				
chi2	0.9558				
chi2-test	68.1675 %				
corr-test	70.8121 %				
fitcycles	6				
maxiter	25				
parasig	1				
chi2sig	1				
fitparameter	5				
Baseline	104517398	104515152	692.58970	1.018	1.008
Total Area	0.00053	0.00088	0.00003	1.125	1.057
Quad split 1	0.55582	0.57349	0.01735	0.949	0.913
Iso shift 1	0.14053	0.16645	0.01028	0.891	0.881
Width 1	0.45440	0.41068	0.02663	1.329	1.089

Figure 4.30 Mössbauer spectrum of 1.40 RD SCS blend coal

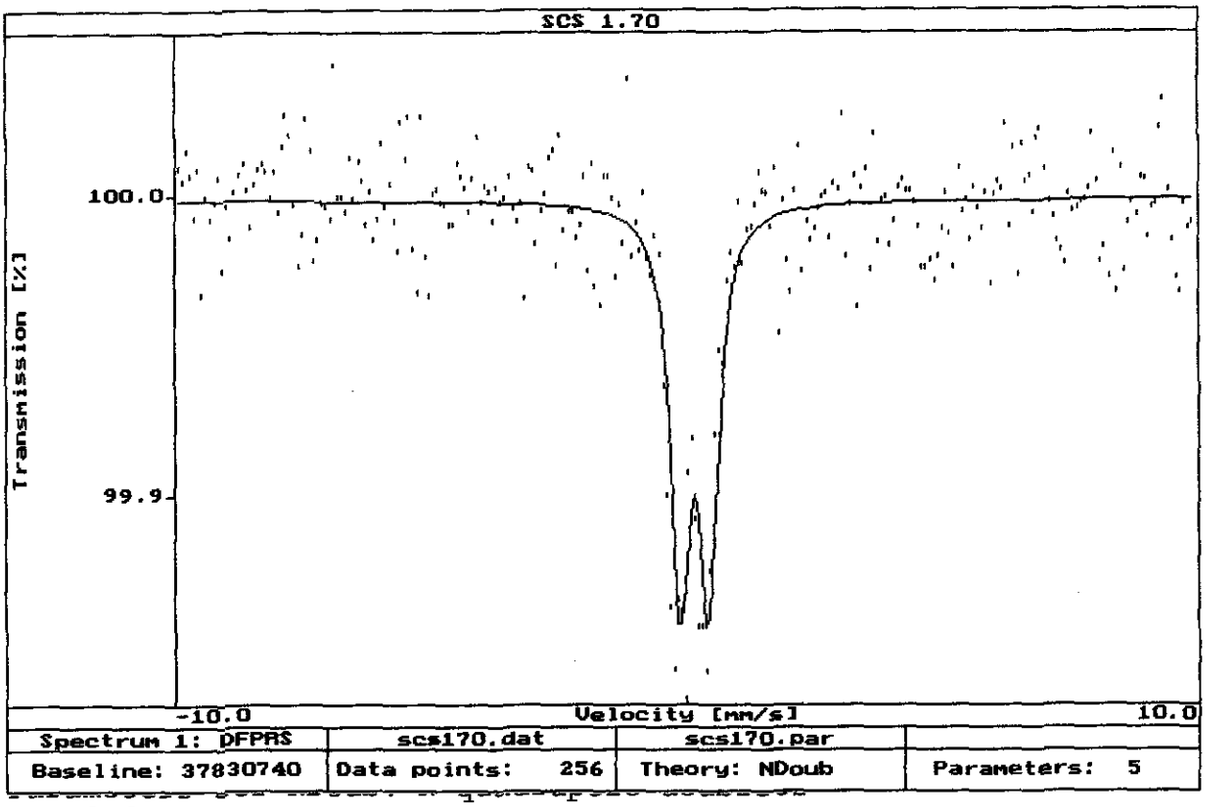

fitresults of data :
SCS 1.70

foldingpoint	255.5				
geometryeffect	0.012 %				
theory	C:\PCMOS\NDoub.exe				
date	Tue Feb 22 23:00:52 2005				
flags	--PCE-				
fitspectra	1				
chi2	0.9720				
chi2-test	61.3035 %				
corr-test	9.7884 %				
fitcycles	4				
maxiter	25				
parasig	1				
chi2sig	1				
fitparameter	5				
Baseline	37831522	37830740	419.25154	1.011	1.008
Total Area	0.00830	0.00113	0.00006	1.093	1.030
Quad split 1	0.61000	0.56111	0.02495	0.947	0.951
Iso shift 1	0.17030	0.17030 F	0.00000	0.000	0.000
Width 1	0.45440	0.44524	0.03995	1.295	1.011

Figure 4.31 Mössbauer spectrum of 1.70 RD SCS blend coal

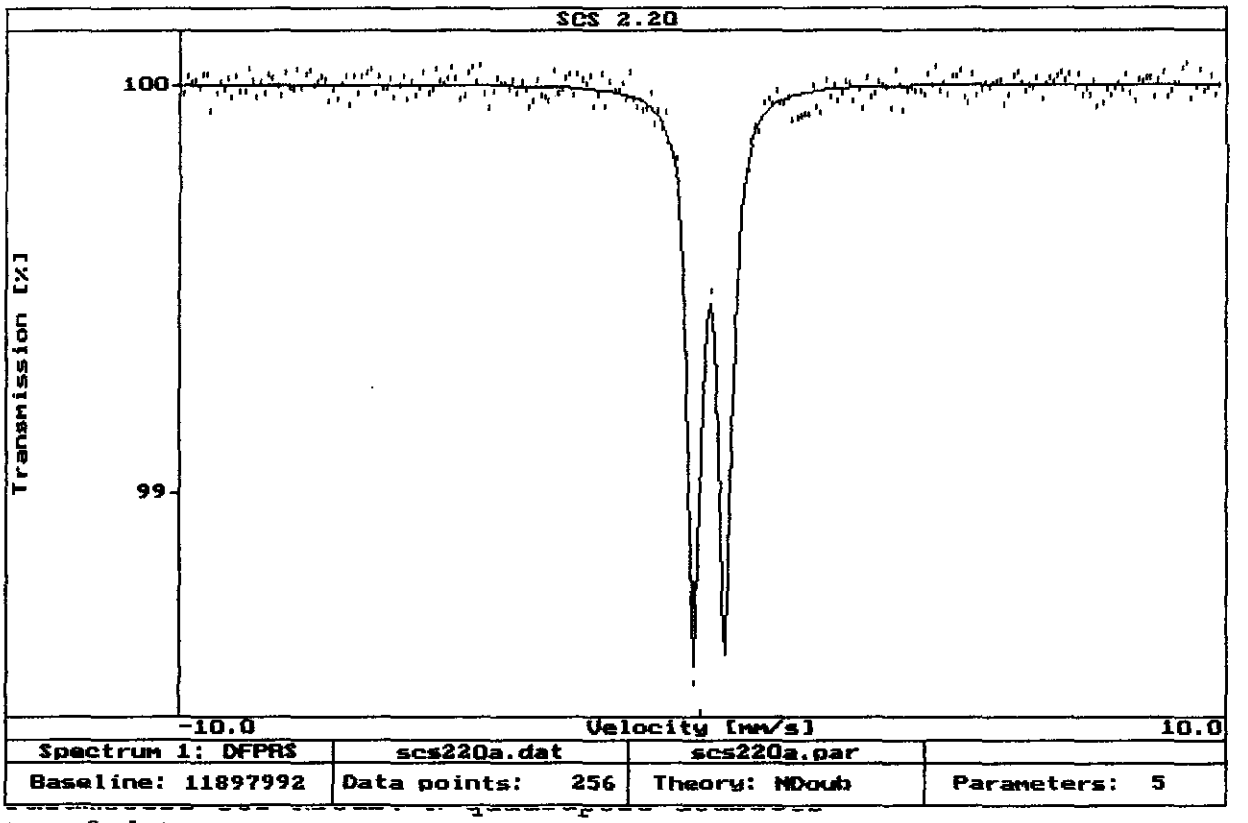

fitresults of data :
SCS 2.20

foldingpoint	255.5				
geometryeffect	0.016 %				
theory	C:\PCMOS\NDoub.exe				
date	Wed May 12 13:03:31 2004				
flags	--PCE-				
fitspectra	1				
chi2	0.8391				
chi2-test	96.9931 %				
corr-test	65.9727 %				
fitcycles	5				
maxiter	25				
parasig	1				
chi2sig	1				
fitparameter	5				
Baseline	11897953	11897992	229.89322	1.000	1.000
Total Area	0.00830	0.00815	0.00009	1.005	0.996
Quad split 1	0.61000	0.60734	0.00363	1.007	1.004
Iso shift 1	0.17030	0.16379	0.00196	1.004	1.003
Width 1	0.45440	0.30372	0.00500	1.018	0.978

Figure 4.32 Mössbauer spectrum of 2.20 RD SCS blend coal

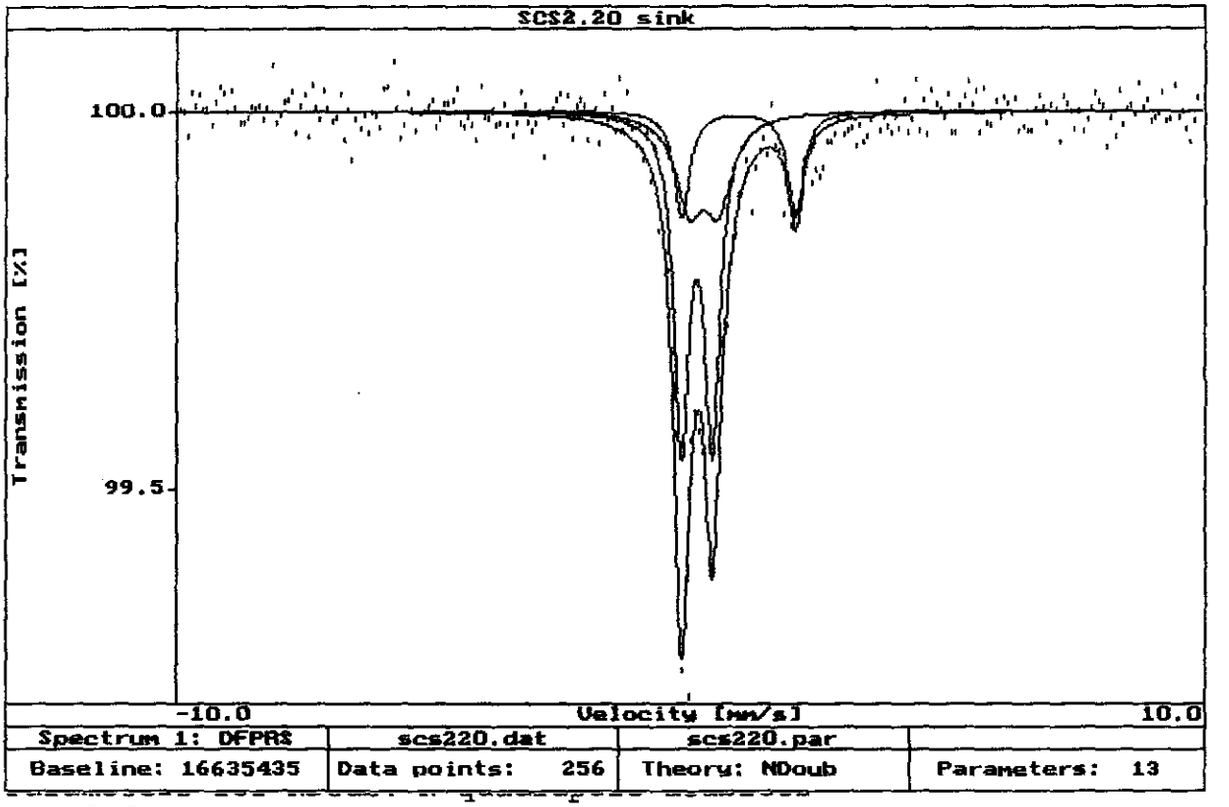

fitresults of data :
SCS2.20 sink

foldingpoint	255.5				
geometryeffect	0.015 %				
theory	C:\PCMOS\NDoub.exe				
date	Wed May 12 12:53:17 2004				
flags	---CE-				
fitspectra	1				
chi2	0.9601				
chi2-test	66.2652 %				
corr-test	43.7931 %				
fitcycles	5				
maxiter	25				
parasig	1				
chi2sig	1				
fitparameter	13				
Baseline	16635129	16635435	287.62891	6.802	9.073
Total Area	0.00530	0.00557	0.00011	94.194	85.904
Quad split 1	0.56600	0.56600 F	0.00000	0.000	0.000
Iso shift 1	0.27030	0.27030 F	0.00000	0.000	0.000
Width 1	0.55440	0.64744	0.05301	380.662	318.042
Quad split 2	2.25000	2.21248	0.81300	1145.539	1218.139
Iso shift 2	0.98230	0.94484	0.40695	1218.312	1145.366
Width 2	0.55000	0.55000 F	0.00000	0.000	0.000
Area 2	0.27700	0.18166	0.01393	27.019	22.488
Quad split 3	0.59900	0.60012	0.26922	1219.733	1145.439
Iso shift 3	0.15230	0.14284	0.13357	1136.795	1221.951
Width 3	0.55000	0.55000 F	0.00000	0.000	0.000
Area 3	0.61700	0.54728	0.08984	27.595	26.486

Figure 4.33 Mössbauer spectrum of 2.20 SINK SCS blend coal

Table 5.1 Type and concentration of minerals in leaching agents after leaching (mg/l)

Leaching agent	Sample	Al	Ca	Fe	K	Mg	Na	Si	Ti
H_2O	Blank	<1	<1	<1	2	<1	1	1	<1
	1.55	<1	12	<1	3	4	65	4	<1
	1.95	<1	37	<1	10	7	152	8	<1
	Sink	2	195	12	15	39	199	5	<1
NH_4OAc	Blank	<1	5	<1	<1	<1	4	7	<1
	1.55	<1	865	1	9	60	143	7	<1
	1.95	<1	847	2	47	61	245	8	<1
	Sink	2	575	2	44	81	175	6	<1
HNO_3	Blank	<1	2	<1	<1	<1	3	1	<1
	1.55	108	2	111	16	872	244	52	1
	1.95	156	4721	377	63	650	314	104	<1
	Sink	250	1942	2310	89	514	261	139	1
HCl	Blank	<1	2	1	1	<1	3	1	<1
	1.55	101	3753	145	14	910	234	50	1
	1.95	164	5452	444	63	700	337	106	<1
	Sink	242	1881	2307	80	509	258	141	<1

Table 5.2 Ash composition of leached SCS blend coal (%)

		SiO_2	Al_2O_3	Fe_2O_3	P_2O_5	TiO_2	CaO	MgO	K_2O	Na_2O	SO_3
H_2O	1.55	42.1	28.1	1.97	1.64	1.67	12.3	4.52	0.66	0.67	5.90
	1.95	57.1	26.8	3.58	0.44	1.80	4.78	1.13	0.95	0.34	2.94
	Sink	66.2	21.0	5.50	0.05	1.19	2.29	0.60	1.78	0.36	1.05
NH_4OAc	1.55	42.6	29.3	2.24	1.62	1.86	8.94	4.61	0.65	0.32	6.38
	1.95	55.6	26.7	4.32	0.48	1.86	4.36	1.08	0.86	0.19	3.14
	Sink	66.6	21.2	4.26	0.04	1.28	1.91	0.55	1.74	0.18	0.62
HNO_3	1.55	54.8	34.5	2.19	1.03	2.14	2.21	0.55	0.86	0.51	1.02
	1.95	59.6	27.6	4.70	0.41	1.96	1.62	0.33	1.02	0.33	0.48
	Sink	67.4	21.1	4.20	0.02	1.47	1.47	0.31	1.76	0.30	0.17
HCl	1.55	54.3	35.2	2.33	1.06	2.25	2.38	0.59	0.80	0.52	0.37
	1.95	60.3	27.5	5.10	0.39	2.04	1.62	0.33	0.90	0.32	0.58
	Sink	68.9	21.2	4.15	0.02	1.37	1.47	0.30	1.81	0.41	0.11

Table 5.3 Ash fusion temperature of leached SCS blend coal (°C)

		DT	ST	HT	FT
H_2O	1.55	1290	1300	1310	1320
	1.95	1380	1400	1440	1450
	Sink	1440	1460	1500	1510
NH_4OAc	1.55	1290	1300	1310	1320
	1.95	1310	1330	1340	1350
	Sink	1410	1430	1450	1460
HNO_3	1.55	>1600	>1600	>1600	>1600
	1.95	1550	1560	1570	1590
	Sink	>1600	>1600	>1600	>1600
HCl	1.55	>1600	>1600	>1600	>1600
	1.95	1440	1460	1490	1520
	Sink	>1600	>1600	>1600	>1600

Table 6.1 Linear correlations (r) between AFT and ash composition on Middelbult, Twistdraai and the SCS blend coal

		SiO_2	Al_2O_3	Fe_2O_3	P_2O_5	TiO_2	CaO	MgO	K_2O	Na_2O	SO_3
Middelbult	**DT**	**0.80**	0.13	-0.03	-0.60	0.67	**-0.75**	-0.72	0.63	-0.61	-0.56
	ST	**0.81**	0.16	-0.06	-0.57	0.69	**-0.75**	-0.72	0.62	-0.58	-0.57
	HT	**0.80**	0.15	-0.08	-0.53	0.69	**-0.72**	-0.70	0.62	-0.55	-0.56
	FT	**0.81**	0.17	-0.10	-0.53	0.70	**-0.73**	-0.71	0.63	-0.54	-0.56
	AFT range	**0.22**	0.21	-0.30	0.13	0.30	**-0.07**	-0.12	0.12	0.13	-0.12
Twistdraai	**DT**	**0.54**	0.11	-0.36	-0.26	0.03	-0.23	-0.37	0.32	-0.17	-0.32
	ST	**0.51**	0.06	-0.31	-0.25	0.00	-0.20	-0.35	0.30	-0.20	-0.31
	HT	**0.52**	0.07	-0.33	-0.26	0.04	-0.20	-0.33	0.30	-0.18	-0.35
	FT	**0.52**	0.07	-0.33	-0.26	0.04	-0.20	-0.33	0.30	-0.18	-0.33
	AFT range	**-0.26**	-0.34	0.23	0.04	0.08	0.23	0.36	-0.21	-0.03	-0.01
SCS blend	**DT**	**0.79**	0.07	0.09	-0.54	-0.20	**-0.78**	-0.62	0.62	-0.55	-0.75
	ST	**0.80**	0.10	0.08	-0.55	-0.22	**-0.80**	-0.62	0.60	-0.54	-0.76
	HT	**0.80**	0.11	0.09	-0.55	-0.22	**-0.81**	-0.62	0.59	-0.54	-0.76
	FT	**0.78**	0.13	0.08	-0.53	-0.21	**-0.80**	-0.61	0.56	-0.53	-0.75
	AFT range	**0.26**	0.22	-0.02	-0.17	-0.10	**-0.34**	-0.19	0.04	-0.15	-0.27
Leached SCS blend	**DT**	**0.62**	0.01	0.14	-0.43	0.06	**-0.82**	-0.69	0.48	0.17	-0.75
	ST	**0.64**	-0.02	0.18	-0.46	0.04	**-0.83**	-0.71	0.50	0.12	-0.76
	HT	**0.68**	-0.06	0.25	-0.51	0.00	**-0.85**	-0.75	0.53	0.09	-0.79
	FT	**0.69**	-0.08	0.31	-0.54	0.00	**-0.86**	-0.77	0.53	0.05	-0.81
	AFT range	**-0.04**	-0.29	0.51	-0.15	-0.24	**0.24**	0.06	-0.05	-0.47	0.15

Table 6.4 Mineral ratios calculated for density fractionated Middelbult coals

	1.40	1.45	1.50	1.55	1.60	1.65	1.70	1.75	1.80	1.85	1.90	1.95	2.00	2.05	2.10	2.15	2.20	Sink
Acidity	2.63	3.17	2.80	3.08	5.79	4.51	8.27	9.30	15.20	11.21	2.30	15.11	31.39	5.18	11.92	4.16	4.56	20.60
% Base	24.87	22.10	24.39	23.29	13.88	17.01	10.28	9.31	5.90	7.83	28.74	5.95	2.95	15.35	7.51	18.70	17.00	4.47
% Acid	66.85	71.43	69.53	73.02	81.79	78.49	86.98	88.33	92.04	89.54	67.63	92.44	95.25	81.71	91.36	79.48	79.67	94.35
Silica factor	0.63	0.67	0.65	0.67	0.80	0.76	0.86	0.87	0.92	0.89	0.60	0.93	0.97	0.79	0.90	0.74	0.78	0.95
Dolomite ratio	0.91	0.90	0.87	0.92	0.86	0.85	0.77	0.78	0.49	0.70	0.19	0.34	0.59	0.29	0.65	0.09	0.41	0.19
SiO_2*CaO	690.3	688.0	706.2	783.7	457.1	523.6	321.5	278.5	118.2	233.2	165.6	81.0	70.8	180.5	279.0	60.1	355.9	34.1
CaO*MgO	91.00	62.24	76.56	71.28	27.69	40.17	12.70	11.78	1.83	5.88	6.72	0.92	0.71	4.05	2.20	0.61	4.04	0.18
CaO+MgO	22.56	19.89	21.14	21.42	11.94	14.39	7.88	7.26	2.92	5.47	5.60	2.00	1.75	4.51	4.90	1.69	6.95	0.85
Base/Acid ratio	0.33	0.28	0.32	0.30	0.16	0.20	0.11	0.10	0.06	0.08	0.40	0.06	0.03	0.18	0.08	0.23	0.20	0.05
Slagging factor	0.20	0.16	0.19	0.15	0.08	0.12	0.09	0.04	0.05	0.06	2.05	0.06	0.01	0.58	0.06	0.83	0.57	0.06
Fouling factor	0.35	0.24	0.22	0.19	0.09	0.13	0.05	0.04	0.02	0.03	0.10	0.03	0.01	0.06	0.02	0.08	0.06	0.01
Acid flux factor	1.58	1.66	1.65	1.77	1.85	1.79	2.03	1.99	1.88	1.96	0.98	2.25	2.22	1.69	2.35	1.26	1.94	2.65
Basic flux factor	0.06	0.05	0.04	0.04	0.07	0.08	0.11	0.09	0.38	0.17	0.11	0.57	0.45	0.21	0.16	0.60	0.11	1.11
Silica module	1.50	1.53	1.54	1.66	1.77	1.71	1.95	1.92	1.79	1.89	0.94	2.15	2.12	1.61	2.27	1.21	1.86	2.57
Alumina module	25.10	23.89	10.90	27.79	26.95	18.27	18.05	20.65	16.52	20.77	1.04	9.43	71.71	2.46	14.11	1.65	2.27	8.92
Hydraulic module	0.26	0.22	0.23	0.24	0.11	0.14	0.06	0.05	0.02	0.04	0.04	0.01	0.01	0.04	0.05	0.01	0.07	0.01
Basic module	0.34	0.28	0.31	0.30	0.15	0.19	0.09	0.08	0.03	0.06	0.08	0.02	0.02	0.06	0.05	0.02	0.09	0.01
Iron index	3.08	3.98	7.25	3.13	6.51	7.32	13.44	13.54	29.82	16.72	55.79	44.57	13.49	54.54	22.78	69.56	45.31	57.28
(Dolomite ratio)^2	0.82	0.81	0.75	0.85	0.74	0.72	0.59	0.61	0.24	0.49	0.04	0.11	0.35	0.09	0.43	0.01	0.17	0.04
New Slagging index	0.38	0.35	0.82	0.30	0.18	0.33	0.18	0.15	0.12	0.12	9.56	0.18	0.01	1.86	0.15	3.76	1.98	0.13
New Fe+Ca index	18.32	17.13	18.84	18.25	9.84	12.10	7.16	6.20	3.88	5.42	26.36	4.10	1.53	13.16	6.25	17.17	15.59	3.18

Table 6.5 Mineral ratios calculated for density fractionated Twistdraai coal

	1.40	1.45	1.50	1.55	1.60	1.65	1.70	1.75	1.80	1.85	1.90	1.95	2.00	2.05	2.10	2.15	2.20	Sink
Acidity	4.06	4.60	4.74	2.44	4.35	1.11	12.33	7.83	7.29	5.32	0.96	9.58	6.36	3.88	1.95	8.58	5.69	17.30
% Base	18.50	16.25	15.93	27.65	17.19	44.42	7.08	10.69	11.53	15.25	47.32	9.11	13.16	19.68	32.69	10.11	14.49	5.29
% Acid	76.55	76.80	77.93	69.93	77.39	50.16	89.34	85.75	85.44	82.44	45.93	89.28	84.60	78.02	64.83	88.05	83.36	92.67
Silica factor	0.73	0.76	0.77	0.62	0.75	0.41	0.91	0.87	0.86	0.79	0.40	0.89	0.84	0.77	0.59	0.89	0.82	0.95
Dolomite ratio	0.83	0.77	0.81	0.74	0.67	0.43	0.50	0.37	0.49	0.13	0.19	0.36	0.35	0.25	0.87	0.37	0.26	0.27
SiO_2*CaO	496.1	434.7	412.3	607.4	312.3	410.7	125.6	184.4	202.6	67.2	190.6	122.8	235.0	172.9	1210	176.6	156.2	48.8
CaO*MgO	50.24	29.45	36.80	90.49	32.57	72.08	2.93	2.54	7.64	0.95	16.37	2.53	3.16	5.91	34.82	2.91	2.65	0.51
CaO+MgO	15.34	12.54	12.92	20.41	11.57	18.90	3.52	3.94	5.65	2.02	8.79	3.28	4.60	4.96	28.48	3.73	3.70	1.45
Base/Acid ratio	0.23	0.19	0.19	0.38	0.21	0.80	0.08	0.12	0.13	0.18	0.90	0.10	0.15	0.25	0.49	0.11	0.17	0.06
Slagging factor	0.14	0.11	0.10	0.40	0.21	3.15	0.05	0.13	0.20	0.30	5.38	0.12	0.25	0.68	0.51	0.14	0.40	0.03
Fouling factor	0.18	0.15	0.15	0.24	0.12	0.32	0.03	0.04	0.04	0.05	0.13	0.04	0.04	0.06	0.16	0.02	0.04	0.02
Acid flux factor	1.65	1.61	1.75	1.57	1.55	0.74	1.92	2.05	2.17	1.36	0.62	1.99	2.27	1.94	2.07	2.88	1.70	1.75
Basic flux factor	0.10	0.11	0.13	0.06	0.14	0.05	0.41	0.40	0.39	0.66	0.07	0.49	0.37	0.39	0.04	0.47	0.51	1.53
Silica module	1.56	1.50	1.62	1.46	1.43	0.69	1.84	1.96	2.10	1.32	0.60	1.92	2.23	1.88	2.00	2.82	1.67	1.71
Alumina module	16.85	12.54	21.37	3.90	7.15	0.78	14.00	4.78	6.72	2.37	0.37	6.41	3.09	1.41	6.59	4.19	2.85	20.19
Hydraulic module	0.14	0.12	0.11	0.19	0.09	0.18	0.02	0.04	0.04	0.01	0.07	0.02	0.04	0.03	0.41	0.03	0.03	0.01
Basic module	0.20	0.17	0.17	0.30	0.15	0.38	0.04	0.05	0.07	0.02	0.19	0.04	0.05	0.07	0.45	0.04	0.04	0.02
Iron index	7.40	11.75	6.91	15.96	19.12	30.66	27.56	43.36	28.08	66.13	42.19	42.20	45.33	52.24	6.03	40.99	52.46	29.00
(Dolomite ratio)^2	0.69	0.60	0.66	0.54	0.45	0.18	0.25	0.14	0.24	0.02	0.03	0.13	0.12	0.06	0.76	0.14	0.07	0.08
New Slagging index	0.41	0.48	0.27	2.41	0.88	21.70	0.17	0.65	0.49	2.20	39.05	0.43	1.07	3.23	1.48	0.53	1.55	0.09
New Fe+Ca index	12.28	11.69	9.99	20.00	10.70	38.10	4.27	8.32	7.07	13.17	44.01	6.27	10.63	15.77	30.13	7.23	11.62	2.45

Table 6.6 Mineral ratios calculated for density fractionated SCS blend coal

	1.40	1.45	1.50	1.55	1.60	1.65	1.70	1.75	1.80	1.85	1.90	1.95	2.00	2.05	2.10	2.15	2.20	Sink
Acidity	3.00	2.57	2.68	4.17	3.42	3.30	3.76	4.49	8.90	7.15	3.69	7.16	7.56	7.63	6.54	7.77	3.46	11.72
% Base	22.13	24.40	24.10	17.19	20.35	20.79	18.64	16.25	9.36	11.45	19.51	11.39	10.70	11.04	12.67	11.04	20.49	7.51
% Acid	68.79	64.66	66.05	74.13	71.95	71.86	73.33	75.71	85.37	84.33	74.34	83.95	82.73	86.07	84.28	87.39	72.26	90.05
Silica factor	0.65	0.62	0.63	0.73	0.70	0.69	0.72	0.76	0.87	0.84	0.73	0.84	0.86	0.85	0.85	0.88	0.73	0.92
Dolomite ratio	0.75	0.83	0.89	0.84	0.80	0.85	0.70	0.44	0.49	0.41	0.63	0.41	0.32	0.27	0.35	0.41	0.41	0.39
SiO_2*CaO	165.6	123.7	56.1	70.1	129.1	624.4	479.1	238.2	184.1	203.7	539.6	191.4	149.1	111.0	179.4	255.4	380.3	136.1
CaO*MgO	119.9	82.91	35.64	44.64	75.56	52.08	26.61	10.23	4.00	3.77	14.28	3.89	1.85	2.07	4.27	2.71	7.59	1.78
CaO+MgO	61.49	52.31	24.14	17.60	36.46	17.72	13.11	7.10	4.55	4.74	12.21	4.66	3.40	3.03	4.44	4.57	8.34	2.94
Base/Acid ratio	0.28	0.32	0.32	0.21	0.26	0.26	0.23	0.19	0.10	0.13	0.24	0.13	0.12	0.12	0.15	0.12	0.26	0.08
Slagging factor	0.23	0.23	0.19	0.13	0.18	0.21	0.32	0.39	0.14	0.24	0.38	0.24	0.31	0.37	0.23	0.23	1.16	0.09
Fouling factor	0.23	0.21	0.26	0.13	0.13	0.11	0.11	0.07	0.04	0.05	0.12	0.05	0.04	0.03	0.05	0.04	0.06	0.02
Acid flux factor	1.34	1.42	1.64	1.62	1.64	1.85	1.68	1.48	1.78	1.76	1.85	1.68	1.81	1.65	2.02	2.77	1.82	2.61
Basic flux factor	0.08	0.05	0.06	0.08	0.07	0.05	0.10	0.19	0.25	0.27	0.11	0.24	0.45	0.41	0.41	0.39	0.14	0.57
Silica module	1.20	1.32	1.49	1.48	1.53	1.70	1.55	1.38	1.70	1.67	1.74	1.59	1.72	1.59	1.97	2.70	1.75	2.52
Alumina module	6.49	7.66	17.68	17.44	8.74	11.48	5.86	3.35	7.74	5.02	3.80	4.99	4.52	4.20	3.70	4.24	1.71	7.90
Hydraulic module	0.20	0.24	0.26	0.15	0.17	0.20	0.14	0.06	0.04	0.04	0.14	0.04	0.03	0.02	0.03	0.04	0.09	0.02
Basic module	0.25	0.32	0.33	0.20	0.23	0.26	0.19	0.10	0.05	0.06	0.17	0.06	0.04	0.04	0.05	0.05	0.12	0.03
Iron index	15.13	10.19	4.47	7.71	11.51	8.00	18.55	40.20	35.64	42.07	24.42	43.64	48.24	54.47	44.18	37.63	42.68	35.72
$(\text{Dolomite ratio})^2$	0.56	0.68	0.79	0.71	0.64	0.73	0.49	0.19	0.24	0.17	0.39	0.17	0.10	0.08	0.12	0.17	0.17	0.15
New Slagging index	1.38	1.24	0.52	0.37	0.83	0.61	1.08	1.67	0.40	0.74	1.55	0.76	0.75	0.87	0.96	0.59	3.12	0.24
New Fe+Ca index	18.60	19.19	18.42	12.60	15.34	16.10	14.85	12.89	7.04	9.17	16.82	9.18	8.50	8.75	9.44	8.54	18.30	4.99

Table 6.7 Mineral ratios calculated for the leached SCS blend coal

	1.55				1.95				Sink			
	H_2O	NH_4OAc	HNO_3	HCl	H_2O	NH_4OAc	HNO_3	HCl	H_2O	NH_4OAc	HNO_3	HCl
Acidity	3.49	4.29	14.13	13.52	7.78	7.61	10.62	10.90	8.28	10.16	11.07	11.01
% Base	20.12	16.76	6.32	6.62	10.78	10.81	8.27	8.00	10.53	8.64	8.14	8.04
% Acid	71.87	73.76	91.44	91.75	85.70	84.16	89.84	89.16	88.39	89.08	91.47	89.97
Silica factor	0.69	0.73	0.92	0.91	0.86	0.85	0.90	0.90	0.89	0.91	0.92	0.92
Dolomite ratio	0.84	0.81	0.44	0.45	0.55	0.50	0.24	0.24	0.27	0.28	0.22	0.22
SiO_2*CaO	517.8	380.8	121.1	129.2	272.9	242.4	97.6	96.5	151.6	127.2	101.2	99.0
CaO*MgO	55.60	41.21	1.22	1.40	5.40	4.71	0.53	0.53	1.37	1.05	0.44	0.46
CaO+MgO	16.82	13.55	2.76	2.97	5.91	5.44	1.95	1.95	2.89	2.46	1.77	1.78
Base/Acid ratio	0.25	0.20	0.07	0.07	0.12	0.12	0.09	0.09	0.12	0.09	0.09	0.09
Fouling factor	0.19	0.07	0.04	0.04	0.04	0.02	0.03	0.03	0.04	0.02	0.04	0.03
Acid flux factor	1.51	1.46	1.58	1.54	1.95	1.87	1.92	1.92	2.54	2.67	2.77	2.72
Basic flux factor	0.08	0.07	0.50	0.44	0.22	0.19	0.63	0.69	0.74	0.78	1.25	1.16
Silica module	1.40	1.35	1.49	1.45	1.88	1.79	1.85	1.85	2.50	2.62	2.72	2.66
Alumina module	14.26	13.08	15.75	15.11	7.49	6.18	5.39	5.87	3.82	4.98	5.11	5.02
Hydraulic module	0.17	0.12	0.02	0.03	0.05	0.05	0.02	0.02	0.02	0.02	0.02	0.02
Basic module	0.24	0.19	0.03	0.03	0.07	0.07	0.02	0.02	0.03	0.03	0.02	0.02
Iron index	7.82	11.13	32.46	32.87	29.63	35.64	56.57	54.05	46.73	45.05	46.83	48.04
$(\text{Dolomite ratio})^2$	0.70	0.65	0.19	0.20	0.30	0.25	0.06	0.06	0.08	0.08	0.05	0.05
New Slagging index	0.55	0.51	0.15	0.17	0.45	0.55	0.47	0.42	0.66	0.41	0.37	0.38
New Fe+Ca index	14.27	11.18	4.40	4.71	8.36	8.68	6.72	6.32	7.79	6.17	5.62	5.67

Table 6.8 Linear correlations (r) between AFT and mineral ratios on Middelbult, Twistdraai and the SCS blend coal

	MIDDELBULT				TWISTDRAAI				SCS				LEACHED SCS			
	DT	ST	HT	FT	DT	ST	HT	FT	DT	ST	HT	FT	DT	ST	HT	FT
Acidity	0.88	0.90	0.90	0.92	0.41	0.39	0.40	0.40	0.80	0.82	0.81	0.81	0.84	0.85	0.83	0.82
% Base	-0.77	-0.76	-0.76	-0.76	-0.46	-0.41	-0.42	-0.42	-0.85	-0.87	-0.87	-0.87	-0.77	-0.79	-0.80	-0.80
% Acid	0.79	0.78	0.77	0.77	0.48	0.43	0.44	0.44	0.87	0.88	0.88	0.88	0.79	0.81	0.83	0.82
Silica factor	0.78	0.77	0.77	0.77	0.48	0.44	0.45	0.45	0.84	0.86	0.86	0.86	0.76	0.78	0.80	0.79
Dolomite ratio	-0.46	-0.44	-0.42	-0.40	-0.03	-0.04	-0.03	-0.03	-0.69	-0.69	-0.69	-0.67	-0.70	-0.72	-0.75	-0.76
SiO_2*CaO	-0.75	-0.73	-0.71	-0.70	-0.15	-0.14	-0.14	-0.14	-0.31	-0.34	-0.35	-0.37	-0.76	-0.78	-0.80	-0.79
CaO*MgO	-0.67	-0.64	-0.63	-0.62	-0.32	-0.30	-0.27	-0.27	-0.61	-0.62	-0.63	-0.62	-0.66	-0.69	-0.73	-0.73
CaO+MgO	-0.74	-0.72	-0.70	-0.69	-0.29	-0.26	-0.26	-0.26	-0.61	-0.62	-0.64	-0.64	-0.73	-0.75	-0.78	-0.78
Base/Acid ratio	-0.73	-0.72	-0.72	-0.72	-0.41	-0.36	-0.37	-0.37	-0.85	-0.87	-0.87	-0.87	-0.76	-0.78	-0.79	-0.79
Slagging factor	-0.16	-0.17	-0.19	-0.20	-0.32	-0.27	-0.29	-0.29	-0.26	-0.27	-0.26	-0.25	0.00	0.00	0.00	0.00
Fouling factor	-0.70	-0.68	-0.67	-0.66	-0.42	-0.38	-0.37	-0.37	-0.71	-0.72	-0.73	-0.73	-0.52	-0.54	-0.56	-0.55
Acid flux factor	0.61	0.61	0.62	0.61	0.59	0.57	0.58	0.58	0.58	0.57	0.55	0.54	0.32	0.33	0.35	0.34
Basic flux factor	0.74	0.73	0.72	0.70	0.13	0.11	0.12	0.12	0.80	0.78	0.77	0.75	0.74	0.75	0.74	0.73
Silica module	0.62	0.62	0.63	0.62	0.59	0.57	0.59	0.59	0.61	0.60	0.58	0.57	0.33	0.34	0.36	0.36
Alumina module	0.32	0.37	0.38	0.43	0.03	0.01	0.02	0.02	-0.26	-0.23	-0.22	-0.17	-0.16	-0.18	-0.24	-0.23
Hydraulic module	-0.72	-0.69	-0.67	-0.66	-0.21	-0.19	-0.19	-0.19	-0.76	-0.78	-0.79	-0.78	-0.71	-0.73	-0.76	-0.75
Basic module	-0.73	-0.71	-0.69	-0.68	-0.32	-0.28	-0.28	-0.28	-0.76	-0.78	-0.78	-0.78	-0.72	-0.74	-0.77	-0.77
Iron index	0.33	0.31	0.30	0.27	0.06	0.05	0.05	0.05	0.67	0.66	0.66	0.64	0.60	0.63	0.67	0.68
(Dolomite ratio)^2	-0.53	-0.50	-0.49	-0.47	-0.11	-0.12	-0.11	-0.11	-0.66	-0.66	-0.66	-0.64	-0.69	-0.72	-0.75	-0.74
New Slagging index	-0.12	-0.13	-0.15	-0.16	-0.31	-0.26	-0.28	-0.28	-0.48	-0.48	-0.47	-0.48	-0.51	-0.49	-0.43	-0.44
New Fe+Ca index	-0.71	-0.70	-0.70	-0.70	-0.43	-0.38	-0.39	-0.39	-0.85	-0.88	-0.88	-0.88	-0.79	-0.80	-0.80	-0.79